Nanoscale Vibration to Modulate Osteoclastogenesis

John William Kennedy

BMSc (Hons) MBChB MRCS

Submitted in fulfilment of the requirements for the Degree of MD

Institute of Molecular, Cell and System Biology

College of Medical, Veterinary and Life Sciences

University of Glasgow

June 2019

Abstract

Mechanical factors have been shown to significantly influence stem cell differentiation and fate. Researchers have demonstrated that nanoscale vibration can promote osteogenesis in isolated mesenchymal stem cell (MSC) cultures. In the bone marrow niche, there is a co-dependent existence between MSCs and cells from the haematopoietic lineage (HSCs), particularly osteoclasts. While MSC derived osteoblasts stimulate new bone formation, osteoclasts resorb bone. Given the close overlap between these two cells types, an investigation in to the effect of nanoscale vibration on osteoclasts was required.

Two culture methods were used: an isolated culture of osteoclasts and osteoclast-precursors, and a co-culture of bone marrow stromal cells and bone marrow haematopoietic cells. Vibration was produced with the Nanokick bioreactor – a recently developed technology that facilitates the delivery of accurate and reproducible nanoscale vertical displacements. This bioreactor allows otherwise standard cell culture techniques to be used. A range of experiments was used to investigate the effect of nanoscale vibration, including immunostaining, resorption analysis, RT-qPCR, ELISA and metabolomics.

Nanoscale vibration was found to influence osteoclast differentiation and function. A reduction in osteoclast numbers was observed in both culture conditions. Furthermore, less resorption occurred in the nanokick group. There was no significant impairment in osteoblast development or function when osteoclasts were present, with evidence of increased cytoskeleton tension and mineralisation following stimulation. A number of changes in gene, protein and regulations were observed, suggesting a state of lower inflammation in the nanokick group.

It is hoped that these results will provide further evidence to validate the use of the nanokick bioreactor as a method of producing tissue-engineered bone graft for clinical applications.

Table of Contents

List of Tables

List of Figures

Acknowledgement

I would like to acknowledge my academic supervisors Professor Matthew J. Dalby, Professor Carl Goodyear and Dr Monica P. Tsimbouri for their invaluable support and advice throughout my MD. I also extend my thanks to my clinical supervisor Professor Dominic Meek for his encouragement and support throughout my career.

I thank Carol-Anne Smith for her help in facilitating experiments over the past 2 years. I acknowledge Dr Paul Campsie for assisting me with interferometry measurements and providing an illustrative figure. I also acknowledge Dr Cecilia Ansalone for their help and advice with CD14+ cell cultures. I thank the Glasgow Polyomics department for their contribution to the metabolomics results.

I extend my gratitude to the Royal College of Surgeons Edinburgh for providing funding for this research.

Finally, I send my deepest gratitude to my loving and supportive wife, Morgan.

Author's Declaration

The research reported within this thesis is the original work of the author except where the assistance of others has been acknowledged and at the time of submission is not being considered elsewhere for any other academic qualification.

John W. Kennedy

June 2019

Definitions/Abbreviations

2D	Two-dimensional
3D	Three-dimensional
α-MEM	Alpha minimum essential media
AhR	Aryl hydrocarbon receptor
AMPK	Adenosine monophosphate-activated protein kinase
Arp2/3	Actin related protein 2/3
BMHC	Bone marrow haematopoietic cell
BMP	Bone morphogenic protein
BSA	Bovine serum albumin
cDNA	Complementary DNA
C/EBP	CCAAT/enhancer binding protein
cf	Compare
CO_2	Carbon dioxide
COX-2	Cyclooxygenase-2
CSF1R	Colony stimulating factor 1 receptor
CXCR2	C-X-C chemokine receptor type 2
DC-STAMP	Dendritic cell-specific transmembrane protein
DMEM	Dulbecco's Modified Eagle Medium
DNA	Deoxyribonucleic acid
ECM	Extracellular matrix
EGFR	Epidermal growth factor receptor
ELISA	Enzyme-linked immunosorbent assay
ERK	Extracellular signal-related kinase
FAK	Focal adhesion kinase
FA	Focal adhesion
FC	Focal complex
FITC	Fluorescein isothiocyanate
Gap DH	Glyceraldehyde 3-phosphate dehydrogenase
HIF1	Hypoxia-inducible factor 1
HMDS	Hexamethyl-disilazane
Hz	Hertz
IGF	Insulin-like growth factor
IFN-ϒ	Interferon-ϒ
IPA	Ingenuity pathway analysis
ITGAM	Integrin subunit alpha M
JNK	c-Jun N-terminal kinase
KEGG	Kyoto encyclopaedia of genes and genomes
LC-MS	Liquid chromatography-mass spectrometry
LDL	Low density lipoprotein
LIPUS	Low-intensity pulsed ultrasound
M-CSF	Macrophage colony-stimulating factor
MSC	Mesenchymal stem cell
mm	Millimetre
NADPH	Nicotinamide adenine dinucleotide phosphate
NFATC1	Nuclear factor of activated T cells 1
NF-κB	Nuclear factor kappa-light-chain-enhancer of activated B cells
nm	Nanometre
NNI	National nanotechnology initiative
NO	Nitric oxide

OCN	Osteocalcin
OSCAR	Osteoclast-associated receptor
OPC	Osteoclast precursor cell
OPN	Osteopontin
PARP	Poly ADP ribose polymerase
PBS	Phosphate buffer saline
pg	Picogram
PGE_2	Prostaglandin E_2
PKC	Protein kinase C
PLA2	Phospholipase A2
pN	Piconewton
PYK-2	Protein tyrosine kinase 2
RANKL	Receptor activator of nuclear factor kappa-B ligand
Rap1	Ras-proximate-1
RNA	Ribonucleic acid
ROCK	Rho-associated protein kinase
RT-qPCR	Reverse transcription quantitative polymerase chain reaction
RUNX2	Runt-related transcription factor 2
SD	Standard deviation
SEM	Scanning electron microscopy
SIRT	Sirtuin
TERM	Tissue engineering and regenerative medicine
TGF	Transforming growth factor
TNF	Tumour necrosis factor
TRAF	TNF receptor associated factor
TRAP	Tartrate-resistant acid phosphatase
tRNA	Transfer ribonucleic acid
TRP	Transient receptor potential
µm	Micrometre
VASP	Vasodilator-stimulated phosphoprotein
WASp	Wiskott-Aldrich Syndrome protein

Chapter 1 Introduction

1.1 Bone

Bone is a complex tissue that is constantly changing in response to structural and hormonal signals. It plays a crucial role in multiple functions, including haematopoiesis, mineral homeostasis and locomotion through the attachment of muscles. The chemical and biological composition of bone renders it ideal for these roles. Regarding composition, it can be split into a cellular and acellular component, the latter of which is further divided into organic and inorganic elements. By weight, the inorganic component composes around 65%, compared to 20% organic and the remainder being water (Xu Feng, 2009). The inorganic matrix is primarily crystalline hydroxyapatite, which provided the compressive strength of bone, and osteocalcium phosphate (brushite). This matrix serves as a reservoir for 99% of the body's calcium, 85% phosphorus and 50% of total sodium and potassium. The organic component comprises over 30 proteins with type 1 collagen representing >90% of these. Type 1 collagen provides tensile strength while proteoglycans, matrix proteins and growth factors influence mineralisation and cell function. The cellular component is comprised of osteoblasts, osteoclasts and osteocytes. Osteocytes represent 90 - 95% of total cell numbers and help orchestrate skeletal metabolism (Schaffler MB et al, 2014). Osteoblasts, derived from mesenchymal stromal cells (MSC), and osteoclasts, formed from haematopoietic stem cells (HSC), are responsible for the formation and resorption of bone, respectively (Xu Feng, 2009). The structure of cortical bone is presented in Figure 1:1. Macroscopically, bone is comprised of compact and trabecular components. Although they are composed from the same matrix components, their density is significantly different. Compact bone is denser and as such has a greater compressive strength. Trabecular bone, conversely, is made up of a network of interconnected trabeculae, leading to a greater surface area. Trabecular bone is also more metabolically active, acting as a reservoir of calcium that is important in maintaining homeostasis (Buckwalter JA et al, 1996).

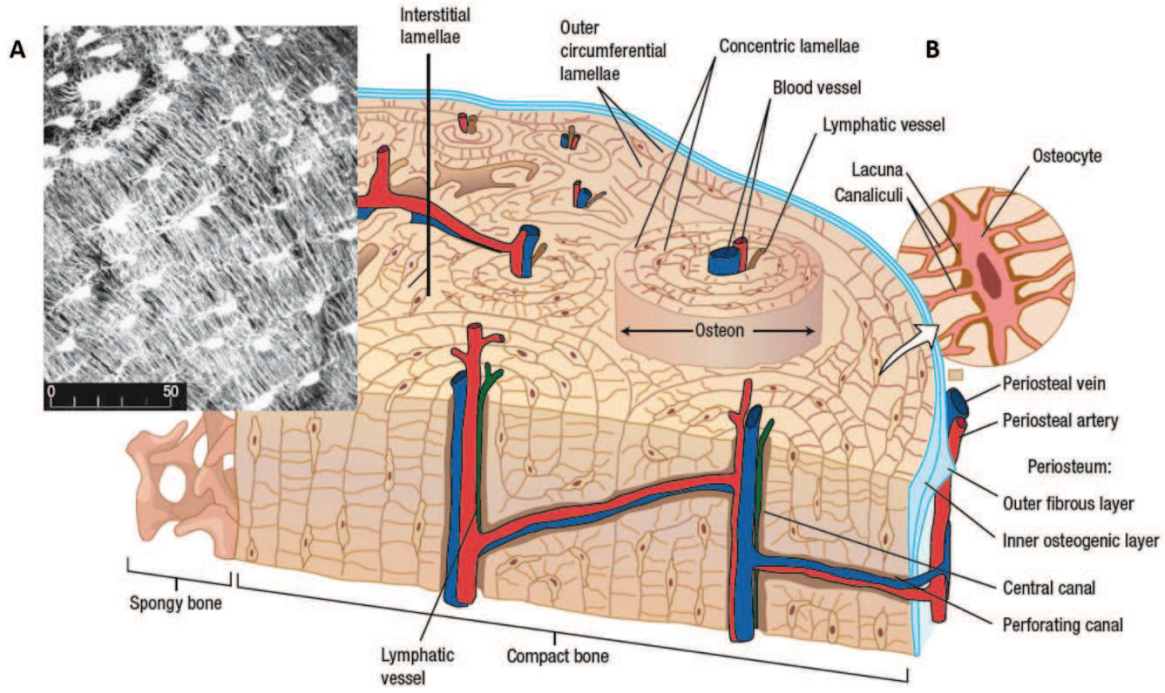

Figure 1:1 Structure of cortical bone.
A – black and white micrography image (scale bar in μm) showing osteocytes (white dots) linked by processes (fine white lines). B – schematic representation of bone in cross section, highlighting compact and trabecular bone. Note the lacuna and canaliculi surrounding the osteocyte processes. These fluid filled spaces help facilitate the detection of hydrostatic pressure change in response to mechanical stimulation by osteocytes. Figure used with permission from the Springer Nature (Taylor D et al, 2007).

1.2 Mesenchymal stem cells

Mesenchymal stem cells are present within bone marrow as undifferentiated cells that have the potential to progress down a range of tissue lineages, including muscle (myocytes), fat (adipocytes) and bone (osteoblasts). They are therefore crucial for tissue regeneration following trauma, age or disease (Pittenger MF et al, 1999). These characteristics have led to detailed investigations by the scientific community into their potential uses in novel cellular therapies. They are defined by three criteria: 1) adherence to plastic, 2) specific surface antigen expression (namely CD105, CD73 and CD90, and lack CD45, CD34, CD14, CD11b, CD79a, CD19 and HLA-DR), and 3) multipotent differentiation (Dominici M et al, 2006). There is no sole marker that is truly MSC-specific (Lv FJ et al, 2014). The route of differentiation can be influenced by a number of chemical, biological and physical factors within the cells' microenvironment (Robertson SN et al, 2018). The exploration of physical factors and mechanical properties has prompted a range of new materials tools to be developed, including nanotopography (McMurray RJ et al, 2011) and hydrogels (Engler AJ et al, 2006). These materials are believed to effect change by altering MSC cytoskeleton dynamics and

intracellular tension (Kilian KA et al, 2010b). More recently, evidence has emerged that mechanotransduction, whereby cells are vibrated at specific frequencies and amplitudes, may play an important role in determining cell fate (Xiao G et al, 2002, Nikukar H et al, 2013, Nikukar H et al, 2016).

1.3 Osteoblasts

Osteoblasts are derived from MSCs through a multi-step differentiation pathway (Neve A et al, 2011). They are mononucleated, measuring around 25 μm in diameter. Their most obvious role is the production of new bone through the secretion of type 1 collagen, which forms the majority of the organic matrix. The collagen molecules arrange in a triple helix to form fibrils, which then produce concentric weaves (Viguet-Carrin S et al, 2006). This configuration improves the strength of bone.

Osteoblasts also closely interact with osteoclasts, which cannot mature and therefore resorb bone without their presence (Young PS et al, 2015). As such, they have a large influence on the overall process of bone remodelling. Osteoblast differentiation and growth is influenced by a number of factors, including bone morphogenic proteins (BMP), insulin-like growth factor (IGF) and mechanical forces (Neve A et al, 2011). As the cells progress in to the mineralisation phase, they produce proteins including osteopontin (OPN) and osteocalcin (OCN) (Neve A et al, 2011). OPN expression is regulated by mechanical stress and influences bone homeostasis (Fujihara S et al, 2006). OCN regulates mineral deposition and promotes osteoblast differentiation and activation (Chenu C et al, 1994). Both OPN and OCN can be used as a marker of mature osteoblasts (Lian JB et al, 1991, Neve A et al, 2011).

1.4 Osteocytes

Osteocytes are the most abundant cell type in bone, making up 90 – 95% of total cell numbers (Schaffler MB et al, 2014). They are formed from osteoblasts that have become enclosed in unmineralised matrix. Structurally, they are dendritic in appearance with long cellular processes that communicate with nearby osteocytes and osteoblasts (Schaffler MB et al, 2014). These processes are elongated through the production of E11/gp38 proteins in response to mechanical stresses (Zhang K

et al, 2006). Similar to osteoblasts, they produce proteins including OPN and OCN as well as dentin matrix protein 1 and proteoglycans (Schaffler MB et al, 2014). Osteocytes are sensitive to mechanical stresses, with elongation of their processes through E11/gp38 proteins in response to tissue strain. It is believed that they recognise mechanical stresses through hydrostatic pressure changes in the pericellular space (see Figure 1.1) (You J et al, 2000). In response to mechanical stimulation, osteocytes upregulate their secretion of a range of molecules, including IGF-1 (Yakar S et al, 2002) and prostaglandin E2 (Somjen D et al, 1980), and reduce production of others such as sclerostin (Robling AG et al, 2008), resulting in increased osteoblast activity. Equally, osteocytes have been shown to influence osteoclastogenesis, whereby apoptosis of osteocytes induce expression of the pro-osteoclastic cytokine receptor activator of nuclear factor kappa-B ligand (RANKL) in neighbouring healthy cells (Schaffler MB et al, 2014). Osteocyte apoptosis is influenced by biomechanical loading, further highlighting the importance of physical factors on cell function (O'Brien CA et al, 2013). Given their close interaction with both osteoblasts and osteoclasts, osteocytes clearly play a crucial role in bone homeostasis.

1.5 Haematopoietic stem cells

Haematopoietic stem cells (HSCs) are self-renewing cells that can give rise to a range of cell types through haematopoiesis (Wu JY et al, 2009). They are non-adherent and round in appearance and can be found in bone marrow and peripheral blood (Suda T et al, 2001). Cell types they can differentiate into include red blood cells, macrophages and lymphocytes (Wu JY et al, 2009).

Within the bone marrow, HSCs are provided with a microenvironment, or niche, that facilitates maintenance, mobilisation and differentiation. HSCs require stromal cells for differentiation, a task which can be performed by cells from the osteoblast lineage (Wu JY et al, 2009). The exact molecular mechanism for this interaction is not completely defined, but studies have suggested factors such as OPN (Stier S et al, 2005), Notch ligand Jagged-1 (Calvi LM et al, 2003) and N-cadherin (Haug JS et al, 2008) play a role. Furthermore, stromal cells and osteoblasts produce macrophage colony-stimulating factor (M-CSF) which promotes osteoclastogenesis further down the HSC differentiation pathway (Suda T et al, 2001).

1.6 Macrophages

Derived from HSCs, macrophages are a white blood cell that play a crucial role in immunity, homeostasis and tissue repair. In response to encountering either damaged tissue or pathogens, molecules are produced by macrophages to exhibit an effect on the surrounding tissue (Mills CD, 2012). This can be categorised as M1 or M2. M1 macrophages exert a pro-inflammatory effect through the production of cytokines including tumour necrosis factor alpha (TNF-α) and interleukin-1 (IL-1). M2 macrophages conversely have anti-inflammatory effects, producing IL-10 and ornithine to promote repair (Mills CD, 2012). This has significance for the success of orthopaedic implants as the phagocytosis of wear debris particles leads to activation of pro-inflammatory M1 macrophages (Rao AJ et al, 2012) which stimulate osteoclastogenesis, predominantly through M-CSF production. This increase in osteoclast activation can lead to loosening of the implant and failure (Landgraeber S et al, 2014).

1.7 Osteoclasts

Also part of the HSC lineage, osteoclasts act alongside osteoblasts to contribute to bone homeostasis. They are formed from the fusion of monocyte progenitors and are the only cells capable of resorbing bone (Roodman GD, 1999). They are multinucleated (typically around 3 – 20 nuclei) with a characteristic ruffled border and sealing zones that act as specialised resorbing structures. They stain intensely for tartrate-resistant acid phosphatase (TRAP), which is their most commonly used histochemical marker (Hayman AR, 2008). They are derived from macrophages that are prompted to proliferate, differentiate and activate in the presence of M-CSF and RANKL, which can be produced by stromal cells and osteoblasts (Figure 1:2). These factors are therefore required when culturing osteoclasts *in vitro* in the absence of stromal cells and osteoblasts (Marino S et al, 2014).

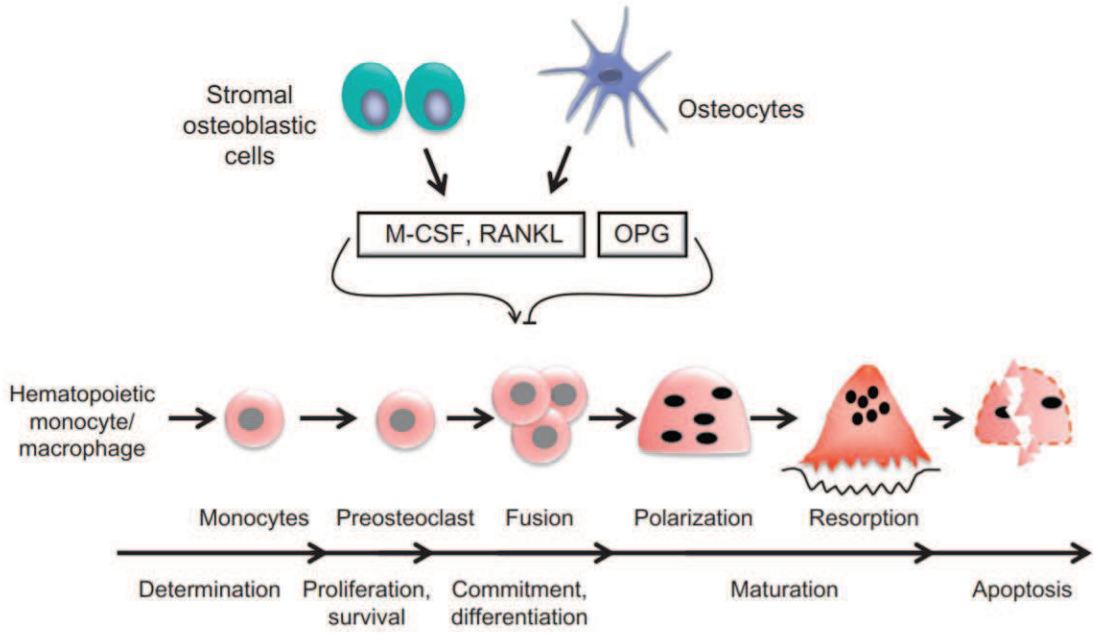

Figure 1:2 Osteoclast generation and fate.
Osteoclasts are derived from the HSC lineage. Mononuclear precursors are promoted to proliferate and fuse under the action of M-CSF and RANKL, both of which are secreted by osteoblasts and osteocytes. M-CSF leads to the proliferation of osteoclast precursors. RANKL then stimulates these precursors to differentiate and fuse into multinucleated osteoclasts. Conversely, OPG – also produced by osteoblasts and osteocytes – has an inhibitory effect on osteoclastogenesis by acting as a soluble decoy receptor for RANKL. Polarisation is the process of cytoskeleton change that facilitates adhesion to the bone surface and, subsequently, resorption. Figure used with permission from Elsevier (Bellido T et al, 2014).

1.8 Osteoclast regulatory cytokines

Given its importance in skeletal and calcium homeostasis, osteoclasts are regulated by a number of cell signalling modulators. The key cytokines that affect activity are discussed hereafter.

M-CSF is crucial for the development of osteoclasts. It binds to the colony stimulating factor 1 receptor (CSF1R) of osteoclast precursors to promote proliferation (Hodge JM et al, 2007) thus expanding the pool size (Jacquin C et al, 2006). The role of M-CSF in survival of osteoclasts is less well understood, however, with conflicting evidence present in the literature (Fuller K et al, 1993, Hodge JM et al, 2007). M-CSF also causes an increase in the production of RANKL from osteoclast precursors (Arai F et al, 1999). Importantly, M-CSF cannot promote the differentiation of precursors to osteoclasts by itself (Boyce BF and Xing L, 2008).

RANKL promotes the final differentiation to mature osteoclasts. It binds to the RANK receptor on the surface of macrophage/monocyte precursors, inducing

downstream intracellular signals that lead to commitment to the osteoclast lineage (Park JH et al, 2017). This is completed through the sequential expression of nuclear factor kappa B (NF-κB), c-Fos and nuclear factor of activated T cells 1 (NFATc1) (Yamashita T et al, 2007). The importance of RANKL has been demonstrated in mice models where deficiency leads to an absence of osteoclasts and high levels of macrophages (Kong YY et al, 1999). It is a member of the TNF family and, although highly expressed by in bone tissue, is also found in a variety of others including lymphoid, lung and mammary tissue (Takayanagi H, 2007). Secretion is mediated by either proteolytic cleavage – through MMP3 or ADAM - or alternative splicing (Boyce BF and Xing L 2008). Although the majority of RANKL production is facilitated through osteoblasts and stromal cells, T cell secretion in patients with inflammatory arthropathies can lead to the joint destruction seen in these conditions (Kearns AE et al, 2008, Boyce BF and Xing L, 2008). Given its involvement in both bone biology and immunity, it is a key factor in the subject of osteoimmunity (Kearns AE et al, 2008, Boyce BF and Xing L, 2008). Furthermore, RANK/RANKL have been implicated in the pathophysiology of several cancers (Renema N et al, 2016).

Closely linked with RANKL is osteoprotegerin (OPG). Also a member of the TNF family (TNFRSF-11B), this cytokine acts to downregulate osteoclast differentiation and function by acting as a soluble decoy receptor for RANKL (Yasuda H et al, 1998). It is expressed in a variety of tissues, including osteoblasts and stromal cells. In bone marrow, the effect of OPG is inhibited by 1,25-dihydroxycholecalciferol and dexamethasone (Yasuda H et al, 1998) and upregulated by transforming growth factor-ß (TGF-ß) (Murakami T et al, 1998). In mouse models where OPG is deficient, severe osteoporosis occurred (Mizuno A et al, 1998), highlighting the significance of this protein in osteoclast function. Interestingly, OPG has been found to be significantly increased during the differentiation of isolated osteoclast cultures. It has been proposed that OPG secretion by osteoclasts may play an auto-regulatory function by inducing apoptosis (Kang JH et al, 2014).

Other cytokines that have multiple roles in bone homeostasis include IL-1, IL-6 and TNF. Early evidence demonstrated all of these cytokines strongly enhance osteoclasts (Lorenzo JA et al, 1987). Both IL-1 and TNF consist of two separate peptides (α and ß) that have similar biological effects. IL-1 is the most potent

stimulator of bone resorption *in vitro* (Lorenzo JA et al, 1987) with direct (Jimi E et al, 1999) and indirect effects on osteoclasts through RANKL (Hofbauer LC et al, 1999) and prostaglandin production (Sato K et al, 1986). IL-6 is produced by osteoblasts and stromal cells, and its production can be increased by TNF and IL-1. It acts to increase resorption by promoting osteoclast precursors to differentiate into mature osteoclasts. *In vivo* analysis has shown TNF administration to raise calcium levels as a result of increased osteoclast formation and activity (Tashjian AH Jr et al, 1987). TNF also enhances the effects of IL-1 to stimulate osteoclasts. However, the effects from these cytokines on bone homeostasis are not restricted to osteoclasts. Recent evidence has demonstrated IL-1 (Lin FH et al, 2010), IL-6 (Franchimont N et al, 2005) and TNF (Glass GE et al, 2011, Gerstenfeld LC et al, 2003) also promote osteoblast differentiation of MSCs. This dual role is a result of dose dependent activity, with osteogenic effects occurring at lower doses (Glass GE et al, 2011, Gerstenfeld LC et al, 2003). This can be seen *in vivo* during fracture healing where pro-inflammatory cytokines migrate to the fracture site and promote local osteogenesis (Glass GE et al, 2011).

1.9 Osteoclast differentiation pathway

In the progression from precursor cell to osteoclast, signalling pathways involving the aforementioned cytokines are crucial. RANKL binds to RANK causing the recruitment of TNF receptor-associated factor (TRAF) proteins, namely 1 – 6 (Darnay BG et al, 1998). Of these, TRAF6 plays the most important role in osteoclast formation by activating several targets including NF-κB, c-Jun N-terminal kinase (JNK) and extracellular signal-regulated kinase (ERK) (Naito A et al, 1999, Kobayashi N et al, 2001, Wong BR et al, 1998). RANKL also strongly induces NFATc1 – via NF-κB and c-Fos – which is the master transcription factor for the terminal differentiation of osteoclasts (Novack DV et al, 2003, Kim JH and Kim N, 2016). The stimulation of NFATc1 is maintained as TRAF-6, NF-κB and c-Fos pathways create a positive autoregulation system. NFATc1 in turn stimulates TRAP, osteoclast-associated receptor (OSCAR) and cathepsin-K, which are responsible for the induction of other osteoclast transcription factors (Matsumoto M et al, 2004, Asagiri M et al, 2005, Kim K et al, 2005). Once fully differentiated osteoclasts can then undertake their role in bone resorption and remodelling (Seeman E and Delmas PD, 2006).

1.10 Osteoclast attachment

The structural appearance of osteoclasts varies depending on their functional state. Different states include moving, resting and absorbing (Jurdic P et al, 2006). The reason osteoclasts are induced to resorb specific sites is not well understood. A potential theory that has been proposed is that micro-fractures within the bone architecture resulting from mechanical loading apoptose osteocytes which in turn signal osteoclasts to migrate to that area (Noble BS et al, 2003). When activated, osteoclasts initiate a resorption cycle. This is a multistep pathway that requires attachment of the osteoclasts to the bone matrix. Attachment is facilitated through focal adhesions (Jurdic P et al, 2006). Adhesions are formed through the interaction between transmembrane cell receptors and surface ligands. OPN is a natural ligand for the vitronectin receptor in bone that accumulates along the bone surface to attract and bind osteoclasts (Reinholt FP et al, 1990).

Integrins are the key group of transmembrane cell receptor responsible for adhesion (Väänänen K, 2005). Osteoclasts express 3 integrin extracellular matrix receptors: αvβ3, α2β1 and αvβ1. In particular, avβ3 has been shown to be crucial to attachment, migration and the formation of the tight seal required for resorption (Väänänen HK and Horton M, 1995). Interruption of integrin binding results in inhibition of bone resorption (Crippes BA et al, 1994). Downstream products of the αvβ3 signalling pathway have also been investigated and shown to be of importance. Tyrosine kinase PYK-2 is phosphorylated by αvβ3 and controls osteoclast attachment. It localises with its attachment protein p130cas to the zone of contact between osteoclasts and bone matrix (Väänänen K, 2005). Blocking the action of PYK-2 in animal models led to osteopetrosis without reduction in osteoclast numbers, highlighting its role in attachment (Nakamura I et al, 2001).

Following attachment, the cell polarises. This enables alterations in the cell shape through changes in the actin cytoskeleton. At this stage, three F-actin and five vinculin distributions are formed (Väänänen HK and Horton M, 1995). Initially, these structures form podosomes. Podosomes are found in cells from a monocytic lineage, such as macrophages and osteoclasts, and are used to adhere and migrate to substrates (Linder S and Aepfelbacher M, 2003). Each podosome is composed of an F-actin cone containing activators of actin polymerisation such as such as

Wiskott-Aldrich Syndrome protein (WASp), Actin related protein 2/3 (Arp2/3), cortactin, and gelsolin (Jurdic P et al, 2006). Initially, they are organised in clusters that subsequently evolve into dynamic rings. With further cell maturation at around day seven, rings expand to the cell periphery to form longer lasting belts that are present in fully differentiated cells (Jurdic P et al, 2006).

Two distinct areas are formed where the osteoclast is in contact with the bone matrix - a sealing zone (SZ) and a ruffled border (Väänänen HK and Horton M, 1995). The sealing zone – adjacent to the ruffled border – provides the required tight attachment to the bone. It is composed of a large ring of actin as discussed above, around 4 µm wide (Jurdic P et al, 2006). However, the SZ is only formed when attached to mineralised matrix; it is not present during adhesion to glass during cell culture (Saltel F et al, 2004). On glass, podosomes arrange to form the aforementioned actin rings and belts, which are similar to the SZ but of a different density (Figure 1:3). The SZ is only observed when the cell is attached during resorption and disappears during migration (Takito J et al, 2018). The ruffled border is an expanded area of the membrane that serves as the exit site of protons and enzymes. The alteration in membrane structure allows for a greater surface area to be presented to the bone surface. In turn, this increases the quantity of secretions and resorbed particles that can pass via the ruffled border (Stenbeck G, 2002).

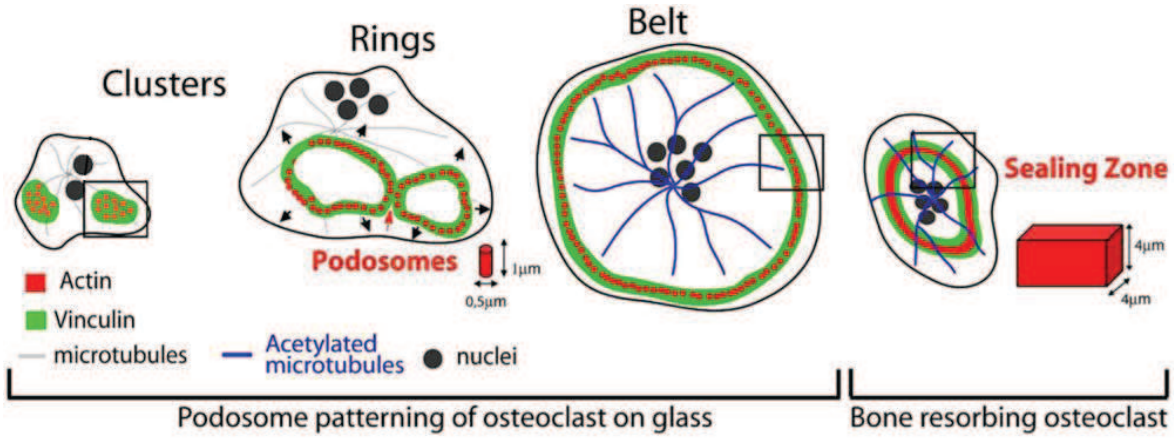

Figure 1:3 Podosome patterning and sealing zone.
Podosomes are initially organised into clusters. As osteoclast differentiation and maturation occurs, they subsequently alter to form rings and then belts. Belts are stabilised by acetylated microtubules. The sealing zone is only evident when osteoclasts are in contact with apatite crystals (e.g. on a bone surface) and measures approximately 4 x 4 µm, compared to the 0.5 x 1 µm podosomes found in rings and belts. The sealing zone is necessary for bone resorption to occur Figure used with permission from Elsevier (Jurdic P et al, 2006).

1.11 Bone resorption

Bone resorption involves dissolution of crystalline calcium phosphate or hydroxyapatite and degradation of fibrillar collagen in the extra-cellular resorption lacunae. This process is facilitated through proteolytic enzymes and requires energy, ion movements and intracellular replacement of materials (Väänänen K, 2005).

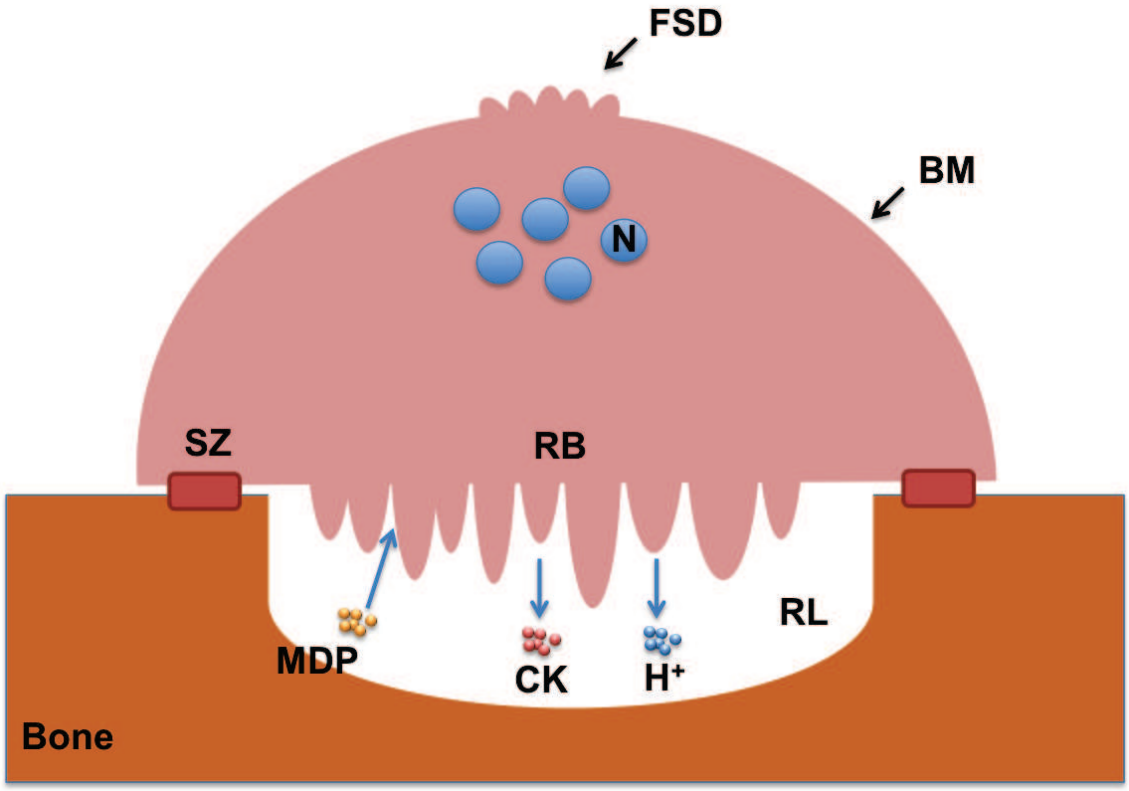

Figure 1:4 Osteoclast attachment and resorption.
Schematic representation of a resorbing osteoclast. Osteoclasts require the presence of the sealing zone to firmly attach to bone and initiate resorption. This feature is only present in mature osteoclasts. H^+ and cathepsin-K are secreted through the ruffled border, creating the acidic environment required to initiate breakdown of the bone matrix. Matrix degradation products are then secreted into the extracellular space at the functional secretory domain via transcytosis. Cytoplasmic ion equilibrium is maintained through ion and bicarbonate production at the basolateral membrane. FSD = functional secretory domain, BM = basolateral membrane, N = nucleus, RB = ruffled border, SZ = sealing zone, RL = resorption lacuna, H^+ = hydrogen ion, CK = cathepsin-K, MDP = matrix degradation particles.

Structurally, the ruffled border is the site of resorption. This occurs within the sealing zone, which provides the tight attachment required (Väänänen HK and Horton M, 1995). As bone matrix is primarily hydroxyapatite ($Ca_3(PO_4)2Ca(OH)_2$), an alkaline salt, dissolution requires protonation, with approximately 2 moles of H^+ for each mole of Ca^{2+}. Upon attachment, acidic vesicles fuse to the bone plasma membrane, releasing acid. This process is maintained via a vacuolar-type proton pump that transports H^+ from the cytoplasm (Blair HC et al, 1989). Chloride

channels are also present in the ruffled border to move chloride anions. Cytoplasmic ion equilibrium is maintained through ion and bicarbonate production at the basolateral membrane. Cathepsin-K is the main protease responsible for matrix degradation. In studies where this enzyme has been blocked, bone matrix contained a build-up of undigested collagen fibrils and thickening of trabeculae (Saftig P et al, 1998). Cathepsin-K is also thought to be responsible for the activation of TRAP; another key enzyme and important cytochemical marker of osteoclasts. In addition to bone dissolution, removal of breakdown products is required. Calcium, phosphate and collagen fragments are endocytosed and transcytosed through the cell before being secreted in to the extracellular fluid via a specialised region of the osteoclast – the functional secretory domain (Väänänen K, 2005, Nesbitt SA and Horton MA, 1997) (Figure 1:4).

1.12 Bone remodelling

Remodelling is a dynamic process whereby bone is removed by osteoclasts and laid down by osteoblasts (Langdahl B et al, 2016). This occurs continually throughout life, with the entire skeleton being replaced every 10 years. It relies upon a close interaction between osteoblasts and osteoclasts and requires a specific balance to maintain bone mass and quality. In cases where this balance is disturbed, disease states occur. For example, osteoporosis occurs when either osteoclasts are overactive or osteoblasts are underactive, leading to reduced bone density (Langdahl B et al, 2016).

The process begins with the activation phase. Changes in the bone microenvironment act as a trigger. These changes include micro-fracture, alterations in mechanical loading and factors such as TNF-α and IGF-1. As previously discussed, micro-fractures potentially stimulate remodelling by inducing osteocyte apoptosis which in turn signal osteoclasts to migrate to the area (Noble BS et al, 2003). Regardless, any of the above changes in the bone microenvironment lead to activation of lining cells. These are cells of an osteoblast lineage that cover non-remodelling surfaces and are involved in the propagation of the activation signal that initiates resorption. The lining cells secrete RANKL that in turn interacts with the RANK receptor of pre-osteoclasts, leading to fusion and activation as detailed above (Miller SC et al, 1989).

Following activation, resorption occurs. This is as described above where osteoclasts polarise, adhere to bone and begin dissolution. Following this, bone lining cells then enter the resorption pits. The lineage of these cells is uncertain, with studies suggesting both monocyte (Tran Van P et al, 1982) and osteoblast lineage (Everts V et al, 2002). It is equally possible that a combination of both cell types are involved. They remove any collagen matrix remnants in order to prepare the bone surface for osteoblast-mediated formation. The cells then produce osteopontin which is incorporated into the mineralised tissue (Takahashi F et al, 2004). Finally, coupling signals are produced to facilitate the final phase of remodelling – formation (Raggatt LJ and Partridge NC, 2010).

The process of resorption leads to the production of growth factors, including IGF-1, BMP and TGF-ß (Tang Y et al, 2009). These in turn assist in the recruitment of osteoblasts to the resorbed area. If osteoclasts are defective in their resorption, leading to these growth factors not being released, osteoblasts are still recruited. It is likely this is a result of coupling factors being produced by osteoclasts (Martin TJ and Sims NA, 2005). These factors rely on both direct contact between cells and soluble signals to stimulate osteoblastogenesis. Osteoblasts then produce initially uncalcified matrix (osteoid) made primarily of type 1 collagen as well as non-collagenous proteins. Finally, hydroxylapatite is incorporated to mineralise the matrix which completes the resorption cycle (Raggatt LJ and Partridge NC, 2010).

1.13 Bionanotechnology

Advances in technology have frequently produced breakthroughs in science and medicine. Nanotechnology represents one such area. This is generally defined by technologies that work with dimensions of 1 - 100 nm (nm = 10^{-9} m) (Kulkarni RP, 2007). It has been subject to intensive development, with a national initiative to promote this research in the United States since the 1990's. Through their National Nanotechnology Initiative (NNI), the US has spent $19.4 billion between 2000 – 2014 (Sargent JF, 2014). Consequently, nanotechnology has found applications is a variety of fields from physics to biology (i.e. bionanotechnology) (Kulkarni RP, 2007).

The origins of bionanotechnology can be considered to trace back to the identification of DNA molecular structure in 1953. This and subsequent research led to an increased understanding of the reactions which drive protein production from DNA (Alberts B et al, 2002). Given the majority of these reactions occur on the nanoscale it was an intuitive progression to develop technologies that manipulate cell function on this level. At present, research has focussed on synthetic nanomaterials and nanoparticles as well as the investigation of nanostructures such as pores. It is hoped these areas will facilitate advancements in diagnostics, treatments and tissue regeneration (Etheridge ML et al, 2013).

Currently, the role of bionanotechnology in healthcare has been limited. An exception to this is cancer research where new diagnostic methods and treatments have been more heavily investigated. The ultimate aim for many of these studies has been the ability to identify cancerous cells at their earliest stage and precisely target them to maximise effectiveness and minimise side effects (Kulkarni RP, 2007). Given the rapid expanse in research, it is likely that the range of medical applications for nanotechnology will increase.

1.14 Tissue engineering and regenerative medicine

Tissue engineering and regenerative medicine (TERM) refers to a broad field of investigation ranging from the molecular level to whole organ systems within the body. There is considerable overlap between tissue engineering and regenerative medicine, although the later often implies the use of stem cells as the source (Berthiaume F et al, 2011). The ultimate goal of TERM is to enhance our understanding and management of degenerative and disease states affecting the body. This can be applied to humans either directly, for example through the implantation of graft tissues, or indirectly via the testing of new drug therapies and precision medicine on engineered tissues (Wobma H and Vunjak-Novakovic G, 2016).

The first engineered tissue was skin. Epidermis was grown from biopsies harvested from patients and co-cultured with mouse mesenchymal cells (Green H et al, 1979). This allowed the production of sheets of tissue that could be applied to areas of significant skin loss, such as following burns. These and subsequent studies effectively introduced the basic principles of tissue engineering. Organs

and tissues that have been targeted have typically been those prone to injury or degeneration, or those with limited regenerative potential. Examples include cornea, neural tissue, pancreas, cartilage and kidney (Shafiee A and Atala A, 2017). Supplying adequate cells or tissue to fulfil the required function is clearly important. Stem cells have therefore played a central role in this field given their potential for high rates of proliferation and pluripotency (Berthiaume F et al, 2011).

Harvesting the correct cell type represents one part of the solution. Equally important is that of the cell environment, both with regard to the chemical and physical aspects. These factors are important for cell stimulation, function and survival (Engler AJ et al, 2006). For example, in the production of engineered liver tissue, cells require low fluid sheer stresses (Park J et al, 2005) and the addition of growth factors such as TGF-α and hepatocyte growth factor (Nagy P et al, 1996). The addition of scaffolds represents a further addition to the cell environmental that can enhance growth. Cell scaffolds allow for cell attachment and migration and offer a form of mechanical stability that is often found in the native tissue. They can either be synthetic (for example poly(ε-caprolactone) (Dong L et al, 2017)) or natural (for example collagen). Given that collagen is such a crucial component of bone, it has significant potential for use as a scaffold in the culturing cells to produce bone graft (Nguyen BB et al, 2017).

With advances in technology across a range of fields, such as bionanotechnology, further developments in TERM have occurred. These include the production of precision-engineered surfaces that have embossed nanoscale features which promote osteogenesis (Dalby MJ et al, 2014) and altering matrix stiffness to guide cell fate (Engler AJ et al, 2006). Such studies have further cemented the link between the cell's environment and its ultimate fate. This has led to the investigation of other parameters that can be altered to manipulate cell differentiation and proliferation.

1.15 Bone tissue engineering

Bone represents the second most commonly transplanted tissue after blood (Wang W and Yeung KWK, 2017). It is required in a range of surgical procedures, across specialities including orthopaedic and maxillofacial surgery. Generally, bone graft

is utilised to assist in the management of healing defects, such as non-unions, where the bone has failed to heal properly following trauma (Delloye C et al, 2007). Within the United States, $2.5 billion is spent annually on the management of bone defects (Amini AR et al, 2013). With the ageing population, it is likely this requirement will rise (Giannoudis PV et al, 2011) given that osteoporotic fractures are common in this demographic and do not heal as readily as those sustained in normal bone (Tarantino U et al, 2011).

At present, the most common graft sources are autograft (i.e. from the same individual) and allograft (i.e. from an individual genetically different to the recipient) (Wang W and Yeung KWK, 2017). Autograft represents the gold standard as they are not associated with immune reactions and contain osteogenic components, including MSCs and growth factors, as well as the required bony scaffold for osteoconduction (Delloye C et al, 2007). They have several limitations, however. Firstly, harvesting of the graft requires a second procedure at a different site, typically the iliac crest. This can be a source of significant morbidity for the patient. Complications that have been documented include significant pain, neurovascular injury, pelvic fracture, herniation of abdominal contents, ureter injury and infection (St John TA et al, 2003, Ebraheim NA et al, 2001). Furthermore, the volume of graft that can be harvested may be insufficient to treat the defect (Amini AR et al, 2013). Finally, they have high direct and indirect costs (St John TA et al, 2003). Allograft has the advantage of being available in a range of forms, such as chips and whole bone segments, however comes with a greater risk of adverse immune reactions and infection transmission (Wang W and Yeung KWK, 2017). Furthermore, given that the graft requires irradiation or freeze-drying prior to implantation (Delloye C et al, 2007), most of the osteoinductive factors are lost, ultimately reducing the effectiveness (Sohn HS and Oh JK, 2019). In the case of both auto- and allograft there are mixed opinions within the literature as to whether there is sufficient supply. There is certainly a perception amongst surgeons that there are insufficient stocks of banked bone graft (Greenwald AS et al, 2001), however a relatively recent paper has reported that, in the United Kingdom at least, this may not be the case (Lomas R et al, 2013). Regardless, taken alongside the aforementioned disadvantages, alternative sources of bone graft have been sought.

The production of tissue engineered bone graft represents an attractive option to the above problem. As such, this has been an area of scientific interest for a number of decades (Amini AR et al, 2013). The ultimate aim of bone tissue engineering is the production of readily available 'off the shelf' bone that avoids the issues of donor site morbidity, immune reactions and limited osteoinduction. Important factors in the fulfilment of this goal include 1) a scaffold to support cell growth, similar to bone extracellular matrix, 2) osteogenic cells, 3) morphogenic signals to influence the route of cell differentiation and growth, and 4) nutrient supply and waste removal (Amini AR et al, 2013). At present, the production of small volumes of tissue within the laboratory setting is possible, however larger production for clinical use represents a greater challenge. Bioreactors represent an option to potentially combat this shortcoming.

1.16 Mechanotransduction

Mechanical forces instigate changes to biological systems across a range of scales, ranging from a cellular level – for example in actin-myosin complexes – to the entire body, as with gravity. Such forces have a significant effect on the formation and maintenance of tissues (He L and Montell D, 2012). Equally, any deficiency can lead to disease states, such as osteoporosis (Hoffman BD et al, 2011). The effect of force on bone and remodelling has been long established, as set out in the 19th Century in Wolff's law (Frost HM, 1994). At the time, however, the mechanism through which organisms respond and adapt to mechanical loads was not known (Frost HM, 2004).

At a cellular level, mechanical forces can have either a direct or indirect effect on cells. Indirect mechanisms require biochemical stimulation, whereas direct involve mechanically stimulating the nucleus. In most scenarios, there is likely to be elements of both direct and indirect mechanisms (Janmey PA and Miller RT, 2011). The process through which cells respond to mechanical stimulation is called mechanotransduction (Wang N et al, 2009).

Integrins are a group of adhesive transmembrane receptors that link the extracellular matrix (ECM) to the internal cytoskeleton of the cell (Goldmann WH, 2012). They transmit forces from the ECM to the actin cytoskeleton and vice versa. The ability to apply force from the cytoskeleton to the ECM is crucial for cell

migration and adherence. In the process of attaching to the cytoskeleton, integrins produce a 2 pN increase in adhesion strength between the ECM and the cytoskeleton (Jiang G et al, 2003). These adhesions produced between the ECM and integrins creates micro-projections, termed lamellipodia and filopodia, which progress to form focal complexes (FC) (Katsumi A et al, 2004). The development from adhesion to FC requires the recruitment of vinculin, which regulates migration and adhesion. Further maturation of FC can occur, leading to the production of larger focal adhesions (FA) through Rho-dependent mechanisms (Galbraith CG et al, 2002). FC are typically 1 μm in size, compared to >5 μm for super-mature FA (Coyer SR et al, 2012). FA consist of three layers: 1) signalling layer, composed of integrins, focal adhesion kinase (FAK) and paxillin which initiate biochemical signalling, 2) a force transduction layer containing talin and vinculin, and 3) an actin regulatory layer comprised of vasodilator-stimulated phosphoprotein (VASP), zyxin and α-actinin (Kanchanawong P et al, 2010). These layers which make up the FA link actin fibres to the main contractile stress fibres of the cell, facilitating the transfer of force from a nanoscale to microscale signal transducer (Dalby MJ et al, 2014).

Ultimately, the signals passed through the cytoskeleton interact with the nucleus, leading to alterations in gene transcription (Ostlund C et al, 2009). Specifically, tension changes produce signalling alterations in the RhoA kinase pathway (ROCK), FAK and ERK (Xiao G et al, 2002, Nikukar H et al, 2013). These cascades are involved in the regulation of transcription factors, including runt-related transcription factor 2 (RUNX2), that alter expression of bone-specific genes such as OCN (Xiao G et al, 2002, Nikukar H et al, 2013).

The ability to alter the production of FA has been a focus of tissue engineering research as this has been shown to alter MSC phenotype and differentiation (Dalby MJ et al, 2014). Specifically, smaller adhesions result in adipogenesis (McBeath R et al, 2004), whereas larger adhesions promote osteogenesis (Kilian KA et al, 2010a). This is thought to be in part due to the geometry of osteoblasts, which are typically large and well spread (Nikukar H et al, 2013). Such geometric features require a highly contracted cytoskeleton in order to support the cell structure. As such, larger FA are required in order to facilitate the increased tension as dictated by their force-balance relationship (Nikukar H et al, 2013).

In addition to FA, ion channels play an important role in the transduction of mechanical stimuli. Piezo1 and piezo2 induce mechanically activated cationic currents in cells (Coste B et al, 2012). When exposed to strain, they facilitate Ca^{2+} influx into cells (Lee W et al, 2014). Similarly, members of the transient receptor potential (TRP) cation channel family are activated by mechanical stimulation (Tsimbouri PM et al, 2017b). Following activation, they produce adaptations in the cell cytoskeleton (Kuipers AJ et al, 2012). TRPV1 has been demonstrated to be the most mechanosensitive protein to nanostimulation. It has downstream effects on protein kinase C (PKC) as part of the TRPV1-PKC-Wnt/ß-catenin axis (Tsimbouri PM et al, 2017b). ß-catenin directly upregulates RUNX2 to stimulate bone formation (Gaur T et al, 2005). Another member of the TRP group, TRPV4, regulates Ca^{2+} influx in osteoclasts, mediating their differentiation and survival. It is not clear what the *in vivo* stimuli for TRPV4 activation in osteoclasts are, however (Masuyama R et al, 2008).

1.17 Bioreactors

The main function of bioreactors is to accelerate tissue growth (Partap S et al, 2010). By definition, they employ mechanical forces to influence biological processes. By stimulating cells to differentiate and mature according to a predetermined objective this allows optimisation of the tissue prior to implantation (Partap S et al, 2010). As the cells are cultured in a controlled and optimised environment this assists in up-scaling tissue production. Several designs have been examined within the literature. This includes spinner flasks, rotating wall bioreactors and perfusion bioreactors.

In the spinner flask, a magnetic stirrer attached to the bottom of the flask produces convective forces. Cells are suspended from needles within a scaffold. The turbulent currents that are produced improve media flow around the cells (Partap S et al, 2010). Studies have demonstrated this results in increased osteogenic cell proliferation and gene expression (Goldstein AS et al, 2001, Partap S et al, 2010, Korin N et al, 2009). This bioreactor also has the advantage of being relatively inexpensive. However, it can lead to uneven cell distribution within the scaffold, with clumping of cells at the periphery (Partap S et al, 2010). Furthermore, the unequal distribution of convective forces within the flask (Bjerre L et al, 2011) can lead to disparities in the osteogenic effect.

Rotating wall bioreactors were initially designed by NASA to protect cell cultures from the extreme forces of shuttle take-off (Partap S et al, 2010). In this bioreactor, the walls rotate to produce an upward drag force and corresponding downward gravitations force, which balance the suspended cell scaffold in the centre of the media (Partap S et al, 2010). The low degree of sheer and high nutrient flow/waste removal aids cell culture. The effect of this bioreactor on osteogenesis is not clear, however, with both positive (Song K et al, 2013, Pollack SR et al, 2000) and negative (Goldstein AS et al, 2001, Sikavitsas VI et al, 2002) findings being described. This may be partly related to limited nutrient transfer to the centre of the scaffold and the osteogenic effect being focussed on the periphery (Sikavitsas VI et al, 2002).

Flow perfusion bioreactors aim to reduce the issues with uneven cell distribution noted in the above two bioreactors. In this system media is pumped by a peristaltic roller through the cell scaffold which is held in a chamber that directs fluid flow (Partap S et al, 2010). Histological examination of seeded scaffolds exposed to flow perfusion demonstrates an equal distribution of cells. The flow rate and character (e.g. continuous, cyclic) can be varied, both of which have been shown to be important factors in upregulating osteogenesis (Li P et al, 2012, Wittkowske C et al, 2016). Limitations to perfusion bioreactors include their complex setup and the inability to upscale to larger cell scaffolds for clinical use (Gardel LS et al, 2014).

The aforementioned bioreactors have all utilised external forces in an attempt to provide a positive influence on osteogenesis. Although each has demonstrated positive results, there have been significant drawbacks to each that ultimately limit their effectiveness in delivering the goal of bone graft production. These technologies highlight the need for a simpler form of bioreactor that can be up-scaled for clinical use.

1.18 Nanokick bioreactor

Collaboration between the University of Glasgow and the University of Strathclyde has led to the development of a new bone bioreactor, called the Nanokick (Figure 1:5). This bioreactor aims to stimulate osteogenesis by transferring nanoscale vibrations to cell cultures. This is achieved primarily through the reverse piezo

effect. The reverse piezo effect is the generation of mechanical force from electrical energy, with the direct piezo effect being the opposite reaction (Tsimbouri PM et al, 2017b). There are several materials which exhibit the piezo effect, including bone (Cerrolaza M et al, 2017a).

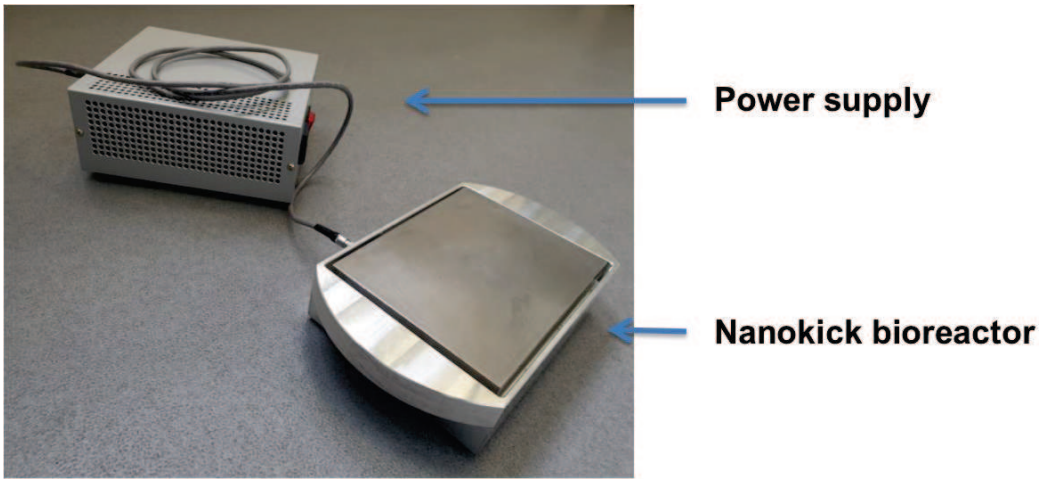

Figure 1:5 The Nanokick bioreactor.
The third generation Nanokick bioreactor and associated power supply.

In the Nanokick, ceramic piezo devices are used to achieve high frequency, low amplitude displacements. These vertical displacements are typically around 30-40 nm at 1000 Hz. This frequency was chosen as it was found to be optimal for osteogenesis (Nikukar H et al, 2013). Furthermore, the optimal piezoelectric frequency for bone is in the kilohertz range (Håkansson B et al, 1994). The amplitude of 30-40 nm was utilised as recent studies demonstrated this promoted osteoblastogenesis in MSCs (Nikukar H et al, 2013, Pemberton GD et al, 2015). Equally, nanotopography research has demonstrated features at this scale are osteogenic (Dalby MJ et al, 2014). The piezo devices – of which there are 13 per bioreactor – are attached to a base plate composed of aluminium bonded with magnetic stainless steel (Figure 1:6). By coupling standard cultureware with magnets, this allows for firm attachment to the Nanokick bioreactor and thus ensures transfer of the nanoscale vibrations. Underneath the piezo devices is a metal baseplate to provide a large mass, ensuring displacement is upwards (Nikukar H et al, 2013). This setup has several advantages. Firstly, magnetically attaching plates to the bioreactor facilitates easy plate removal for cell feeding. Also, by using standard plates that rely of familiar culture techniques this reduces consumable costs and technique complexity. In turn, this limits issues with sterility that come with complex set-ups and autoclaving reusable components.

Finally, the bioreactor can be up-scaled based on its modular design to allow for greater throughput.

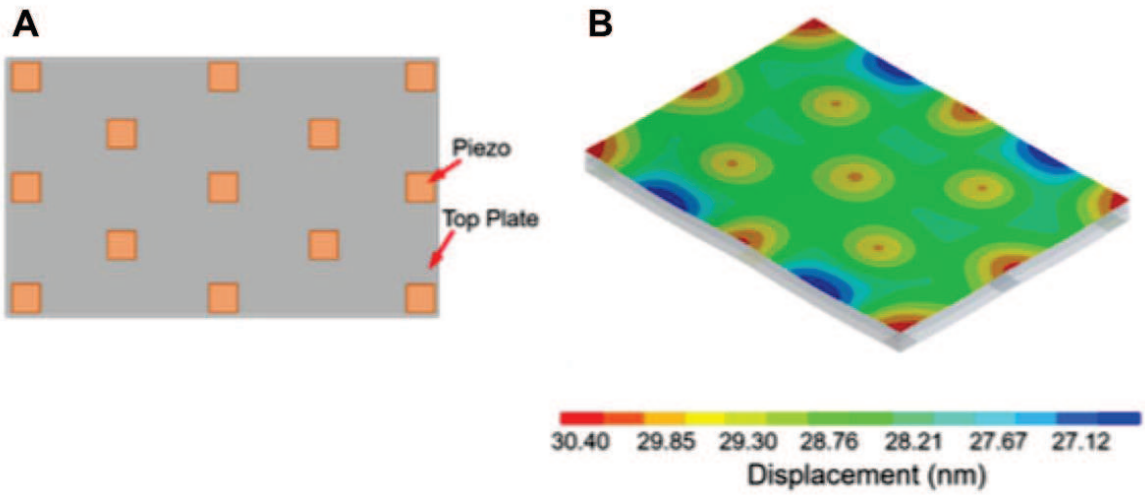

Figure 1:6 Piezo layout and FEA analysis.
A – diagram of the 13 piezo arrangement. This layout was found to produce the most consistent displacements across the top plate. Note a checkerboard layout rather than aligned rows was utilised, as that latter can lead to areas of reduced displacement. B – Finite element analysis performed with ANSYS workbench demonstrating predicted displacements with 13 piezo arrangement. Presented with permission of the authors (Campsie P et al, 2019).

Recent publications have demonstrated the efficacy of the Nanokick bioreactor in stimulating osteogenesis (Pemberton GD et al, 2015). Pemberton *et al* combined nanoscale vibration and nanotopography to assess their effect on osteogenesis. MSCs were vibrated at 1000 – 5000 Hz with 16 – 30 nm vertical displacements. They noted increases in osteogenic genes, including OCN, OPN and BMP-2. Protein analysis suggested nanoscale vibration was more stimulatory than nanotopography alone. They noted little benefit in frequencies above 1000 Hz, whilst going below 500 Hz did not stimulate osteogenesis (Pemberton GD et al, 2015).

Nikukar *et al* exposed MSCs to nanoscale vibration between 25 – 1000 Hz. They demonstrated increased cell spreading, increased proliferation and increased F-actin stress fibres at 1000 Hz (Nikukar H et al, 2016). In a separate study (Nikukar H et al, 2013) the authors illustrated that 500 Hz leads to changes in gene expression but did not alter BMP-2 and RUNX2 suggesting this frequency was not sufficient to promote osteogenesis. Conversely, 1000 Hz produced significant changes in BMP-2 and RUNX2. This frequency also led to greater cell spreading and larger FA, indicative of increased intracellular tension. Furthermore, the ROCK pathway was shown to be stimulated. Stimulation below 500 Hz did not produce any significant change (Nikukar H et al, 2013).

Tsimbouri *et al* examined the effect of nanovibrations in 3D collagen gel scaffolds. These gels were found to transmit the vibrations produced to the contained cells. They demonstrated that the bone marrow stromal cells exhibited an upregulation of osteogenic markers, including osterix, alkaline phosphatase and OPN. It was noted that inhibition of the ROCK pathway downregulated gene expression, but this was to a lesser extent than in 2D models. Further investigation into the underlying mechanism revealed that the TRVP1-PKC-Wnt/ß-catenin axis played a significant role in osteogenesis. This suggests mechanosensitive ion channels in addition to adhesion and cytoskeleton tension are important in 3D models (Tsimbouri PM et al, 2017b).

1.19 Hypothesis

It has been established that mechanical forces represent a crucial factor in influencing cell differentiation and survival. Multiple studies have highlighted that increasing intracellular tension through a variety of means can promote osteogenesis in MSCs. It has also been demonstrated that osteoblasts and osteoclasts are both crucial for the process of normal bone remodelling, with imbalances in the function of either leading to disease states. Furthermore, there exists significant co-dependence between these two cell types, with significant overlap in regulatory cytokines and growth factors. Investigation into the effect of nanoscale vibration on osteoclastogenesis is therefore required. It is hypothesised that nanoscale vibration will promote osteogenesis without upregulating osteoclastogenesis.

1.20 Aims

The aim of this study is to examine the effect of exposing osteoclasts to nanoscale vibration through use of the Nanokick bioreactor. This will be undertaken in two culture models. Firstly, a culture of macrophages and osteoclasts, and secondly a co-culture of both osteoblasts and osteoclasts. Given the need for tissue engineered bone graft, the aim will be to stimulate osteogenesis without upregulating osteoclastogenesis.

Chapter 2 Materials and methods

2.1 Introduction

In this section, the methods involved in establishing cell cultures, bioreactor calibration and experimental analyses will be discussed. As aforementioned, one benefit of the Nanokick bioreactor is the ability to use standard cell culture techniques. As such, the details below represent the standard tissue culture principles employed by most laboratories. Sterile conditions were maintained throughout through the use of lab coats, gloves and class II biological safety cabinets cleaned with 70% ethanol before each use. The Nanokick bioreactors were kept in incubators at 37°C and 5% CO_2 for the duration of each experiment. Removal was only performed to carry out calibration. The cable connecting the bioreactor to the external power supply was passed outside the incubator through the door seal to avoid disturbing the conditions. 2D cell cultures refers to the standard seeding of cells directly on to culture plates. 3D cultures involve mixing cells into a type 1 collagen gel prior to pipetting on to the plate. For experiments with multiple donors, each donor was seeded separately and analysed independently prior to pooling of results for statistical analysis.

2.2 2D cell culture technique

2.2.1 CD14+ Isolation

Buffy coats – the fraction of blood containing white blood cells and platelets – were received from the Scottish National Blood Transfusion Service. These were diluted 1:1 with phosphate buffered saline (1 x PBS) and mixed by inversion. In a 15 ml conical centrifuge tube 10 ml of buffy coat/PBS were overlaid on 4 ml of Ficoll-Paque (Sigma-Aldrich, Dorset, UK) at room temperature and centrifuged at 400 x gravity (*g*) for 30 minutes. After centrifugation, the monocyte layer was aspirated using a Pasteur pipette and transferred to a 50 ml conical centrifuge tube, before resuspending the cells with addition of 1 x PBS to 50 ml total volume. The cells were washed twice with PBS and centrifuged at 200 x *g* for 10 minutes for platelet exclusion. The monocyte pellet was resuspended with 10 ml specific cell separation media (2% foetal bovine serum (FBS) and 1 mM EDTA in 1 x PBS) and mixed. A cell count was then performed with a 10 x dilution (10 µl cells added

to 80 µl 1 x PBS and 10 µl trypan blue) using a haemocytometer. Cells were further centrifuged at 350 x *g* for 5 minutes and resuspended to obtain 1 x 10^8 cells/ml. The suspension was transferred to a 6 ml round bottomed polystyrene tube. Magnetic selection was performed using EasySep Human CD14 positive selection kit (Stemcell Technologies, Cambridge, UK). 100 µl/ml of CD14 positive selection cocktail was added and incubated at room temperature for 15 minutes. Magnetic nanoparticles were vortexed and 50 µl/ml added before incubating at room temperature for 10 minutes. The suspension was made up to 2.5 ml with the addition of cell separation buffer and the tube placed in a specialised magnet for 5 minutes. The magnet was then inverted to pour off the negative fraction. The tube was removed from the magnet and a further 2.5 ml cell separation buffer added prior to placing back in the magnet for a further 5 minutes. This process was repeated a further two times. The cells were finally re-suspended at 1 x 10^6 cells/ml in alpha minimum essential media (α-MEM) supplemented with 10% FBS, 0.02 mM L-glutamine, 10 U/ml Penicillin, and 0.1 µg/ml Streptomycin. This cell concentration was chosen based on publications relating to osteoclast culture from monocytes (Toyosaki-Maeda T et al, 2001) and work carried out by other researchers in the department who found this to be optimal for osteoclast differentiation.

2.2.2 2D CD14+ culture

Following suspension at 1 x 10^6 cells/ml, 25 ng/ml of recombinant human M-CSF (Peprotech, London, UK) was added. Cells were plated in 24 well plates and incubated overnight at 37°C and 5% CO_2. After approximately 18 hours incubation 25 ng/ml of human RANKL (Peprotech, London, UK) was added to a proportion of the wells. These concentrations of M-CSF and RANKL were chosen based on work carried out by other researchers in the department. They demonstrated that 25 ng/ml was optimal for osteoclast growth. This value is in keeping with other studies in the literature (Marino S et al, 2014). Those wells with M-CSF and no RANKL were used as a negative control of osteoclastogenesis. Medium was refreshed on days 4 and 7 if required.

2.2.3 MSC/BMHC isolation

Human bone marrow was aspirated from patients undergoing elective hip and knee arthroplasty and stored for transfer (1 x PBS, 0.53 mM EDTA, and antibiotics (6.74 U/ml Penicillin-Streptomycin, 0.2 µg/ml Fungizone)). The bone marrow aspirate was diluted with 10 ml modified Dulbecco's Modified Eagle Medium (mDMEM) (DMEM (D5671), 10% FBS, 100 mM sodium pyruvate, 200 mM L-glutamine (Invitrogen, Paisley, UK), and antibiotics). This was then centrifuged at 350 x *g* for 10 minutes, repeated twice. The cell pellets were re-suspended in mDMEM and overlaid on a Ficoll-Paque gradient. This was then centrifuged at 450 x *g* for 45 minutes (with no speed brake) and the subsequent mononuclear interface layer aspirated and resuspended in mDMEM. The cells were washed a further three times and plated at a density of 1 x 10^6 in a 75 cm^2 vented cell culture flask and incubated at 37°C with 5% humidified CO_2.

2.2.4 2D MSC/BMHC co-culture

At day 3 non-adherent cells were removed and cultured separately at a density of 1 x 10^6 in a 75 cm^2 vented flask and incubated at 37°C with 5% humidified CO_2, with three times weekly media change. This non-adherent fraction contained mainly bone marrow haematopoietic cells (BMHC), macrophages and osteoclast precursors. The remaining adherent cells were assumed to be MSCs, osteoprogenitors, osteoblasts and osteocytes and were cultured for a further 7 - 10 days until an approximately 80% confluent layer was obtained. The adherent cells were then detached with 0.05% trypsin/0.53 mM EDTA, centrifuged and resuspended in mDMEM to a concentration of 3 x 10^4 cells/ml. 1 ml of cell suspension/well was pipetted onto a 24 well plate. The media was replaced on day 3. At day 7, 1 ml of BMHC suspension/well was added at a concentration of 1.2 x 10^5/ml. These cell concentrations were chosen based on published work on the co-culture technique (Young PS et al, 2015). This co-culture was maintained with media changes three times a week.

2.3 3D cell culture technique

2.3.1 3D CD14+ culture

CD14+ cells were isolated as per the 2D technique laid out above. They were then centrifuged at 400 x *g* for 5 minutes to produce a cell pellet. The cells were then resuspended in 10% FBS and 10 x DMEM (Sigma-Aldrich, Dorset, UK). The collagen gel was then prepared, with the total volume required to produce a concentration of 1 x 10^6 cells/ml. This stage of the experiment was performed on ice to avoid the gel setting early. Sodium hydroxide (NaOH) was combined with rat tail collagen (Sigma-Aldrich, Dorset, UK). The resuspended cells were then added to the NaOH/collagen mix. 1 ml of gel/cell suspension was then pipetted onto each well of a 24 well plate. Plates were then placed in an incubator (37°C and 5% CO_2) for 30 minutes to allow the gels to set. 1 ml of α-MEM (supplemented with 10% FBS, 0.02 mM L-glutamine, 10 U/ml Penicillin, and 0.1 µg/ml Streptomycin) containing 25 µl/ml M-CSF was then added on top of the gels. After 18 hours RANKL, at a concentration of 25 µl/ml, was added to a proportion of the wells. Those wells with M-CSF and no RANKL were used as a negative control of osteoclastogenesis. Media was replaced on days 4 and 7 as required.

2.3.2 3D co-culture

Human bone marrow was processed as described in for 2D above. At day 3, non-adherent cells were removed and cultured separately. Both adherent and non-adherent flasks were cultured until a confluent layer was achieved. In the 2D model, adherent cells were plated first, with non-adherent cells being added after 7 – 10 days. Given it would not be possible to add additional cells once the gel had set, cells from both flasks were combined prior to combining with the gel. The adherent cells concentration was 3 x 10^4 cells/ml and the non-adherent concentration 1.2 x 10^5 cells/ml as per the 2D model. Cells were detached with 0.05% trypsin and counted. They were then centrifuged at 400 x *g* for 5 minutes to produce a cell pellet. The cells were then resuspended in 10% FBS and 10 x DMEM before adding to the NaOH/collagen mix. Further NaOH was added drop-wise while agitating the mix until the colour changed from yellow to pink, indicating the correct pH had been achieved. 1 ml of gel/cell suspension was then pipetted onto each well of a 24 well plate. Plates were then placed in an incubator

(37°C and 5% CO_2) for 30 minutes to allow the gels to set. 1 ml of mDMEM was subsequently added on top of the gels (Figure 2:1) and replaced three times per week.

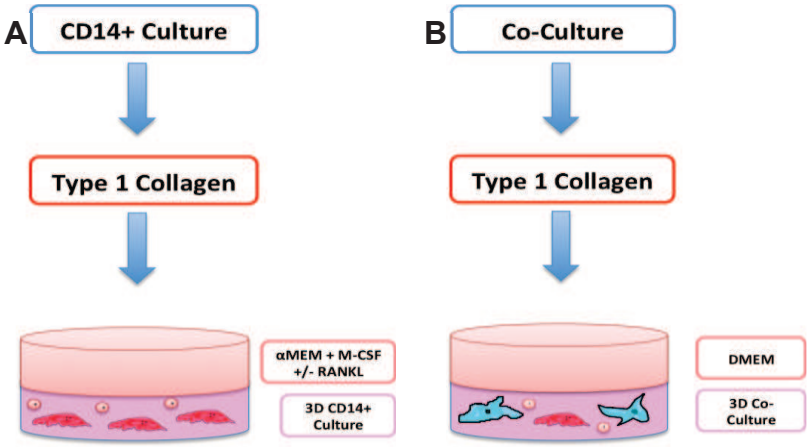

Figure 2:1 3D culture technique.
Schematic representation of 3D culture technique for both cell types. Cells were isolated for each of the CD14+ and co-culture as detailed in the 2D technique. Cells were then mixed into a type 1 collagen gel. The gels containing cells were seeded on to 24 well plates and left to settle for 30 minutes. Following this, media +/- growth factors were pipetted on top of the gels. Figure A represents the CD14+ culture, where M-CSF +/- RANKL was included in the media. Figure B illustrates the co-culture.

2.4 Vibration production and measurement

Following cell isolation and plating, samples were splint into a nanoscale vibration ("nanokick") and control group. For those in the nanokick group, self-adhesive magnetic sheets were applied to the base of the plate before cell seeding, ensuring all wells were covered. This allowed for coupling with the Nanokick bioreactor. In this study, the third generation bioreactor was utilised (Tsimbouri PM et al, 2017a). This differed from previous incarnations in both appearance and ease of use. In addition to a slimmer profile, ergonomic handles were added to the sides of the bioreactor, making lifting in and out of incubators by the user easier. Vibration production also no longer required a multistep process with manual input of frequency and amplitude into an amplifier. Instead, the bioreactor is connected to an amplifier with one switch that, when on, is programmed to deliver 30-40 nm vertical displacements at 1000 Hz.

To ensure accurate and reproducible vibration delivery, the bioreactors are calibrated at regular intervals. This is performed using laser interferometry, which is used in a range of other scientific fields, including gravitational wave astronomy

(Abbott BD *et al*, 2009). These devices are highly sensitive, and can detect displacements in the order of 10^{-20} m. The device used in this study was the Model ST-S 120, (SIOS Meßtechnik GmbH, Ilmenau, Germany), which can detect displacements of 0.1 nm (Figure 2:2). A helium-neon laser is directed vertically towards the culture plates, which are in turn reflected back allowing detecting of vertical displacement changes. Ensuring correct alignment of the reflected beam is achieved by passing the signal through an oscilloscope and obtaining a ring-shaped trace. The signal is then passed to a data processing unit, which can select the desired frequency (i.e. 1000 Hz) and plot the corresponding amplitude. Each well in a 24 well plate was measured three times and mean displacements for each well calculated. The principles of laser interferometry are presented in Figure 2:3.

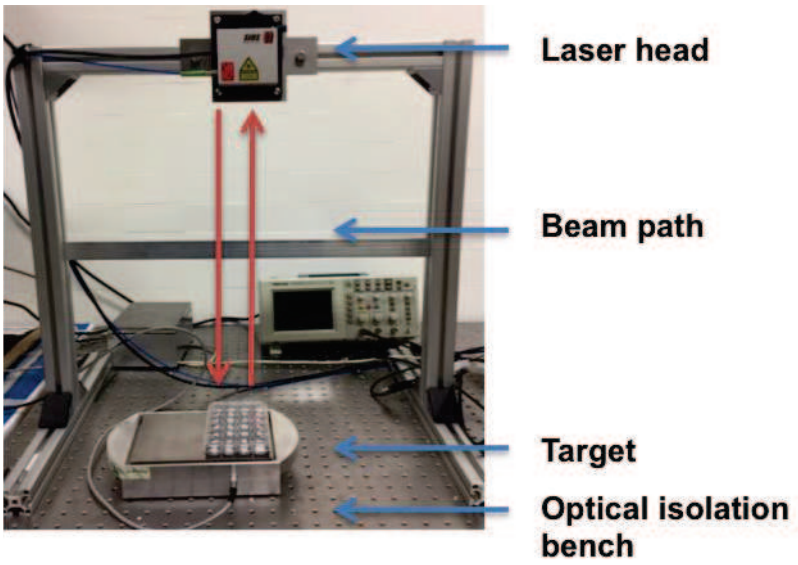

Figure 2:2 Laser interferometry set-up.
The bioreactor and magnetically attached culture plate are place on an optical isolation bench, which reduces background vibration to limit interference. Prismatic tape is present in the base of each well which reflects the laser beam back towards the head and facilitates measurement of the vertical displacement.

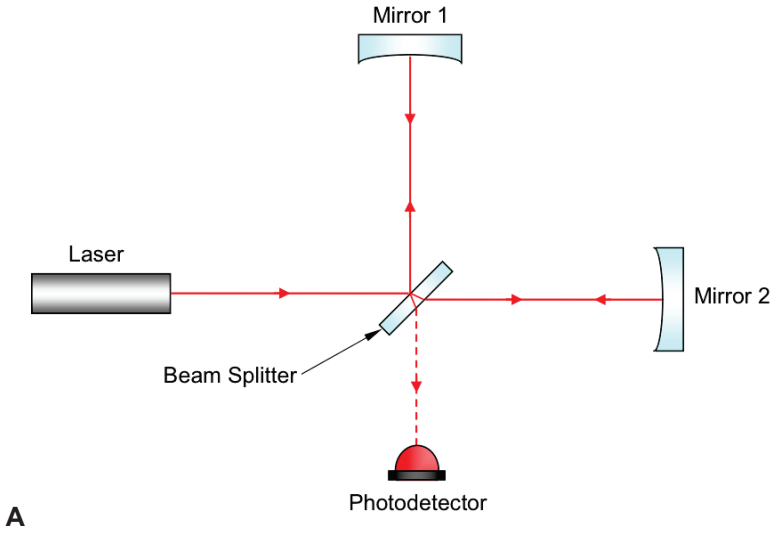

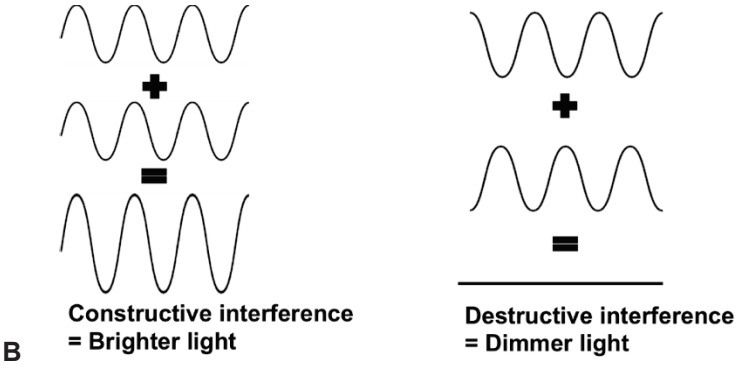

Figure 2:3 Principles of laser interferometry.
A - A light beam is emitted from the laser and is subsequently split into two separate arms travelling at 90 degrees to one another. Each beam then reflects off a mirror and is returned towards the beam splitter. Both beams then recombine and travel towards the photodetector. In doing so, an interference pattern is produced depending on how well aligned they are. Their alignment is dependent on the difference in distance each beam has travelled. If one beam has travelled further, it will take longer to return to the photodetector. If both arms of the beam are the same length, each will cancel the other out i.e. destructive interference. Alternatively, differences in length result in constructive interference, leading to the emission of light that is identified by the photodetector. The interferometer can identify displacements of 0.1 nm (Campsie P et al, 2019) Figure produced by Dr Paul Campsie. B – diagrams illustrating complete constructive and destructive interference.

2.5 TRAP staining

TRAP (Tartrate-Resistant Acid Phosphate) was used as per manufacturer's instructions (Acid Phosphatase, Leukocyte (TRAP) kit, No.387A, Sigma-Aldrich, Dorset, UK). Fast Garnet solution (25 µl Fast Garnet and 25 µl Sodium Nitrite) was mixed by inversion for 30 seconds and left to stand for 2 minutes. 400 µl of fixative (12.5 ml Citrate solution, 32.5 ml Acetone and 5 ml Formaldehyde) was added to the base of each well for 30 seconds. This was then washed three times with warm water. 400 µl TRAP staining solution (4.5 ml warm water, 50 µl Fast Garnet solution, 50 µl Napthol, 200 µl Acetate, 250 µl Tartrate) was added and incubated

at 37°C for 30 minutes in the dark. The TRAP staining solution was then removed. Samples were washed three times with warm water and allowed to air dry.

Digital images of the wells were acquired using an EVOS® FL Auto 2 Cell Imaging System (Thermo Fisher Scientific, Loughborough, UK). Osteoclasts were identified as TRAP positive cells with ≥3 nuclei and quantified by both number and area using Fiji software (Image J). Cell numbers were determined by counting all osteoclasts in the entire well of each replicate. Area was calculated by manually delineating the cell border of 100 cells/well and using the area calculation tool in Image J.

2.6 Immunofluorescence

Co-culture samples were cultured for 28 days. Cells were fixed (4% formaldehyde, 1 x PBS with 1% sucrose) at 37°C for 15 minutes. The samples were washed with PBS and a permeabilising buffer (10.3 g of sucrose, 0.292 g of NaCl, 0.06 g of $MgCl_2$, 0.476 g of HEPES buffer, 0.5 ml of Triton X, in 100 ml of deionised water, pH 7.2) at 4°C for 5 minutes, then incubated at 37°C for 5 minutes in 1% bovine serum albumin (BSA)/ 1 x PBS. The BSA/PBS was removed and different antibodies added for one hour at 4°C. Specific primary antibodies used were:

Vimentin (1:50 in 1% BSA/1 x PBS)

Tubulin (1:50 in 1% BSA/1 x PBS)

Vinculin (1:150 in 1% BSA/1 x PBS)

Simultaneously, rhodamine-conjugated phalloidin was added for the duration of this incubation (1:100 in 1% BSA/1 x PBS, Thermo Fisher Scientific, Loughborough, UK). The samples were then washed in 0.5% Tween 20/PBS at 37°C for 5 minutes. A secondary antibody – anti-mouse IgG (1:50 in 1% BSA/1 x PBS, Vector Laboratories, Peterborough, UK) – was added for 1 hour at 37°C followed by washing in 0.5% Tween 20/PBS. Fluorescein isothiocyanate (FITC)-conjugated streptavidin was then added (1:50 in 1% BSA/1 x PBS, Vector Laboratories, Peterborough, UK) at 4°C for 30 minutes, with samples covered in foil to protect them from direct light. A final wash in 0.5% Tween 20/1 x PBS was performed. Nuclear stain 4',6-diamidino-2-phenylindole (DAPI, Vectashield, Vector

Laboratories, Peterborough, UK) was added to each well and a coverslip placed on top. Samples were viewed using a fluorescence microscope (Zeiss Axiovert 200M, 10 x magnification, Fisher Scientific, Loughborough, UK). Staining intensity was calculated with Fiji software (Image J). Images were thresholded to minimise background noise. The threshold for each antibody was maintained for the assessment of all respective images.

2.7 Actin ring staining

Cells were cultured for 28 days. Medium was removed and cells were fixed with 3.7% methanol-free formaldehyde (Sigma-Aldrich, Dorset, UK) for 10 minutes at room temperature in the dark. Samples were then washed twice with 1 x PBS and permeabilised with 0.1% Triton x-100. A further wash x 2 with 1 x PBS was performed. Rhodamine-Phalloidin (1:40 PBS, Thermo Fisher Scientific, Loughborough, UK) was added to sufficiently cover the cells prior to incubating in the dark at room temperature for 20 minutes. Samples were given a final wash x 2 with 1 x PBS. Cover slips were applied and fluoroscopy images acquired using an EVOS® FL Auto 2 Cell Imaging System.

2.8 Von Kossa staining

Samples were cultured for 28 days. They were then fixed (4% formaldehyde/1 x PBS with 2% sucrose) at 37°C for 15 minutes. 5% silver nitrate was added to cover the cells before exposing to UV light for 30 minutes. Samples were then rinsed three times with deionised water. 5% sodium thiosulphate was then added for 10 minutes to remove excess silver nitrate. They were then rinsed three times with deionised water. Counterstaining with 0.1% nuclear fast red for 10 minutes was then performed before a further rinse x 3 with deionised water. A final rinse with 70% ethanol was performed. Digital images of the entire wells were acquired using an EVOS® FL Auto 2 Cell Imaging System. The percentage surface area stained was then calculated using Fiji software (Image J).

2.9 Scanning electron microscopy

Cells were fixed with buffered fixative (1.5% glutaraldehyde, 0.1 M sodium cacodylate) for 1 hour at 4°C. Samples were then rinsed with 0.1 M sodium

cacodylate for 3 x 5 minutes. Postfix in 1% osmium tetroxide for 1 hour at room temperature was then performed followed by 3 x 10 minutes wash with distilled water. A dehydration process was performed using an ethanol series (30, 50, 70 and 90% for 5 minutes each x 2, followed by 100% for 5 minutes x 4, and dried absolute ethanol for 5 minutes x 4). Hexamethyl-disilazane (HMDS) was then applied to samples and left overnight for drying. An 18 nm gold palladium coating was overlaid on the sample surface using a Polaron SC515 SEM Coating System (Quorum Technologies, Sussex, UK). Finally, samples were attached to aluminium stubs and analysed on a Carl Zeiss Sigma variable-pressure analytical SEM (Carl Zeiss Ltd, Cambridge, UK). The accelerating voltage was 10 kV, with a working distance of 5 nm and 30 µm aperture.

2.10 AlamarBlue assay

Cell viability was assessed at defined time points using an alamarBlue assay (Thermo Fisher Scientific, Loughborough, UK) according to the manufacturer's instructions. A 10% solution was produced (1 ml alamarBlue, 9 ml media). Media was removed from the wells and 500 µl of 10% alamarBlue added. Both the stimulated and control samples were then incubated at 37°C for 4 hours in the dark. 150 µl/well of 10% alamarBlue was then transferred in triplicate to a 96 well plate. The remainder of 10% alamarBlue was discarded before washing three times with HEPES saline and adding fresh media. The absorbance was measured at 570 nm and 600 nm using a Multiskan FC Microplate Photometer (Thermo Fisher Scientific, Loughborough, UK).

2.11 Live/dead stain

An assessment of the proportion of live:dead cells in the 3D collagen gel was performed at defined time points. Media was first removed from the wells. A 1:1000 dilution of ethidium homodimer and calcein AM (Thermo Fisher Scientific, Loughborough, UK) was made, and 400 µl added to each well. Plates were then incubated at 37°C for 45 minutes. The stain was then removed and 400 µl fresh warmed media added to the wells. The entire wells were then imaged with a fluorescent microscope (EVOS® FL Auto 2 Cell Imaging System) using both the green (470/22 nm excitation, 510/42 nm emission) and red (531/40 nm excitation, 593/40 nm emission) filters.

2.12 RT-qPCR

2.12.1 2D RNA extraction

After culture for defined time points, media was removed from the samples and the wells gently washed with sterile 1 x PBS. They were then lysed using RLT buffer (QIAGEN, Manchester, UK). Lysates from wells were homogenised and then transferred to 1.5 ml nuclease free tube. RNA was extracted using RNeasy Micro Kit (QIAGEN, Manchester, UK) following the manufacturer's instructions. 14 µl of RNase-free water was used to elute RNA. Nucleic acid quantification was performed using a Nanodrop 1000 spectrophotometer (Thermo Fisher Scientific, Loughborough, UK). Reading distilled water absorbance acted as a blank, and the samples were read at 260 nm to give quantification and the ratio of 260/280 used for purity estimation. RNA was then either immediately used for cDNA generation or stored at -80°C for later use.

2.12.2 3D RNA extraction

Attempts to employ the same technique for RNA extraction in 3D as 2D were unsuccessful. Measurement of RNA in the 3D cultures led to values so low that it was suspected the technique was inappropriate. Specifically, it was postulated that the collagen gels were blocking the RNeasy MinElute spin column membrane (QIAGEN, Manchester, UK) used to elute RNA. As an alternative to these spin columns a precipitation technique was employed, as described below.

After culture for defined time points, media was removed before gently washing with sterile 1 x PBS. The gel was then disrupted with a pipette tip and transferred to an eppendorf. 350 µl TRIzol (Thermo Fisher Scientific, Loughborough, UK) was added and the tube vortexed to further disrupt the gel. Samples were incubated for 10 minutes to allow for cell lysis and subsequently centrifuged at 12000 x *g* for 15 minutes at 4°C. The pellet was discarded and the RNA in solution transferred to a clean eppendorf. 100 µl chloroform was added before mixing vigorously for 20 seconds then incubating at room temperature for 3 minutes. Samples were centrifuged at 12000 x *g* for 15 minutes at 4°C and the upper aqueous phase transferred to a clean tube. 1 µl glycoblue (Thermo Fisher Scientific, Loughborough, UK) was added to aid with visualisation of the pellet and 250 µl isopropanol (Sigma-Aldrich, Dorset, UK) mixed in to samples. The eppendorfs were

then incubated at -20°C for 1 hour and then centrifuged at 12000 x *g* for 15 minutes at 4°C. The supernatant was discarded without disrupting the blue pellet. The RNA pellet was then washed twice with 70% ethanol and centrifuged 7500 x *g* for 5 minutes at 4°C. The ethanol was removed and the tube air-dried. The pellet was re-suspended in 20 µl RNase-free water and incubated at 60°C for 10 minutes to ensure full re-suspension. Nucleic acid quantification was performed using a Nanodrop 1000 spectrophotometer. Reading distilled water absorbance acted as a blank, and the samples were read at 260 nm to give quantification and the ratio of 260/280 used for purity estimation. RNA was subsequently either immediately used for cDNA generation or stored at -80 °C for later use.

2.12.3 cDNA generation

100 – 300 ng of RNA was used to generate cDNA using QuantiTect Reverse Transcription Kit (QIAGEN, Manchester, UK) following the manufacturer's instructions. RNA, RNase free water and gDNA Wipeout Buffer were combined to produce a volume of 14 µl and incubated for 2 minutes at 42°C. A master mix containing Quantiscript Reverse Transcriptase, Quantiscript RT buffer and RT Primer Mix was then produced, providing a total reaction volume of 20 µl. The samples were incubated at 42°C for 15 minutes and then 95°C for 3 minutes to terminate the reaction. cDNA was finally further diluted to a concentration of 5 ng/µl and stored at -20°C.

2.12.4 RT-qPCR

Using a 96 well PCR plate, each sample was run in duplicate. A master mix was prepared using 10 µl SYBR Green (QIAGEN, Manchester, UK), 0.1 µl forward primer, 0.1 µl reverse primer and 7.8 µl nuclease free water. This was added to each duplicate alongside 2 µl of cDNA, producing a volume of 20 µl per PCR well. The plate was then sealed using an adhesive PCR plate cover and centrifuged at 200 x g for 1 minute. Primers were provided by Eurofins (Eurofins, Hamburg, Germany) and the sequences shown in Table 2:1. An Abi7500 thermal cycler PCR machine (Thermo Fisher Scientific, Loughborough, UK) was used to run the samples. The primer sequences for the genes were validated by dissociation curve/melt curve analysis. The GapDH housekeeping gene primer/probe set was used (ABI predesigned amplification reagent) for normalisation. The ΔCT of each sample was

calculated with normalisation against GapDH. Blanks (no cDNA) were used to act as controls.

Table 2:1 Forward and reverse primer sequences for RT-qPCR.

Target Gene	Forward Sequence	Reverse Sequence
ALP	AGAACCCCAAAGGCTTCTTC	CTTGGCTTTTCCTTCATGGT
Cathepsin-K	GCCAGACAACAGATTTCCATC	CAGAGCAAAGCTCACCACAG
IL-6	GATGAGTACAAAAGTCCTGATCCA	CTGCAGCCACTGGTTCTGT
M-CSF	GAACTGCCAGTGTAGAGGGAAT	GCTGGTCAGACAACATCTGG
OSCAR	CCAGCTCTAGCGGGTATCTG	GACGGAGTGATGTCTGTGTGAC
OPN	AGCTGGATGACCAGAGTGCT	TGAAATTCATGGCTGTGGAA
OPG	GAAGGGCGCTACCTTGAGAT	GCAAACTGTATTTCGCTCTGG
RANKL	TGATTCATGTAGGAGAATTAAACAGG	GATGTGCTGTGATCCAACGA
TNF- α	CAGCCTCTTCTCCTTCCTGAT	GCCAGAGGGCTGATTAGAGA
TRAP	GGACTGAAGGGACTCCTGAAT	GGTCCCTGAGCCTTTATTCC

2.13 ELISA

Cells were cultured for defined time periods, with regular media changes. The supernatant was removed and stored pending analysis at -80°C. The media was last changed 72 hours prior to removal for analysis. 96 well ELISA plates were prepared according to the manufacturer's instructions (R&D Systems, Abingdon, UK). The capture antibody was diluted to the working concentration and 100 µl/well added. The plates were sealed and left overnight at room temperature. Wells were then aspired and washed with 400 µl wash buffer (0.05% Tween 20 in 1 x PBS) x 3. Plates were then blocked with 300 µl/well reagent diluent (1% BSA in 1 x PBS) for 1 hour. A further wash x 3 with wash buffer was performed. 100 µl/well of either samples or standard was added, with duplicate technical replicates, and incubated at room temperature for 2 hours. A further wash x 3 was performed. 100 µl/well of detection antibody diluted in reagent diluent was added for 2 hours. A further wash x 3 was performed. 100 µl/well of Streptavidin-HRP was added for 20 minutes, avoiding direct light exposure. A further wash x 3 was performed. 100 µl/well of substrate solution (1:1 mixture of Colour Reagent A and B) was added for 20 minutes, avoiding direct light exposure. Finally, 50 µl/well of Stop Solution was added. The optical density was calculated at 450 nm using a

Multiskan FC Microplate Photometer. A standard curve was created with Prism v6 (GraphPad Software, California, USA) and the results interpolated from this.

2.14 Osteoclast functional assessment

The Osteo Assay Surface is a multiple well plate. The base of each well is coated with a synthetic inorganic bone surface. As osteoclasts resorb this surface coating, the plate can be used to determine the function of osteoclasts by measuring the area resorbed. CD14+ cells were selected as per the technique described above. Cells were then seeded at a concentration of 1 x 10^6 /ml onto a 24 well Osteo Assay Surface plate (Corning, Flintshire, UK). The RANKL was added at a concentration of 25 ng/ml after approximately 18 hours incubation. Media was refreshed twice weekly. After 7 days incubation, the cell layer was removed by adding 10% chlorine solution (Sigma-Aldrich, Dorset, UK) to the wells at room temperature for 10 minutes. The wells were examined to ensure all cells had been removed before rinsing thoroughly with deionised water and leaving to dry. Images were then captured using an EVOS® FL Auto Cell Imaging System and the area of resorption calculated using Fiji software (Image J).

2.15 Metabolomics

Cells were cultured for defined time periods. All the media was removed from the wells and then gently washed with 1 x PBS at 4°C. All the PBS was removed before adding 500 µl/well of chilled extraction solvent (1:3:1 chloroform: methanol: water). Solvent was also placed in a well without cells to produce a blank. Plates were then sealed with parafilm and vigorously agitated on a rotary shaker for 1 hour at 4°C. The solvent was removed from the wells and placed in an eppendorf before centrifuging at 1300 rpm for 3 minutes. The supernatant was removed and placed in a new eppendorf. 50 µl of each sample was placed in a separate tube to produce a pooled sample of each condition. Samples were stored at -80°C pending transfer to the Glasgow Polyomics department.

2.15.1 Liquid chromatography-mass spectrometry

This stage of the experiment was conducted by the staff of the Glasgow Polyomics department. This technique involves separation of the components of the mixture based on chemical properties, before quantifying the mass of the varying analytes

based on their mass: charge ratio (Clish CB, 2015). Utilising standards of known metabolites then helps identify the specific constituents. The Glasgow Polyomics department used the UltiMate 3000 RSLC and Orbitrap Q-Exactive (Thermo Fisher Scientific, Loughborough, UK).

2.15.2 Data analysis

The data produced by LC-MS was converted to an IDEOM file by the Polyomics staff. This Excel file details the varying metabolites identified and their respective quantities. Furthermore, the metabolites are linked to the KEGG database (Kyoto Encyclopaedia of Genes and Genomes) which facilitates examination of varying chemicals and biological pathways (Fiehn O, 2002). The files were generated containing the metabolite KEGG IDs and their ratio to the specified control. These files were analysed with IPA (Ingenuity Pathway Analysis); a programme that identifies and predicts alterations in pathways and networks.

2.16 Statistical analysis

The appropriate statistical analyses were preformed using GraphPad Prism software (version 6). Normally distributed data were analysed with the t-test. Conversely, if the data were not normally distributed the Mann-Whitney U test was utilised. Statistically significant results were defined as those having a *p* value of 0.05 or less.

Chapter 3 Nanoscale vibration of CD14+ culture

3.1 Introduction

The primary aims of this project are to examine the effects of nanoscale vibration on 1) osteoclasts, and 2) a co-culture of MSCs and BMHCs. The results of osteoclasts will first be discussed. Osteoclasts were obtained by selection CD14+ cells from blood, as discussed in Chapter 2.2. Within this culture, there were two main cell types – macrophages and osteoclasts. As osteoclasts would only form in the presence of RANKL (Zhang S et al, 2017), the production of two different conditions was established: 1) an M-CSF group, where only macrophages would be present, and 2) an M-CSF + RANKL group, containing osteoclasts, pre-osteoclasts and macrophages. It was beneficial to have a relatively pure culture of macrophages and osteoclasts for investigation in addition to the co-culture, as this allowed an assessment of the effects on nanoscale vibration without the influence of MSCs.

In addition to assessing the impact of nanoscale vibration on these cell cultures, it was equally important to measure the nanoscale displacements themselves. This was to ensure the bioreactor was correctly calibrated and would produce the correct displacements using a 24 well plate. Thermal imaging and shear flow measurements were not undertaken as this work has already been carried out by other authors, demonstrating no significant heat transference to the cell culture or production of fluid shear stress (Tsimbouri PM et al, 2017b, Nikukar H et al, 2016).

3.2 Materials and methods

Experiments were conducted as laid out in the Materials and Methods chapter. Cells were cultured using standard laboratory techniques, including sterile working conditions, laminar flow cabinets and incubators at 37°C with 5% CO_2. Cell numbers were kept standard across all experiments as were frequency of media changes and volume of media used (2 ml/well for 2D culture, 1 ml/well for 3D). Maintaining the same volume ensured the vertical pressure of the media on the cells was comparable throughout. 24 well plates were used for all

experiments. Following seeding of cells, plates were left for 4 hours to allow cells to settle on the cultureware surface prior to placing on the Nanokick bioreactor.

The initial attempts to differentiate osteoclasts proved unsuccessful. Macrophages were present however there was no evidence of fusion despite the addition of RANKL. Following a number of changes, including cell count and well size, it was found that the batch of FBS used was not conducive to osteoclast differentiation. Although no changes to manufacturer were made, once a new batch was used osteoclasts were successfully produced. Going forward, this batch was stored and used. When depleted, small experiments were conducted to ensure any new batch of FBS facilitated osteoclast formation prior to larger experiments being established.

A number of time points were used for different experiments. These included days 1, 2, 3, 5 and 7. With the addition of RANKL to the culture, osteoclasts were present from around day 3 onwards – a finding consistent with other papers in the literature (Marino S et al, 2014) – and were mature by day 7. Extended cultures beyond day 7 was not felt to be beneficial for this reason.

3.3 Results

3.3.1 Bioreactor calibration

As each bioreactor can accommodate 2 x 24 well plates, 48 separate displacement measurements were taken (Figures 3:1 and 3:2). The set-up of the laser interferometer and bioreactor is illustrated in the Materials and Methods chapter. The mean displacement was found to be 40.6 nm (Table 3:1). Measurement of the bioreactor was undertaken periodically to ensure no change in displacement had occurred.

There were no significant peaks or troughs in vertical displacement identified across the bioreactor surface. Previous ANSYS finite element modelling had suggested the corners of the bioreactor would potentially produce higher displacements (Figure 1:6) but this was not found to be the case in any of the calibrations. This could potentially be attributed to evolution of the Nanokick bioreactor design from the 1st to the 3rd generation.

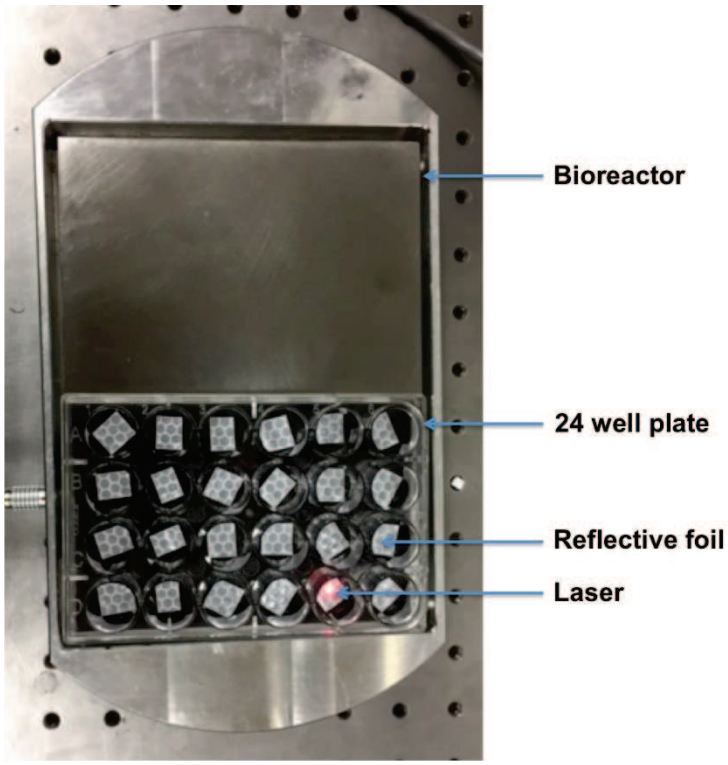

Figure 3:1 Measurement of vertical displacements with laser interferometry.
The Nanokick bioreactor is placed on an anti-vibration table to minimise background interference. Magnetic sheets are fixed to the 24 well plate to facilitate attachment of cultureware onto the bioreactor. Prismatic tape is placed in the base of each well to reflect the laser and measure vertical displacements, as detailed in Chapter 2.4.

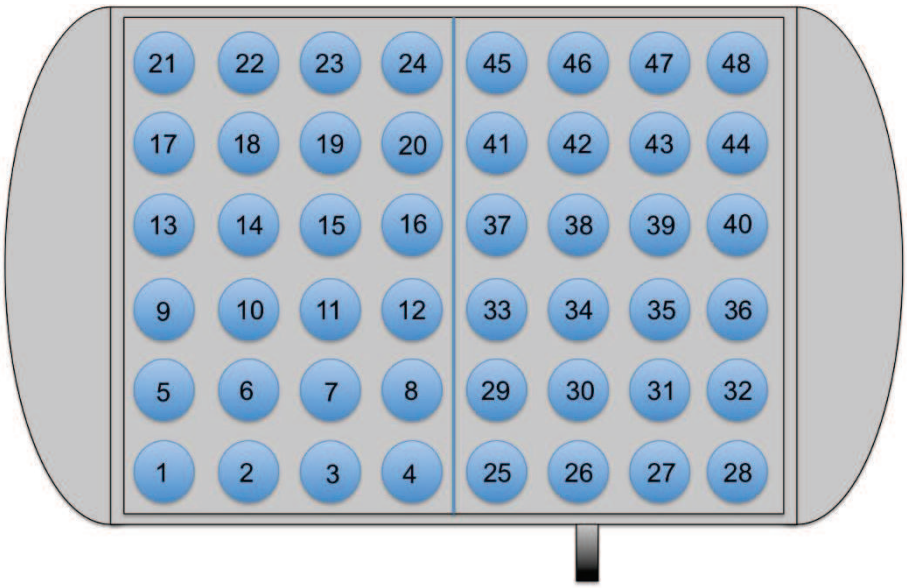

Figure 3:2 Interferometry measurement locations on Nanokick bioreactor.
Each bioreactor has space for two standard culture plates. Each number (1 – 48) corresponds to a single well of a 24 well plate where a laser interferometry measurement was taken. Values 1-24 and 25 – 48 represent to the two plate locations. The power input cable is depicted at the bottom right of the bioreactor.

Table 3:1 Vertical displacement measurements for the Nanokick bioreactor.
48 well positions were measured, as depicted in the figure above. The mean vertical displacement was 40.6 nm (SD 9.8 nm). Although there was variation between wells none were felt to be significantly different.

Well	Vertical displacement (nm)	Well	Vertical displacement (nm)
1	44	**13**	46
2	69	**14**	31
3	45	**15**	26
4	31	**16**	32
5	33	**17**	39
6	39	**18**	41
7	74	**19**	40
8	50	**20**	30
9	30	**21**	39
10	29	**22**	40
11	36	**23**	40
12	40	**24**	42

Well	Vertical displacement (nm)	Well	Vertical displacement (nm)
25	33	**37**	45
26	34	**38**	45
27	28	**39**	42
28	24	**40**	39
29	37	**41**	51
30	41	**42**	50
31	34	**43**	46
32	29	**44**	43
33	39	**45**	57
34	42	**46**	53
35	38	**47**	49
36	37	**48**	47

3.3.2 Osteoclast differentiation

As previously noted, osteoclasts stain intensely for TRAP. Other cell types including macrophages and dendritic cells also stain for TRAP, however. To differentiate between osteoclasts and the other cell types, they were identified as those that were TRAP positive with three or more nuclei. This allowed measurement of cell number and area to be performed. This experiment was a useful starting point as it allowed a quick determination on whether osteoclasts

were formed and an objective assessment of morphological change between groups.

The results shown below are only for the samples with RANKL added. Those with only M-CSF did not show evidence of osteoclast differentiation as expected. In the nanokick group, a significant reduction in the number of osteoclasts per well was found (Figure 3:3, p=0.034). Similarly, a significant reduction in mean osteoclast area was found in the nanokick group (Figure 3:4, p<0.001). The cell count and area were reduced by approximately 32% and 34%, respectively. Figure 3:5 illustrates a typical TRAP stain image.

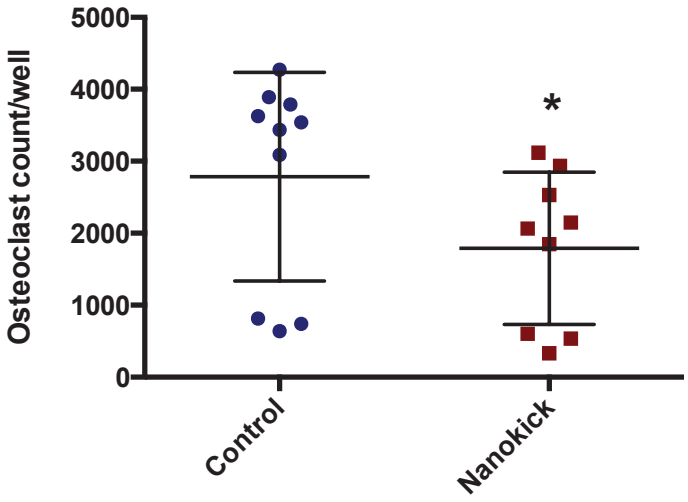

Figure 3:3 Osteoclast cell count.
A significant reduction in osteoclast numbers was observed in the nanokick group following 7 days of culture. One donor was found to have a viably lower number of osteoclasts present, as can be seen in the data plots above. However, in this donor there was still a reduction in cell numbers in the nanokick group. Graph shows mean +/- SD. * = p<0.05, by Mann-Whitney U test. N=3 cell donors.

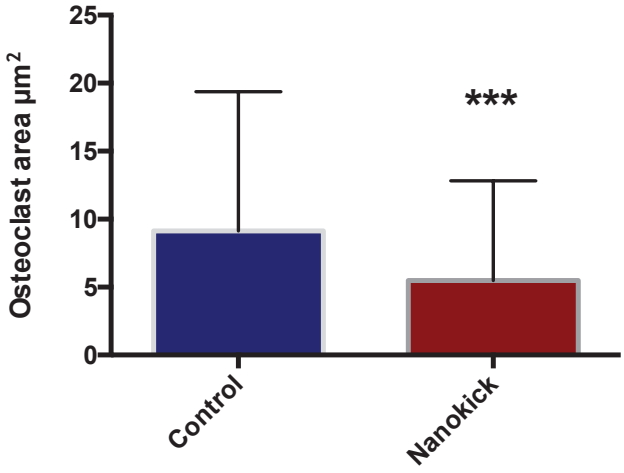

Figure 3:4 Osteoclast area measurement.
A significant reduction in osteoclast area was demonstrated in the nanokick group. As the data points illustrate, there is a potentially wide variation in the cell size observed within each culture. Graph shows mean +/- SD. *** = p<0.001, by t-test. N=3 cell donors.

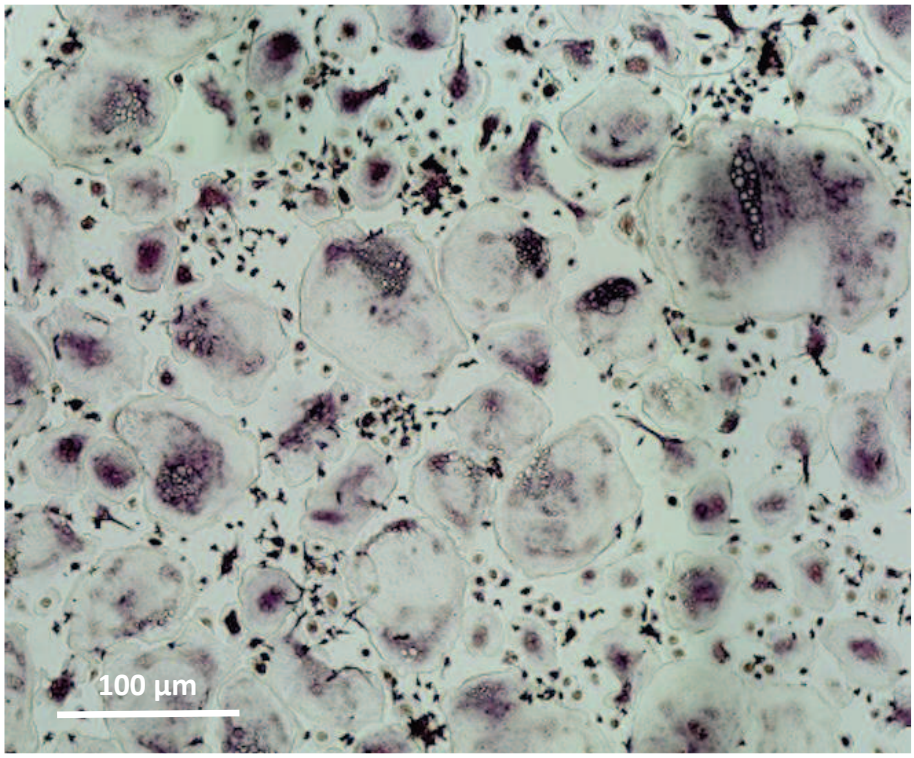

Figure 3:5 TRAP stained CD14+ culture image.
10 x magnification brightfield microscopy image. This image demonstrates numerous osteoclasts (those cells with three or more nuclei) surrounded by smaller macrophages following 7 days of culture with RANKL. This figure illustrates the potentially variable osteoclast cell size that can be present within a culture, as also noted in Figure 3:4.

3.3.3 AlamarBlue cell viability assessment

TRAP staining demonstrated a reduction in osteoclast numbers. Moving forward, cell viability was assessed to determine whether this reduction could be attributed to lower cell metabolism or viability. This was performed for the +RANKL culture given osteoclasts were the cell of interest that had demonstrated an effect following nanoscale vibration. The alamarBlue cell viability reagent assay was therefore performed. This assay quantifies cell viability by measuring their ability to reduce resazurin to resorufin (Back SA et al, 1999). A significant increase in the percentage of alamarBlue reduced was found in the nanokick group at day 3 (Figure 3:6, p=0.003). This suggests increased cell viability in the nanokick group at this stage. By day 7, there was no difference between the two groups.

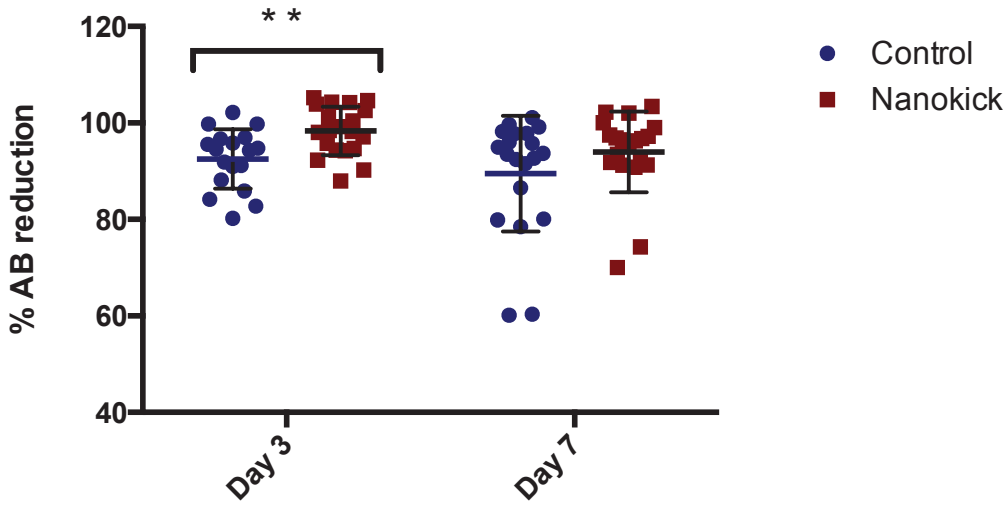

Figure 3:6 alamarBlue cell viability reagent assay of CD14+ culture.
A significant increase in percentage alamarBlue reduction was observed in the nanokick group at day 3. No difference was found at day 7. This suggests increased cell death was not the cause of the reduction in osteoclast numbers observed in the nanokick group. Graph shows mean +/- SD. ** = $p<0.01$, by t-test. N=3 cell donors.

3.3.4 Scanning electron microscopy

TRAP staining had demonstrated a reduction in osteoclast numbers and area. To gain further insight into other potential morphological changes, scanning electron microscopy (SEM) was undertaken. This facilitated more detailed examination of the cells structure. Three main cell types were identified: macrophages, osteoclasts precursors and osteoclasts. Osteoclast precursors were less spherical in appearance than macrophages, but lacked the size of osteoclasts. It is likely these cells are in the early stages of fusion. There were no obvious changes in appearance between the control and nanokick group, however. Subjectively, a lower density of osteoclasts was observed in the nanokick group, conforming with the TRAP stain data, but those cells which were present did not display differing features. Macrophages were frequently seen in clusters around larger osteoclasts, potentially indicating they were in the stage prior to fusion.

Osteoclasts demonstrated the typical filopodia seen in this cell type. Filopodia were observed on the periphery of the osteoclasts, which are known to play a role in cell-cell fusion (Song RL et al, 2014). Phagocytotic pits were also observed in mature osteoclasts; a feature noted by other authors (Young PS et al, 2015) (Figure 3:7).

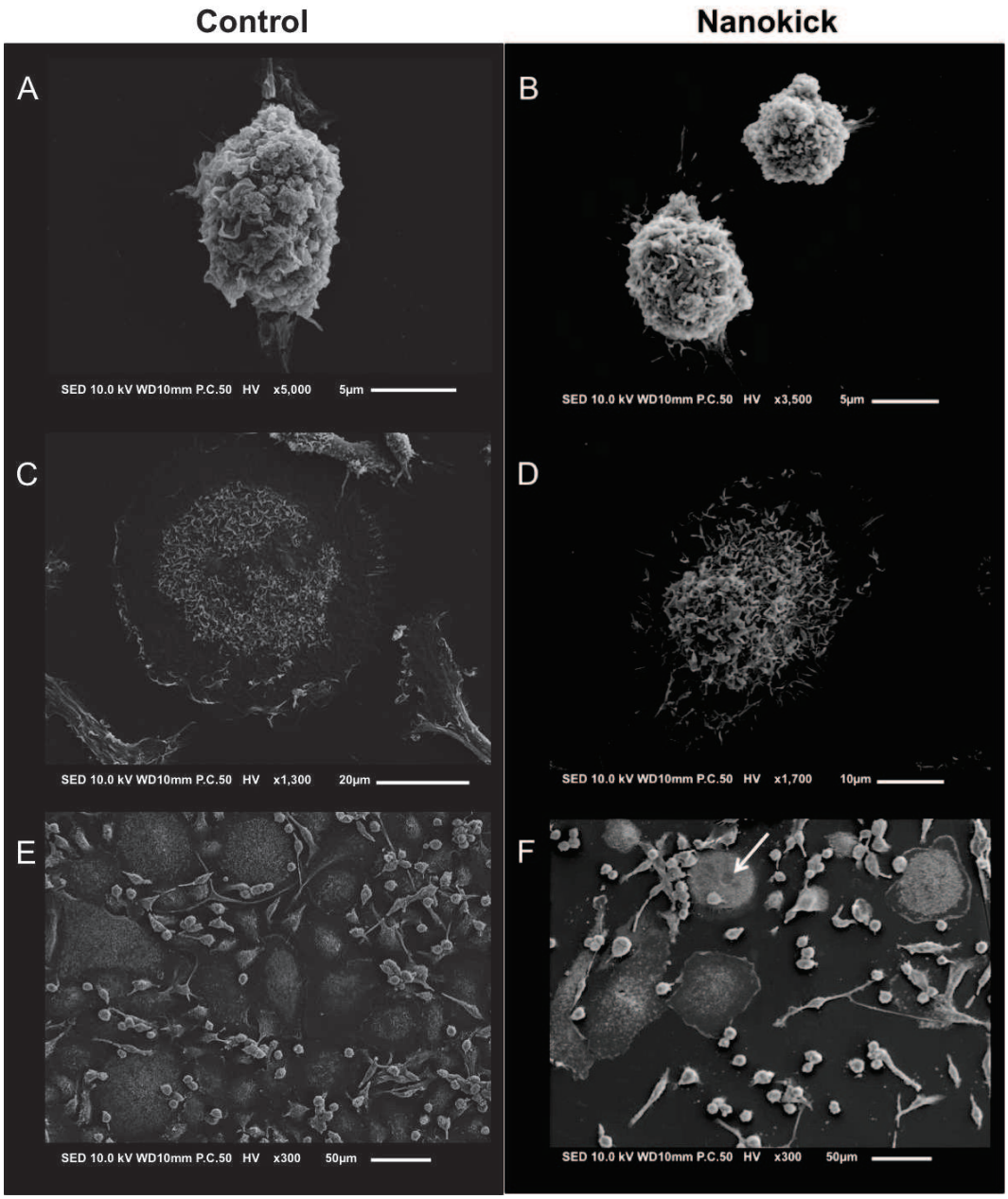

Figure 3:7 SEM images of CD14+ culture.
A and B show macrophages. C and D: osteoclast precursors appear less spherical than macrophages, but are smaller than mature osteoclasts. E and F: lower magnification images showing multiple osteoclasts surrounded by the smaller, more spherical macrophages. Arrow indicates phagocytosis pit. Note the lower density of osteoclasts observed in the nanokick group.

3.3.5 Osteoclast functional analysis

The initial experimental results had demonstrated a reduction in osteoclasts numbers. While this is significant, potentially of more importance is the functionality of the osteoclasts. Specifically, their ability to resorb bone. Cells were seeded onto the Osteo Assay surface plate and the area of collagen resorbed measured. A significant reduction in surface area resorbed at day 7 was observed in the nanokick group (Figure 3:8, p=0.04). This result refers only to the +RANKL

group; as expected there was no resorption demonstrated in the M-CSF group where only macrophages would be present (Figure 3:9).

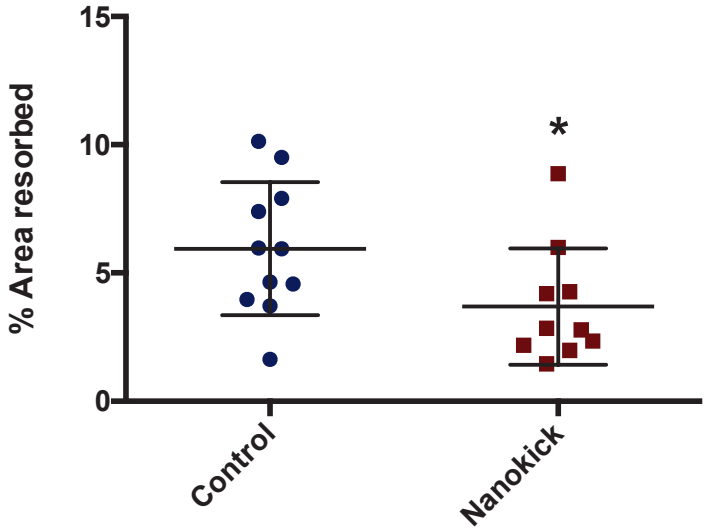

Figure 3:8 Osteoclast-mediated resorption of Osteo Assay surface plate.
Measurement of percentage surface area resorbed was performed. A significant reduction (p=0.04) was found in the nanokick group 7 days following seeding of the CD14+ culture with RANKL added. This result is not surprising given the lower number of osteoclasts observed, but is important as it indicates there is no increase in activity. Graph shows mean +/- SD. * = p<0.05, by t-test. N=3 cell donors.

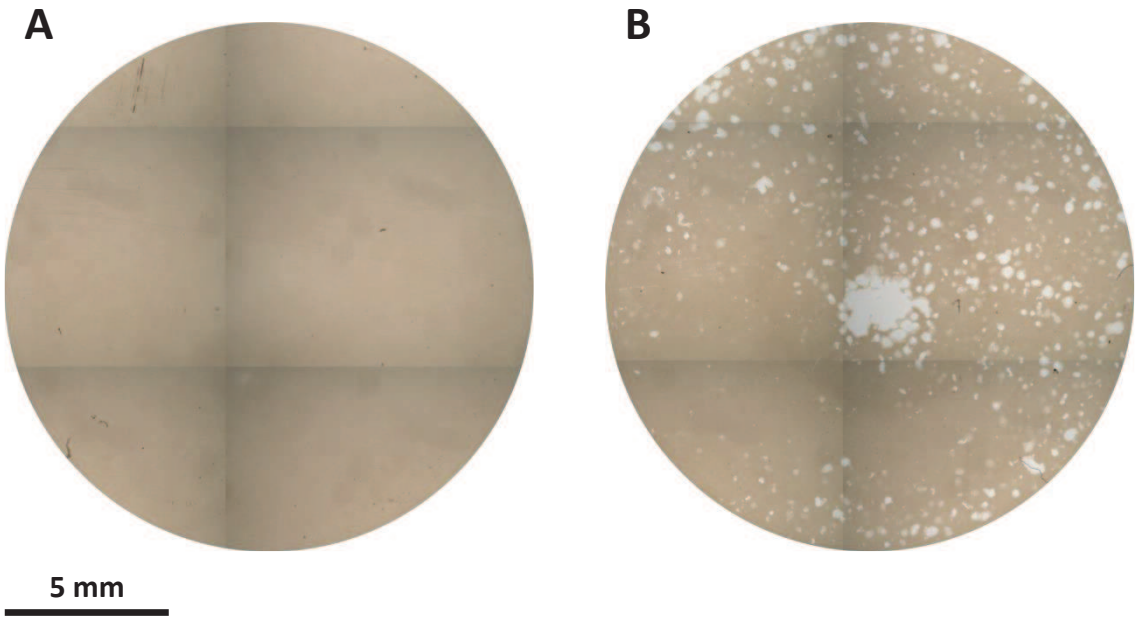

Figure 3:9 Images of Osteo Assay surface demonstrating osteoclast-mediated resorption.
2 x magnification brightfield microscopy images of entire well of a 24 well Osteo Assay surface plate. Image A shows no resorption has taken place in the M-CSF group. The lighter coloured areas present in image B illustrate where osteoclasts have resorbed the collagen surface coating.

3.3.6 Cell viability in 3D collagen gel

To ensure the CD14+ culture was viable in the collagen gel for progression to 3D models, a live/dead stain was performed, using the methodology set out in Chapter 2.11. This demonstrated >99% living cells present in the culture after 7 days incubation (Figure 3:10). This therefore confirmed the 3D technique was able to support this cell culture.

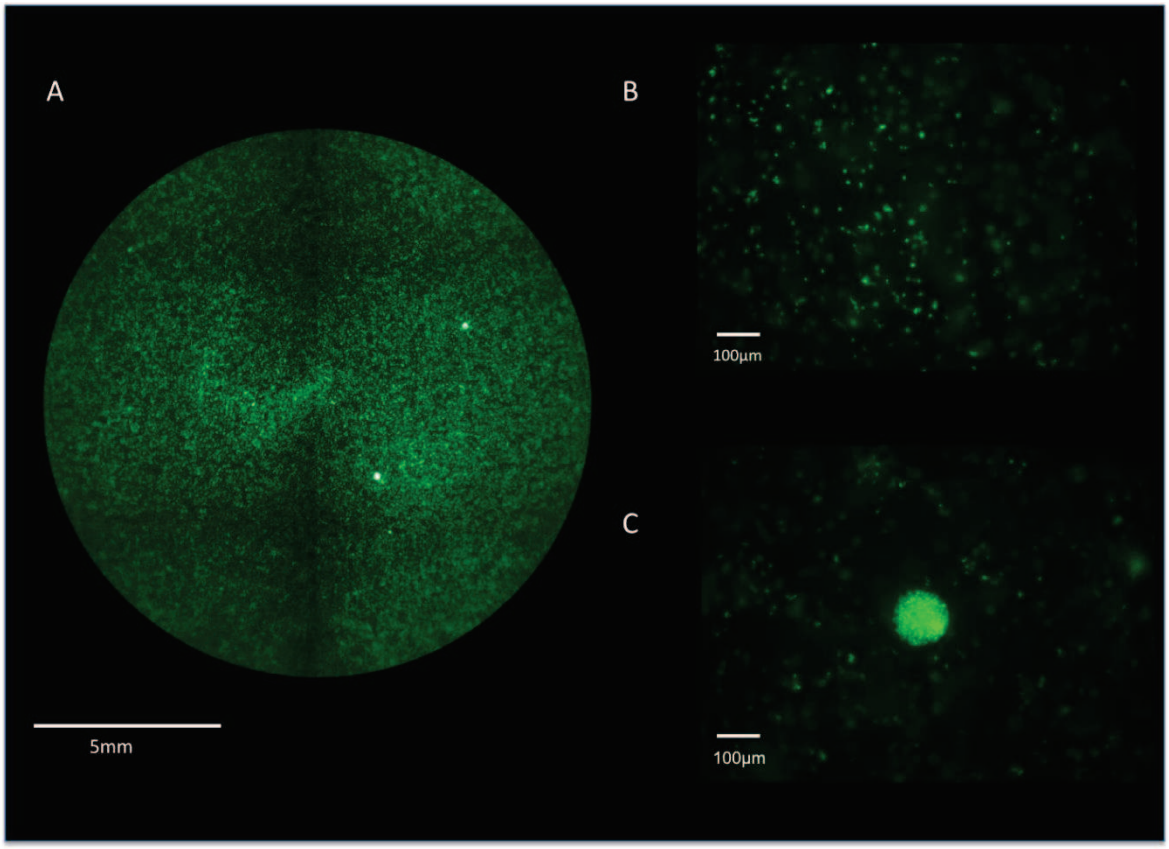

Figure 3:10 Live-dead stain microscopy images of 3D CD14+ culture.
A – 2 x magnification image of entire well in 24 well plate. Cells stained green are living. Conversely red cells are dead. This highlights >99% living cells utilising the collagen gel model after 7 days, which represent the longest time point in the CD14+ culture. B – 10 x magnification image of M-CSF group, illustrating macrophages seeded throughout the gel. C – 10 x magnification of +RANKL group. The large cell in the centre of the image is consistent in appearance with an osteoclast, suggesting fusion of macrophages to form osteoclasts occurs in the collagen gel.

3.3.7 Gene expression

RNA was extracted using the techniques detailed in Chapter 2.12 (with different approaches for 2D and 3D) and subsequently used for cDNA synthesis and qPCR. GapDH was used as the housekeeping gene. Osteoclast stimulatory (TRAP, OSCAR, cathepsin-K, IL6, RANKL and TNF-α), macrophage stimulatory (M-CSF) and osteoclast inhibitory genes (OPG) were assessed.

3.3.7.1 2D M-CSF group

Four time points were assessed: days 1, 2, 3 and 7. Across these stages, there was a general trend towards increases in osteoclast stimulatory genes in the nanokick group (Figure 3:11). However, there were only two statistically significant results: an increase in cathepsin-K and day 1 (Figure 3:12) and an increase in OPG (Figure 3:13) at day 7. This paints a conflicting picture given that cathepsin-K is a pro-osteoclast gene, whilst OPG inhibits osteoclast differentiation. The heatmaps below demonstrate the trends observed. The statistically significant results are illustrated in greater detail through the corresponding Figures.

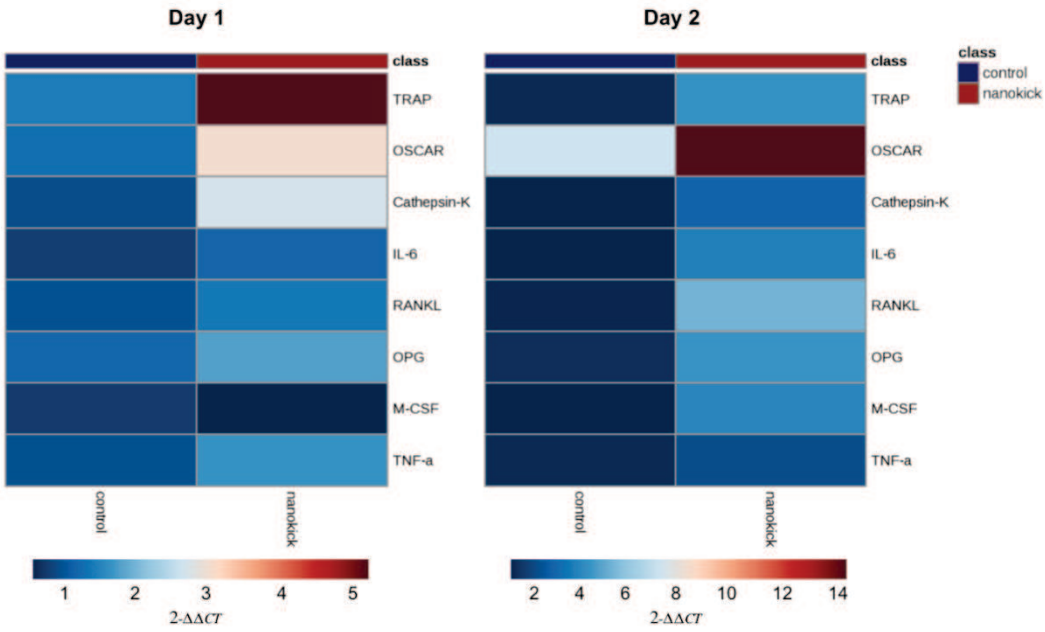

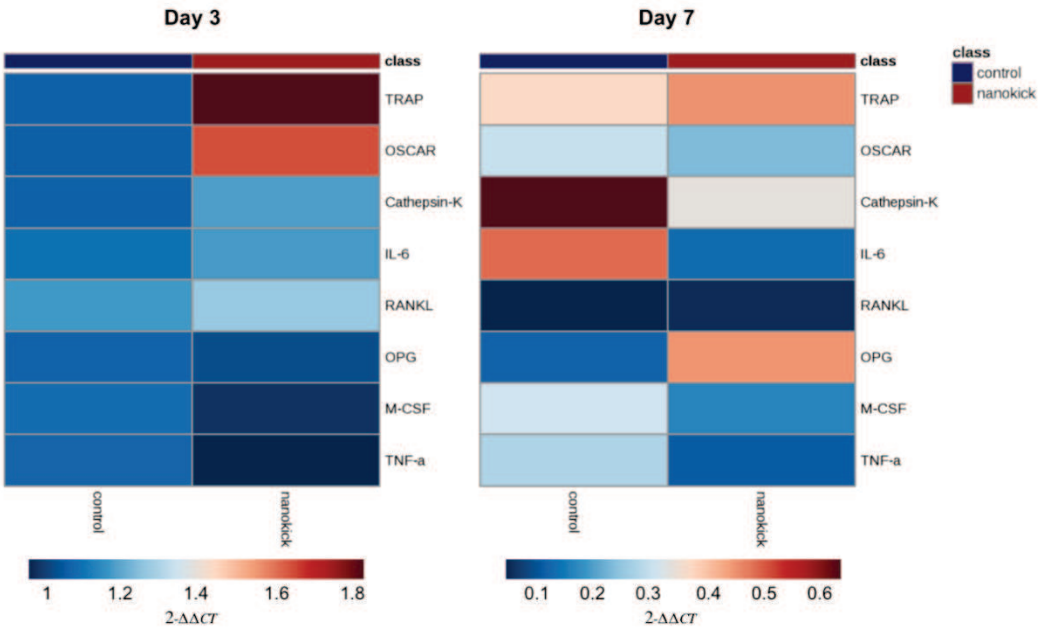

Figure 3:11 RT-qPCR heatmaps of 2D M-CSF group.
The M-CSF group comprises macrophages only, as osteoclast differentiation requires the addition of RANKL. The general trend that can be observed is an increase in osteoclast stimulatory genes in the nanokick group. Significant increases in both cathepsin-K and OPG were observed in the nanokick group.

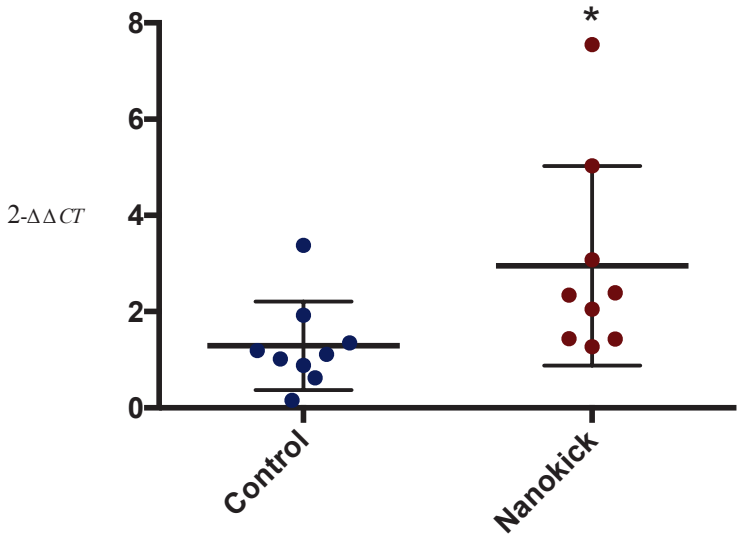

Figure 3:12 Cathepsin-K RT-qPCR result of 2D M-CSF group at day 1.
A significant increase in cathepsin-K expression – a pro-osteoclast gene – was found in the nanokick group. Cathepsin-K is an enzyme release by osteoclasts to promote bone resorption and so would not be secreted by this culture of isolated macrophages. However, it suggests nanoscale vibration may be priming macrophages for bone resorption. Graph shows mean +/- SD. * = p<0.05, by t-test. N=3 cell donors.

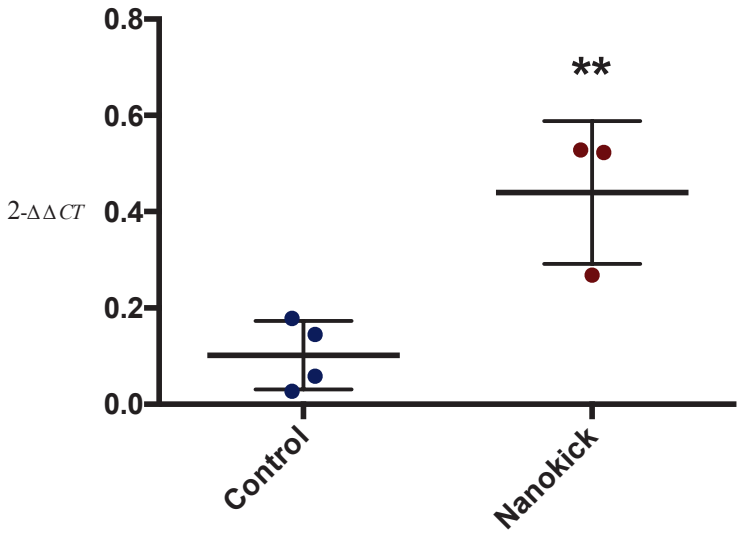

Figure 3:13 OPG RT-qPCR result of 2D M-CSF group at day 7.
A significant increase in the osteoclast inhibitory gene OPG was found in the nanokick group at this time point. OPG inhibits the differentiation and function of osteoclasts (Udagawa N et al, 2000). Graph shows mean +/- SD. ** = p<0.01, by t-test. N=1 cell donor.

3.3.7.2 2D +RANKL group

The +RANKL group comprised a culture of osteoclasts and macrophages. There was a significant increase in cathepsin-K at day 1 in the nanokick group (Figure 3:15). However, in subsequent time points there was a non-significant reduction in this gene in the nanokick group. Similarly, the pro-osteoclast genes TNF-α, M-CSF and IL-6 were reduced at day 3, although the difference did not reach statistical significance. OSCAR, M-CSF and TNF-α had a similar non-significant reduction at day 7 in the nanokick group. These trends are highlighted in Figure 3:14.

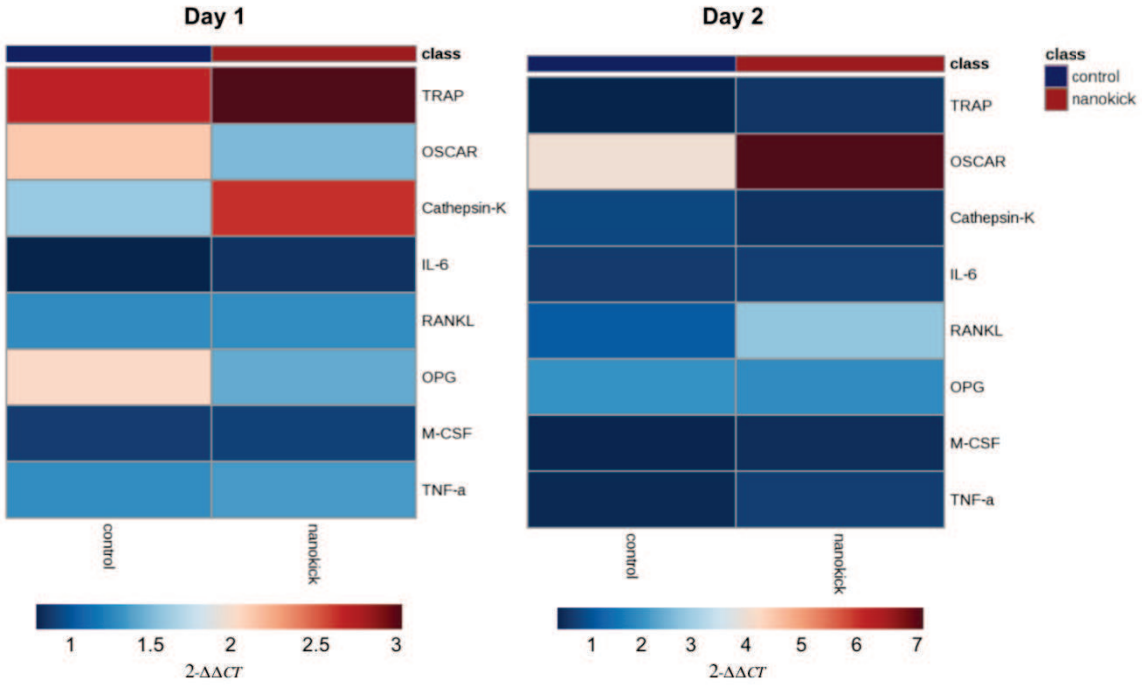

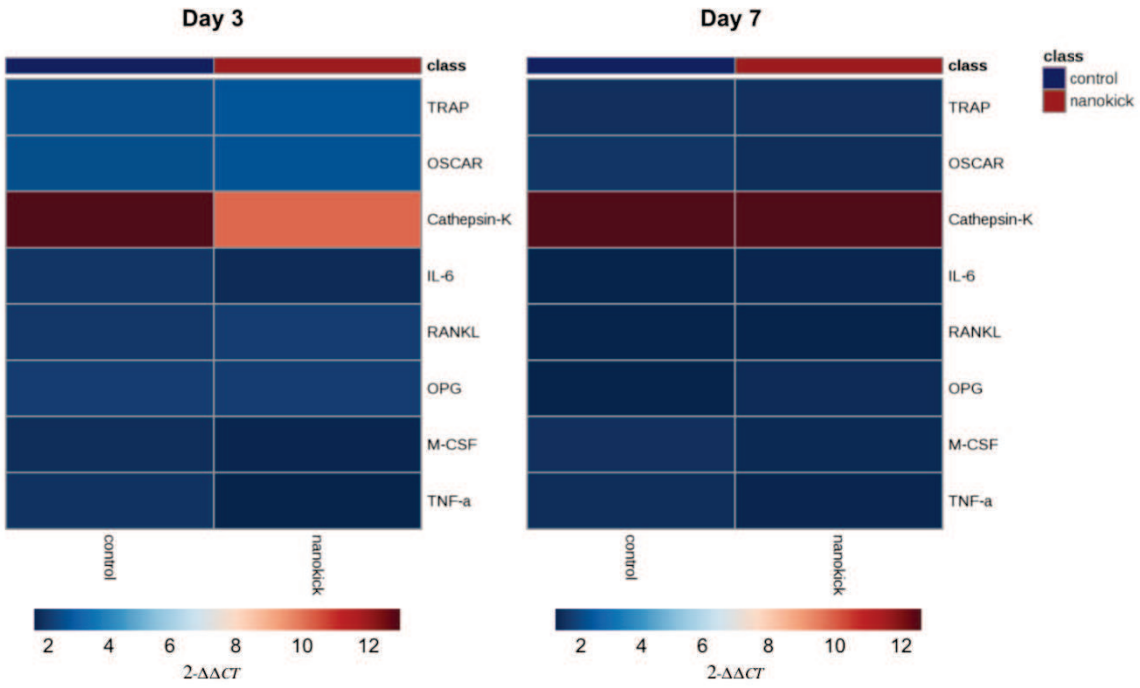

Figure 3:14 RT-qPCR heatmaps of 2D +RANKL group.
The only significant difference identified was an increase in cathepsin-K at day 1 in the nanokick group. A non-significant reduction was subsequently observed at all future time points. Although reductions in certain pro-inflammatory and osteoclast-stimulatory genes were found in the nanokick group, the differences in gene expression were largely subtle at all time points.

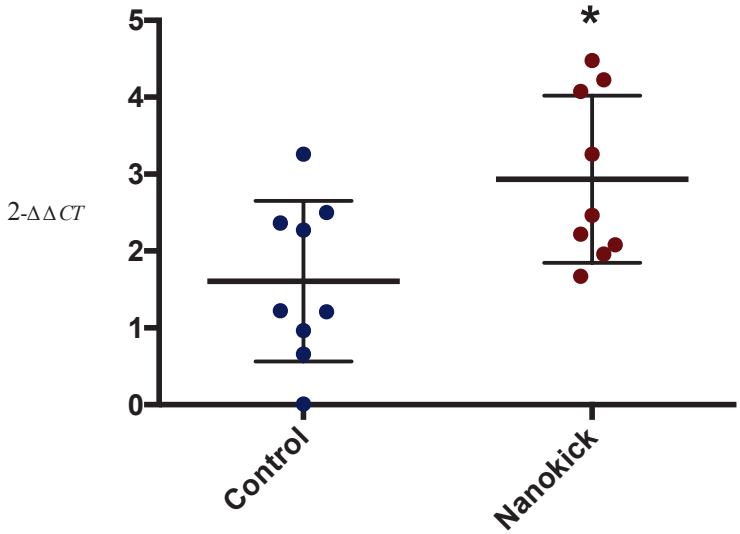

Figure 3:15 Cathepsin-K RT-qPCR result of 2D +RANKL group at day 1.
Similar to the M-CSF group, cathepsin-K expression was found to be significantly increased in the nanokick group. As noted above, this enzyme promotes bone resorption. Interestingly, there was a non-significant reduction in the expression of cathepsin-K in the nanokick group at subsequent time points. Graph shows mean +/- SD. * = $p<0.05$, by t-test. N=4 cell donors.

3.3.7.3 3D M-CSF group

The same 4 time points were assessed in 3D as in 2D (Figure 3:16). In this culture, a significant decrease in cathepsin-K (Figure 3:17), M-CSF (Figure 3:18) and TNF-α (Figure 3:19) was observed in the nanokick group. This suggests lower levels of inflammation and osteoclast stimulatory genes were present following exposure to nanoscale vibration. Again, it is interesting that cathepsin-K levels were found to be significantly different given that this enzyme is produced by osteoclasts and the M-CSF group only contains macrophages.

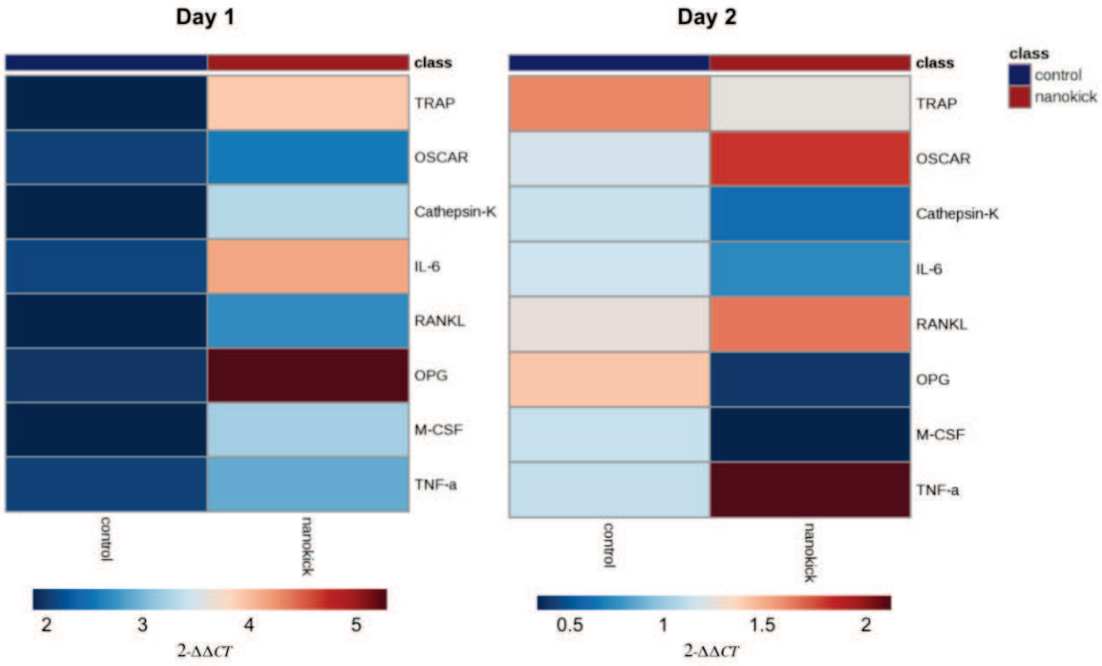

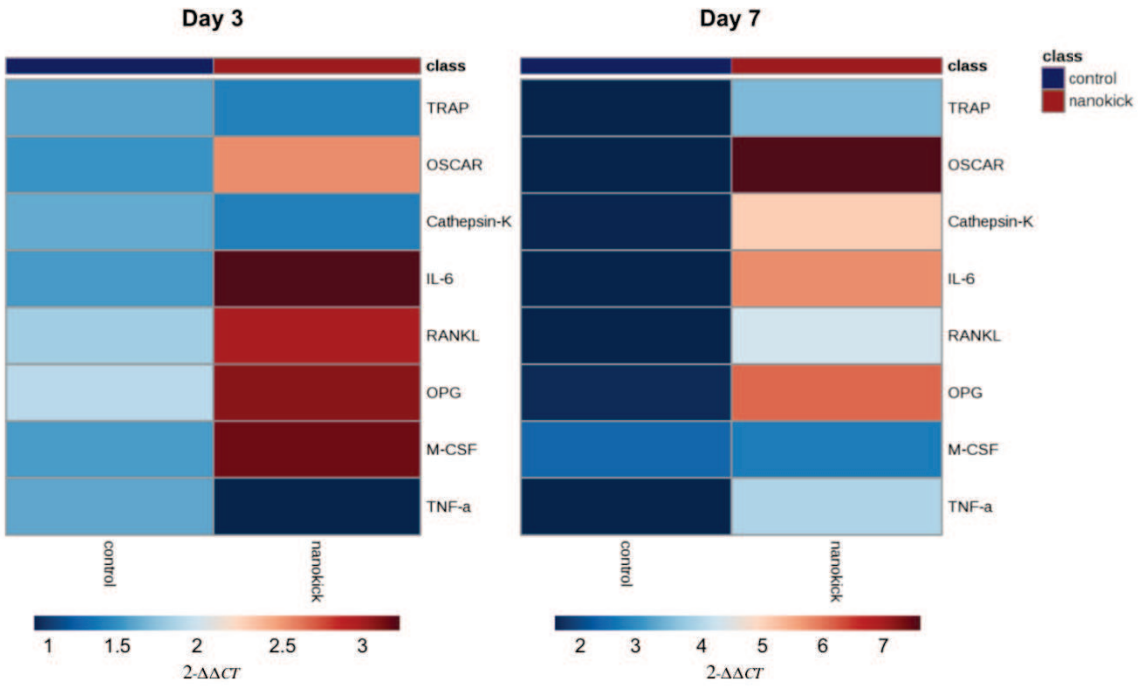

Figure 3:16 RT-qPCR heatmaps of 3D M-CSF group.
Although there were three different significantly different genes identified, it is difficult to discern the overall trend in this experimental condition. Most genes were elevated in the nanokick group at day 1. In the remaining time points, there was a fairly even split of upregulation and downregulation between the groups.

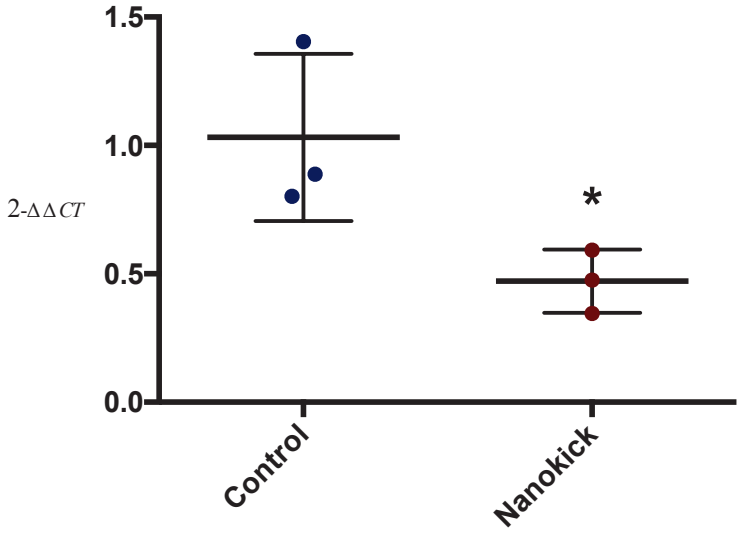

Figure 3:17 Cathepsin-K RT-qPCR result of 3D M-CSF group at day 2.
A significant reduction in the pro-osteoclast gene was observed in the nanokick group. This differs from the result obtained in the 2D culture, where cathepsin-K was significantly increased at day 1, and a nonsignificant increased observed at day 2. Graph shows mean +/- SD. * = p<0.05, by t-test. N=1 cell donor.

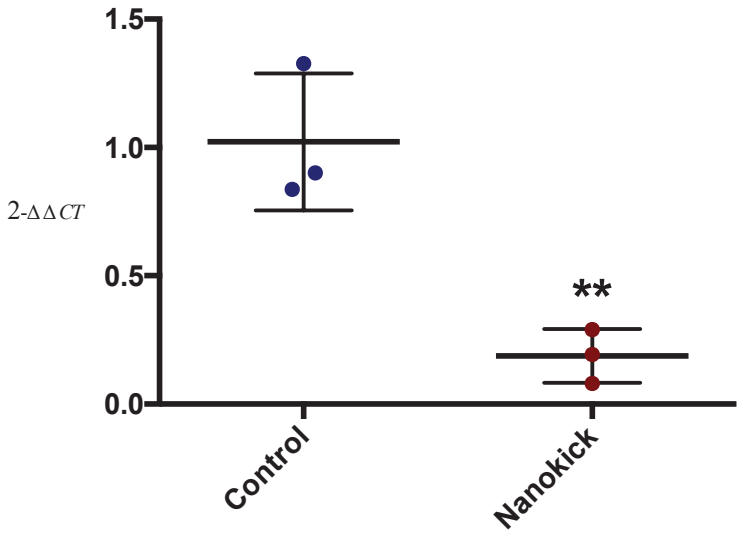

Figure 3:18 M-CSF RT-qPCR result of 3D M-CSF group at day 2.
A significant reduction in M-CSF expression was found in the nanokick group. This suggests nanoscale vibration may inhibit proliferation of macrophages in 3D conditions. Graph shows mean +/- SD. ** = p<0.01, by t-test. N=1 cell donor.

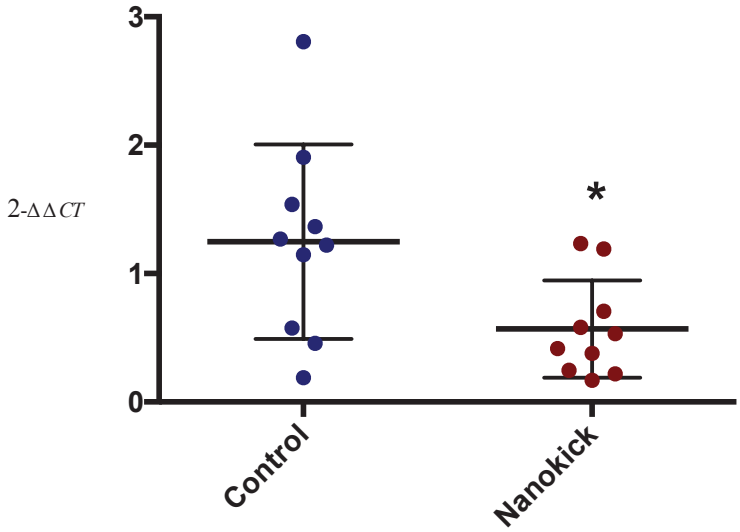

Figure 3:19 TNF-α RT-qPCR result of 3D M-CSF group at day 3.
A significant reduction in the expression of pro-inflammatory gene TNF-α was exhibited in the nanokick group. TNF-α has multiple functions including initiating and perpetuating inflammation, prolonging macrophage survival and inducing osteoclast formation (Parameswaran N and Patial S, 2010). Graph shows mean +/- SD. * = p<0.05, by t-test. N=4 cell donors.

3.3.7.4 3D +RANKL group

Similar to the M-CSF group, differences in gene expression trends were not consistent. There was potentially a trend towards increases in osteoclast stimulatory genes in the nanokick group, but changes were subtle (Figure 3:20). OSCAR was elevated at day 3 (Figure 3:21), but reduced at all other time points. Many of the genes were upregulated in the nanokick group at the early time points,

but subsequently downregulated by day 7, suggesting nanoscale vibration may induce gene level changes early in the differentiation stage.

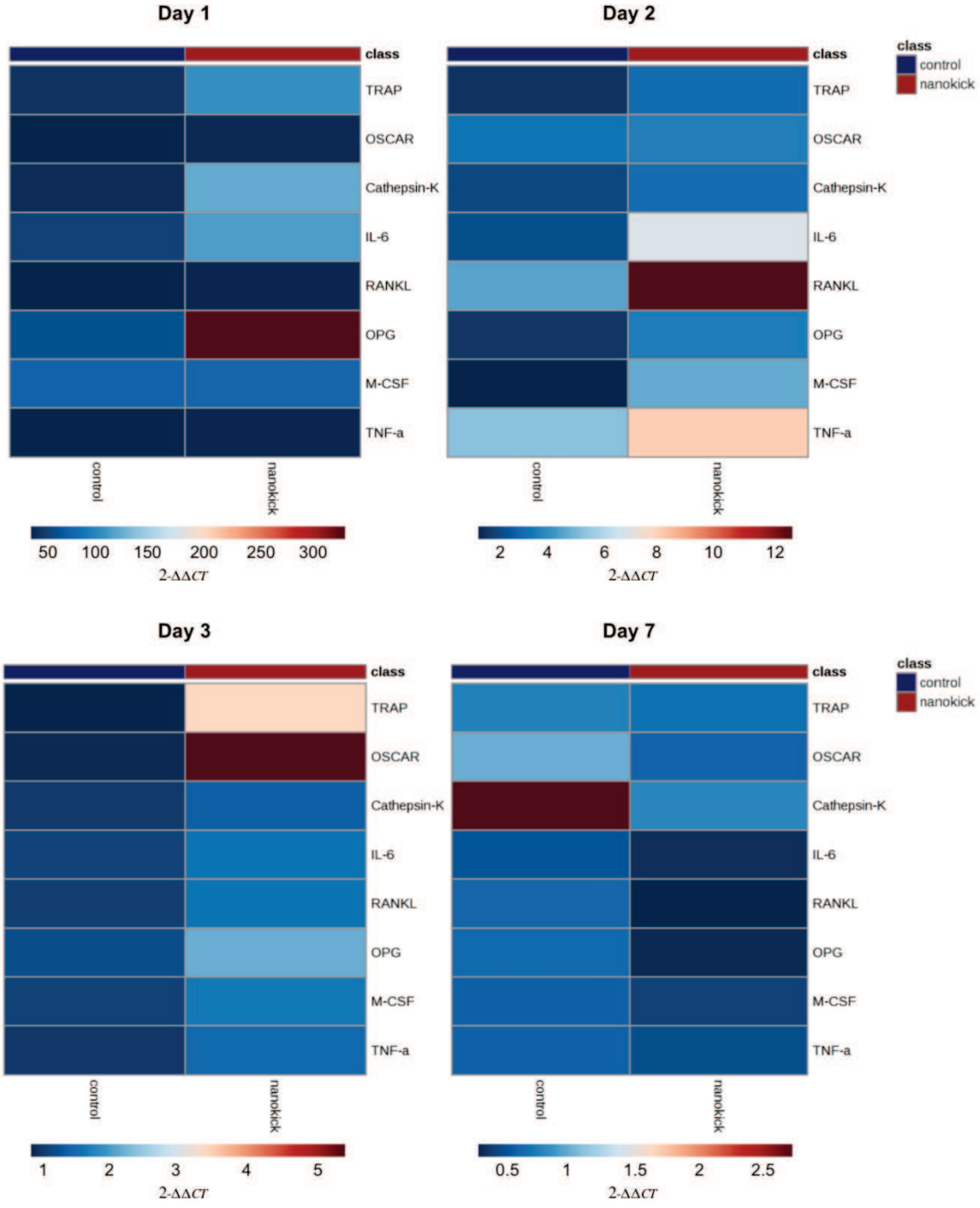

Figure 3:20 RT-qPCR heatmaps of 3D +RANKL group.
Many of the genes were found to be upregulated in the nanokick group at days 1 – 3. However, by day 7, all were reduced. OSCAR was significantly elevated at day 3, but reduced in all other time points.

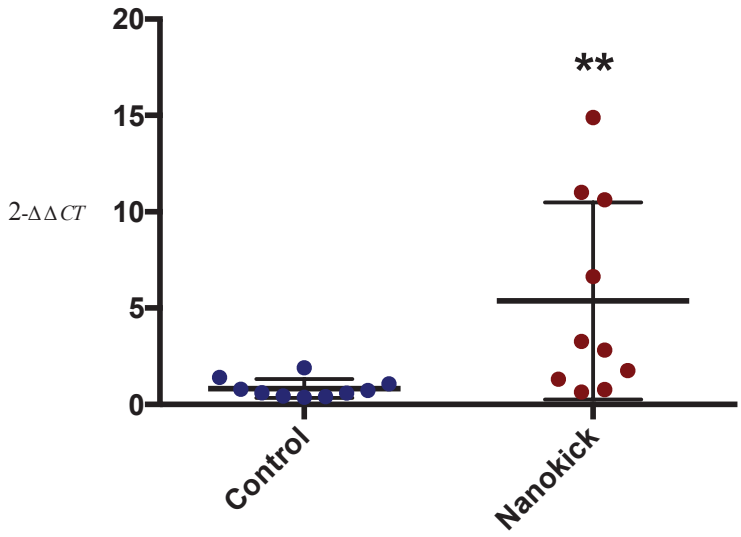

Figure 3:21 OSCAR RT-qPCR result of 3D +RANKL group at day 3.
A significant increase in the expression pro-osteoclast gene OSCAR was observed in the nanokick group. OSCAR plays an important role in osteoclast differentiation (Nemeth K et al, 2011). Graph shows mean +/- SD. ** = p<0.01, by t-test. N=4 cell donors.

3.3.8 Protein assay

Similar to the RT-qPCR experiments, ELISA was performed for both the M-CSF and RANKL groups in both 2D and 3D and days 3 and 7. Osteoclast stimulatory (IL-6 and TNF-α) and inhibitory (OPG) proteins were quantified. This was performed given the ambiguity of the RT-qPCR results. Furthermore, gene level changes detected through RT-qPCR may not result in alterations in protein levels and so performing ELISA was a useful next step.

3.3.8.1 2D M-CSF

At day 3, a significant reduction in OPG was found in the nanokick group. This contrasted with the day 7 RT-qPCR result as OPG was elevated in the nanokick group. Although OPG is an inhibitor of osteoclastogenesis (Boyce BF and Xing L, 2008) there were no osteoclasts present in these cultures. Macrophages have been shown to be a source of inflammatory cytokine IL-1 when under the influence of elevated OPG, leading to more invasive breast tumours in cancer models (Chung ST et al, 2017). It is therefore challenging to interpret the ultimate outcome of OPG in this culture condition. There was no significant difference at day 7 (Figure 3:22).

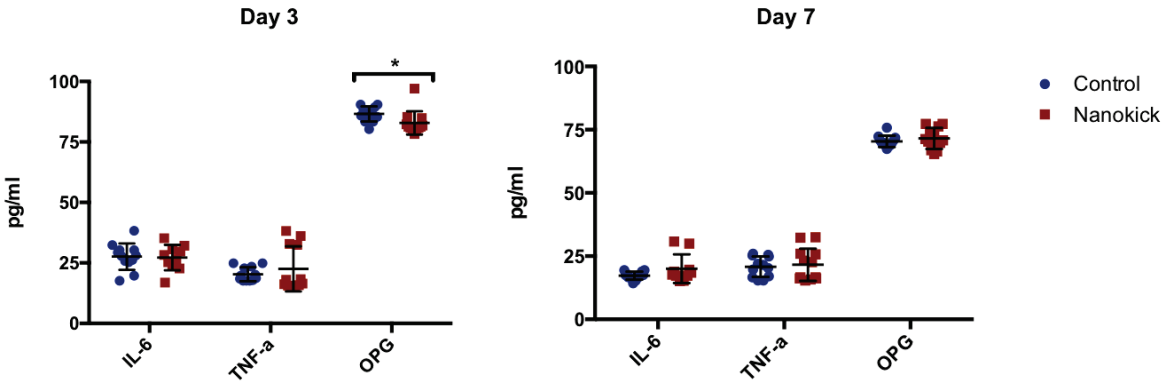

Figure 3:22 ELISA results for 2D M-CSF group.
A significant reduction in OPG was found in the nanokick group at day 3 (86.5 *cf* 82.9 pg/ml). No difference was present at day 7. Graph shows mean +/- SD. * = $p<0.05$, by t-test. N=3 cell donors.

3.3.8.2 2D +RANKL

A significant reduction in pro-inflammatory cytokine IL-6 was demonstrated in the nanokick group at day 3. IL-6 has been shown to promote osteoclastogenesis (Wu Q et al, 2017) and so the lower levels observed tie in with the reduction in osteoclast numbers observed. By day 7, however, there was no significant difference (Figure 3:23).

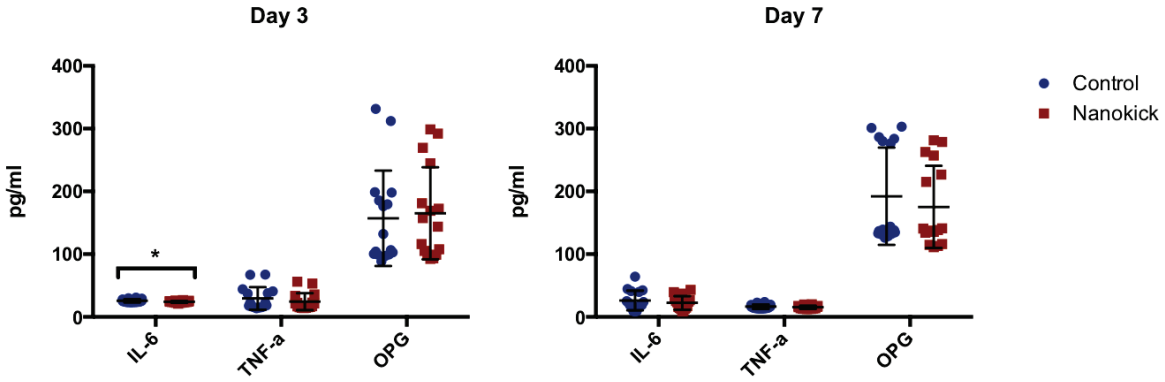

Figure 3:23 ELISA results for 2D +RANKL group.
A significant reduction in pro-inflammatory cytokine IL-6 was observed in the nanokick group at day 3 (25.7 *cf* 24.1). No significant differences were found at day 7. Graph shows mean +/- SD. * = $p<0.05$, by t-test. N=3 cell donors.

3.3.8.3 3D M-CSF

Similar to the 2D M-CSF group, reductions in OPG were observed in the nanokick group at both day 3 and 7 (Figure 3:24). As noted, the role of OPG in macrophages is multimodal, with both inhibition of osteoclastogenesis and promotion of IL-1 secretion.

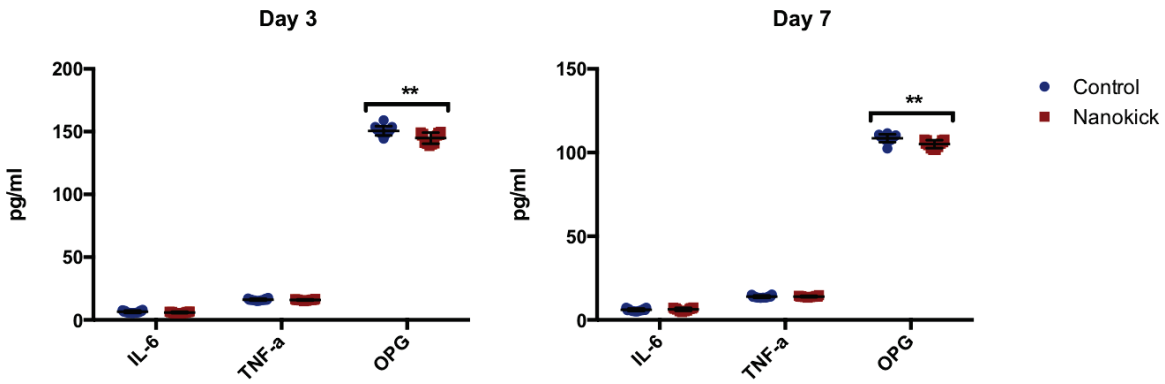

Figure 3:24 ELISA results for 3D M-CSF group.
A significant reduction in OPG was found in the nanokick group at day 3 (150.6 *cf* 144.8) and day 7 (108.6 *cf* 105). Graph shows mean +/- SD. ** = $p<0.01$, by t-test. N=3 cell donors.

3.3.8.4 3D +RANKL

The trend towards a reduction in OPG continued in the +RANKL group at day 7 (Figure 3:25). As noted in Chapter 1.8, OPG has been shown to be produced by osteoclasts as part of a self-regulatory function when MSCs are not present (Kang JH et al, 2014). It is possible the lower number of osteoclasts present in the nanokick group has led to lower levels of OPG being secreted through this auto-regulatory mechanism. It should be noted that in all the experimental conditions, the absolute differences in protein concentrations were relatively small and so this must be borne in mind when interpreting the significance of the results observed.

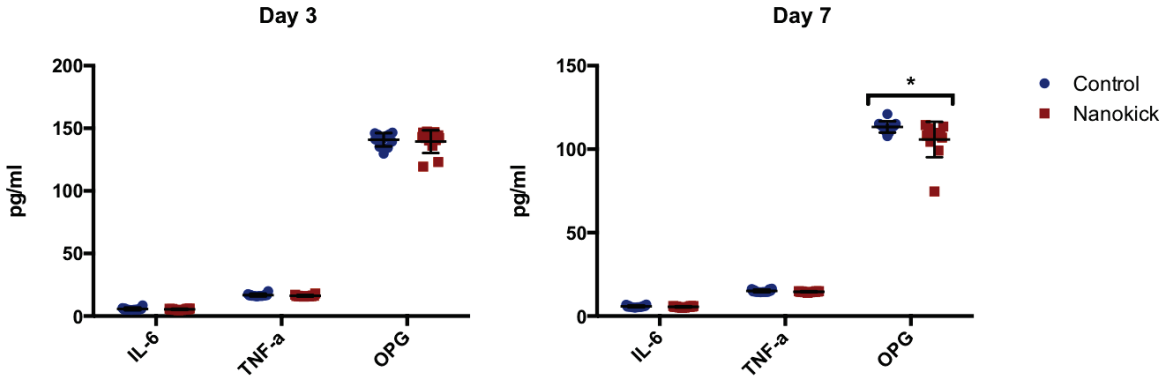

Figure 3:25 ELISA results for 3D +RANKL group.
A significant reduction in OPG was observed in the nanokick group at day 7 (113.3 *cf* 105.8). Graph shows mean +/- SD. * = $p<0.05$, by t-test. N=3 cell donors.

3.3.9 Metabolomics

Metabolomics refers to the comprehensive identification and quantification of metabolites in a biological specimen (Clish CB, 2015). It has the benefit of being highly sensitive and unbiased. Metabolites are the end product of cellular

processes and as such can be viewed as a marker of genetic and environmental change in that biological system (Fiehn O, 2002). Recent research has demonstrated metabolomics can be utilised to investigated stem cell responses to topographical changes (McNamara LE et al, 2012). Stem cells have been found to be metabolically inactive when compared to the increased metabolic activity observed in actively differentiating cells. Metabolome analysis can therefore provide a snap shot in to biological activity and phenotype (Tsimbouri PM et al, 2012). Given the large quantity of data produced, which has been cited as a potential issue with this field (Daviss B, 2005), it is beneficial to focus on pathways and networks relevant to the area of research.

3.3.9.1 M-CSF group

The M-CSF group was cultured for three days before metabolite extraction was performed. The results presented are the main pathways and top scoring networks identified on IPA, using the methodology presented in Chapter 2.15.2. Pathways related to amino acid synthesis were found to have the greatest reduction in Z-scores (i.e. standard deviations away from the mean) in the nanokick group. Specifically, tRNA charging, arginine and lysine had reductions in Z-scores in the nanokick group (Figure 3:26). tRNA is responsible for amino transport (Lodish H et al, 2000), and high levels of amino acid synthesis are associated with self-renewal, differentiation and proliferation (Zhao T et al, 2012, Sampath P et al, 2008).

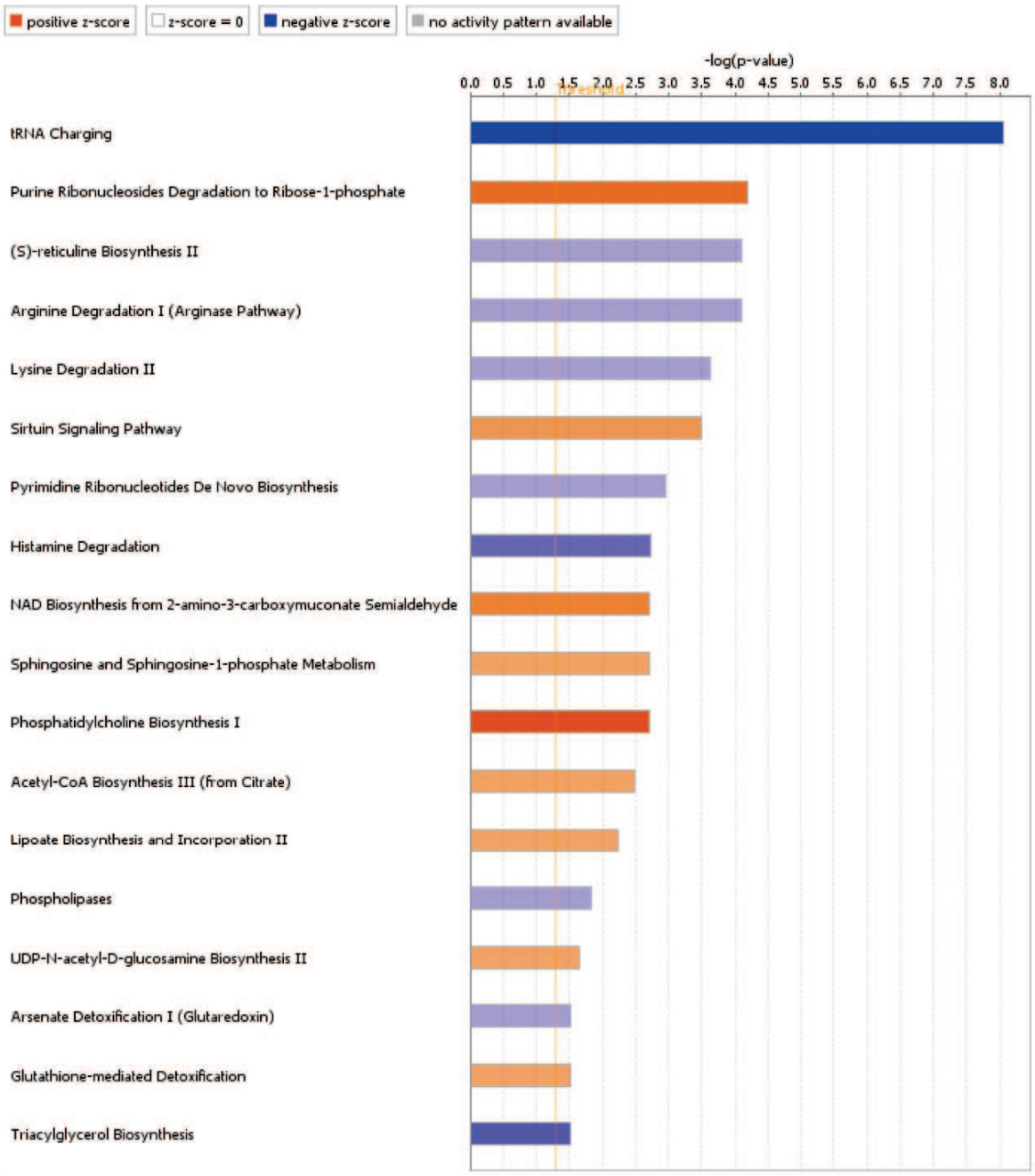

Figure 3:26 Pathway analysis of M-CSF group.
Metabolite analysis with IPA identified a number of changes between the control and nanokick group. The greatest changes identified were reductions in tRNA and amino acid degradation in the nanokick group. Sirtuin was found to be increased, which acts to inhibit macrophage driven inflammation (Liu P et al, 2018). The threshold for significance is p <0.05 with Fisher's exact test. N=3 cell donors.

Examination of the top scoring networks predicted inhibition of several key complexes in the nanokick group, including IL-1, TNF, NF-κB, JNK and pro-inflammatory cytokine. JNK is an important factor in osteoclast survival, and NF-κB is essential for the osteoclastic action of RANKL (Ikeda F et al, 2008). When pathways for IL-6 and role of osteoblasts, osteoclasts and chondrocytes in rheumatoid arthritis were included in the network, almost every complex was found to be inhibited (Figure 6:1). This is of interest given the reduction in TNF-α and IL-6 found with RT-qPCR and ELISA, respectively. ALP – an osteogenic marker

– was the only upregulated complex. Table 3:2 highlights the key complexes that were altered. The full network analysis is presented in the Appendices.

Table 3:2 Selected complexes activated and inhibited in metabolomics network analysis of nanokick M-CSF group

Inhibition	Activation
HIF1	ALP
NF-κB	LDL
JNK	
IFN-ϒ	
IL-1	
TNF	
Pro-inflammatory cytokine	
C/EBP	
PARP	

3.3.9.2 +RANKL group

The +RANKL samples were also cultured for three days prior to metabolite extraction. Analysing the top scoring networks and pathways revealed some similarities with the M-CSF group. The greatest reductions in Z-score were found for tRNA charging and amino acid metabolism in the nanokick group (Figure 3:28). As noted above, amino acids are crucial for self-renewal, differentiation and proliferation. Citrulline was one of the most significantly inhibited amino acids. This amino acid, which can be synthesised from arginine (also inhibited), has been implicated in osteoclast differentiation and bone resorption in rheumatoid arthritis (Harre U et al, 2012). The amino acid serine was also inhibited, which is required for NFAT2 induction by RANKL and, therefore, plays a role in upregulating osteoclastogenesis (Ogawa T et al, 2006, Pollari S et al, 2011).

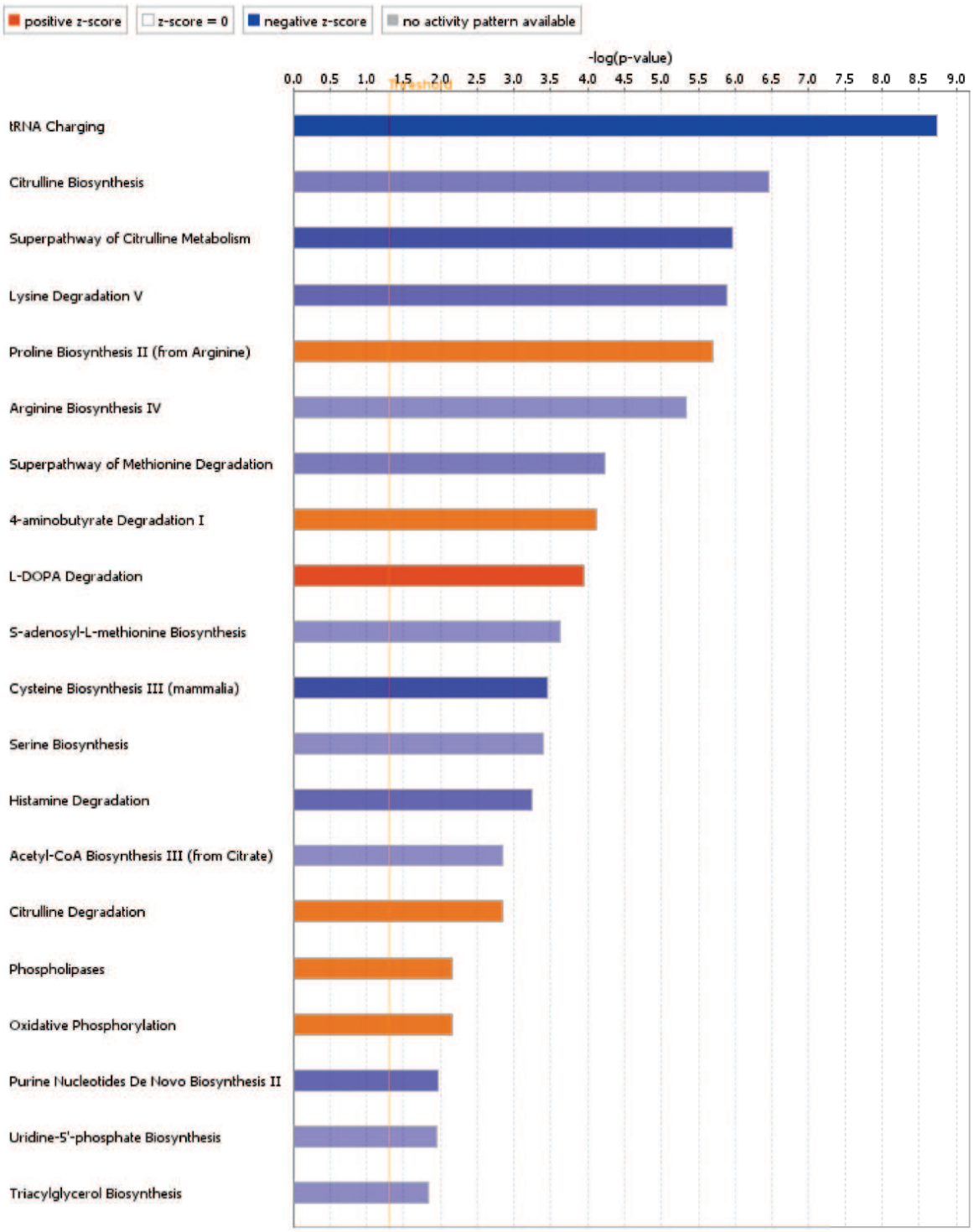

Figure 3:27 Pathway analysis of +RANKL group.
Metabolite analysis with IPA identified a number of changes between the control and nanokick group. The significant changes were similar to those identified in the M-CSF group, namely reductions in tRNA and amino acid metabolism in the nanokick group. The threshold for significance is p <0.05 with Fisher's exact test. N=3 cell donors.

On analysis of the top scoring networks, an inhibition of several pro-inflammatory and osteoclast stimulatory markers was predicted. These include TNF, NF-κB, pro-inflammatory cytokine, poly ADP ribose polymerase (PARP) and nicotinamide adenine dinucleotide phosphate (NADPH) oxidase. PARP stimulates osteoclastogenesis (Beranger GE et al, 2006) and NADPH oxidase has been show to

promote osteoclast differentiation by stimulating NFATc1, a downstream factor of RANKL (Kang IS and Kim C, 2016). Phospholipase A2 (PLA2) was also reduced. Inhibition of PLA2 *in vitro* has been shown to suppress osteoclastogenesis (Allard-Chamard H et al, 2014). Sirtuin 6 (SIRT6) was increased, which has been shown to inhibit osteoclastogenesis by inhibiting NF-κB (Zhang D et al, 2018). Adenosine monophosphate-activated protein kinase (AMPK) was similarly increased, which although promotes the survival of osteoblasts, negatively impacts osteoclast differentiation by suppressing RANKL (Lee YS et al, 2010). Conversely, low density lipoprotein (LDL) and aryl hydrocarbon receptor (AhR) were increased, both of which have been shown to promote osteoclast survival (Luegmayr E et al, 2004, Izawa T et al, 2016). When the canonical pathways for IL-6 and roles of osteoblasts, osteoclasts and chondrocytes in rheumatoid arthritis were overlaid on to the network, the majority of complexes were inhibited. As with the M-CSF group, the osteogenic marker ALP remained elevated (Figure 6:2). Table 3:3 highlights the key complexes that were altered. The full network analysis is presented in the Appendices.

Table 3:3 Selected complexes activated and inhibited in metabolomics network analysis for nanokick +RANKL group

Inhibition	Activation
HIF1	ALP
NF-κB	LDL
NADPH	SIRT6
PLA2	AMPK
IL-1	AhR
TNF	
Pro-inflammatory cytokine	
C/EBP	
PARP	

3.4 Discussion

In this chapter we examined the effects of nanoscale vibration on a culture of macrophages and osteoclasts. No other studies thus far have done so. It is necessary to assess the response of osteoclasts to nanoscale vibration when attempting to produce tissue engineered bone given their close interaction with osteoblasts (Chen X et al, 2018). Doing so first in insolation – i.e. not in a co-culture alongside MSCs and osteoblasts – enabled a true portrayal of their response to vibration.

Nanoscale vibration was produced by the Nanokick bioreactor, with vertical displacements in the order of 40 nm at 1000 Hz. This stimulation resulted in a reduction in the number of osteoclasts produced. The reduction was approximately 30% in all donors. It was interesting that this inhibition of osteoclast formation was relatively uniform across all the donors as this suggests the effect of vibration is constant irrespective of patient-to-patient variation. The osteoclasts were not just fewer in number, but also smaller in size. This confirmed that the reduction in number was not due to their fusion into larger cells. Given the same number of cells were seeded in both the control and nanokick groups, this suggests more macrophages and osteoclast progenitors (i.e. cells with less than 3 nuclei) would be present in the nanokick group. Other authors have found a similar pattern, demonstrating a reduction in osteoclast numbers when exposed to mechanical stimulation (Kameyama S et al, 2013, Kulkarni RN et al, 2013). Although not utilising nanoscale vibration or human cells, these studies do lend support to the results observed.

SEM was used to analyse the appearance of the osteoclasts in more detail. Similar cell types were observed in both the control and nanokick groups, namely macrophages, osteoclast precursors and osteoclasts. Filopodia and phagocytotic pits were present; these features are important for cell migration and bone resorption and their presence infers mature osteoclastogenesis was achieved in both groups (Young PS et al, 2015, Song RL et al, 2014). Subjectively, however, a lower density of osteoclasts was observed in the nanokick group. Given the lower cell number of osteoclasts observed, alamarBlue assay was performed to determine whether increased cell death could be responsible. An increase in cell metabolic activity and viability was found in the nanokick group at day 3, indicating increased cell death was not the cause of the disparity. This result made inhibition of osteoclast differentiation and maturation a more likely hypothesis.

The primary function of osteoclasts is to break down bone (Kim JH and Kim N, 2016). The ability of the cells in this culture to resorb a collagen-coated surface was therefore tested. A significant reduction in osteoclast-mediation resorption was observed in the nanokick group at day 7. This could be considered more significant than purely the number of osteoclasts present, as a small number of highly “aggressive” osteoclasts would be detrimental to new bone formation and graft production. Importantly, however, osteoclast function was not completely

impaired. Normal bone remodelling relies upon the coordinated action of osteoblasts and osteoclasts, and without the presence of the later abnormal bone would form, as in osteopetrosis (Chen X et al, 2018).

RT-qPCR was undertaken with the aim of providing an insight into the underlying mechanism behind the lower osteoclast number and resorption ability. Unfortunately, no clear picture emerged from this. Varying time points in both 2D and 3D showed increases and decreases in osteoclast stimulatory and inhibitory genes. It is therefore difficult to determine what gene changes are of significance to the morphological changes observed. It is possible that the primary genes responsible were not tested in this study. A broad range of primers was utilised, with both osteoclast stimulatory and inhibitory roles, in an effort to capture the underlying mechanism. It was not exhaustive, however, and so in an effort to gain greater clarity, ELISA was performed to examine for potentially significant changes in protein production. This result was again slightly conflicting. IL-6 – an osteoclast stimulatory cytokine (Wu Q et al, 2017) – was found to be significantly reduced in the nanokick group. Conversely, OPG – an inhibitor of osteoclastogenesis (Boyce BF and Xing L, 2008) – was also reduced. The cause for this reduction is not clear given the lower number of osteoclasts observed. It has been noted by other authors that OPG production from osteoclasts (rather than osteoblasts) is significantly elevated in the late phase of osteoclastogenesis, and so potentially the lower concentration identified is a result of the nanokick group not having many terminally differentiated osteoclasts. Furthermore, silencing of osteoclast-derived OPG is associated with lower levels of TRAP and cathepsin-K, and therefore, reduced bone resorption (Kang JH et al, 2014). This conforms to the osteoclast functional assessment result presented earlier in the chapter.

Finally, metabolomics analysis was undertaken to gain further insight into the underlying mechanisms that potentially drive the changes observed. In both the M-CSF and RANKL group similar trends were observed. Specifically, there were reductions in the synthesis of key amino acids and inhibition of inflammatory pathways. This is potentially significant given both IL-6 and TNF-α were found to be reduced in preceding experiments. In a separate study examining the effects of vibration on macrophages, Pongkitwitoon *et al* found a similar pattern, with a significant reduction in IL-6, TNF-α and IFN-ϒ, and promotion of a M2 macrophage

phenotype following stimulation (Pongkitwitoon S et al, 2016). Regarding osteoclasts, Kulkarni *et al* found their differentiation to be reduced following mechanical stimulation secondary to inhibition of DC-STAMP – a downstream factor stimulated by RANKL (Kulkarni RN et al, 2013). Taken collectively, the RT-qPCR, ELISA and metabolomics results indicate a trend towards a lower inflammatory state in the nanokick group which would support the observations of reduced osteoclast numbers and function. Although this is promising, it is difficult to draw definitive conclusions from the metabolomics data and so further experiments would need to be conducted to validate the results seen.

Chapter 4 Nanoscale vibration of co-culture

4.1 Introduction

In the previous chapter, the effects of nanoscale vibration on a CD14+ culture were discussed. By studying this cell type in relative isolation, this allowed an assessment of how macrophages and osteoclasts respond to vibration without the influence of MSCs and osteoblasts. Ultimately, however, these cells do not exist in isolation. Rather, in the bone marrow niche, they are one component of a larger environment that functions through the complex interplay between differing cell types (Chen X et al, 2018).

As discussed in Chapter 1.1, bone is a complex environment containing cells that both generate and remove bone, allowing for normal homeostasis. Bone remodelling relies on a continual process of formation (by osteoblasts) and resorption (by osteoclasts) and is dependent on the interaction between the two cell types. Osteoblasts are derived from undifferentiated MSCs in contrast to osteoclasts which originate from HSCs (Buckwalter JA et al, 1996). Osteoblasts express receptor activator RANKL, which binds to its receptor, RANK, on osteoclasts and their precursors, leading to their activation and increased bone resorption. In contrast, OPG is a soluble decoy receptor, also produced by osteoblasts that binds to RANKL, preventing its interaction with RANK and therefore limiting bone resorption (Roodman GD, 1999). Given the close interaction between osteoblasts and osteoclasts, it is likely that a more bone like environment can be generated within the Nanokick bioreactor through use of both MSCs and BMHCs. A recent development in the area of tissue culture has been the co-culture technique (Young PS et al, 2015). This method involves combining MSCs and BMHCs from the same human bone marrow. It allows for a more accurate representation of the *in vivo* environment, enabling us to study how well the two cell types interact and generate more bone-like graft materials. The technique for processing this culture is detailed in Chapter 2.2. In a further effort to produce an environment more akin to the bone marrow niche, some experiments will be performed in 3D as well as 2D given these cells will normally interact in three dimensions.

4.2 Materials and methods

Experiments were conducted as detailed in the Materials and Methods chapter. As with the CD14+ culture, standard laboratory techniques and practices were followed. Cell numbers were kept standard across all experiments and 24 well plates used. Different time points were chosen from the CD14+ culture. As RANKL was not added, osteoclast formation was not present until around day 14. Furthermore, certain experiments that assess osteoblast function, such as Von Kossa staining, require a greater period of culture time for the desired effect to be observed (e.g. mineralisation). As such, the time points chosen were days 7, 14, 21 and 28.

4.3 Results

4.3.1 Osteoclast differentiation

As with the CD14+ culture, osteoclasts were defined as TRAP positive cells containing three or more nuclei. This allowed differentiation from other TRAP positive cells that would be present in the co-culture, namely macrophages.

A significant reduction in osteoclast number was observed in the nanokick group after 28 days of stimulation (Figure 4:1, mean cells per well 1641 in control group *cf* 1077 in nanokick, p=0.0019). Although the number of osteoclasts observed varied between donors, the reduction in the nanokick group was present throughout. This 34.4% reduction is comparable to the reduction in osteoclasts numbers observed in the CD14+ culture. The time point was different for the CD14+ culture (day 7 *cf* day 28) due to the addition of RANKL in this condition as discussed in Chapter 4.2, but mature osteoclasts were present in both cell cultures at their respective end points.

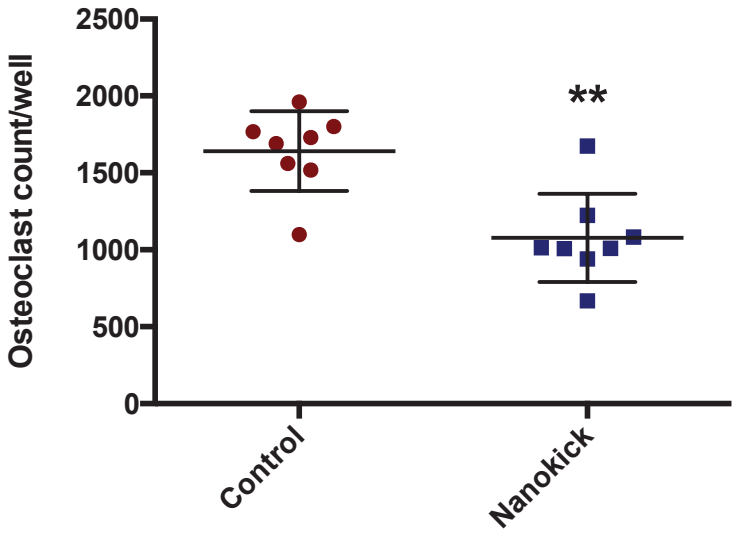

Figure 4:1 Co-culture osteoclast count.
Following 28 days of culture, TRAP staining demonstrated a significant reduction in osteoclasts numbers in the nanokick group. This reduction was of a comparable proportion to the CD14+ culture. Graph shows mean +/- SD. ** = p<0.01, by t-test. N=3 cell donors.

Just as with the CD14+ culture, measurement of mean osteoclast area in the co-culture demonstrated a reduction in the nanokick group (Figure 4:2, 5.5 mm^2 *cf* 4.1 mm^2, p=0.03). Given that osteoclasts are formed through the fusion of smaller cells, there can be a wide range of potential areas observed, as illustrated in Figure 4:3. This helps explain the large standard deviation present.

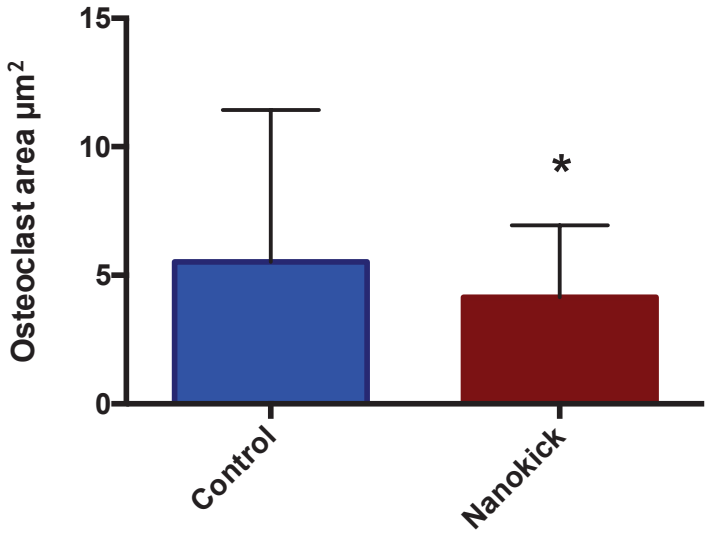

Figure 4:2 Co-culture osteoclast area.
Similar to the CD14+ culture, a significant reduction in osteoclast area was observed in the nanokick group after 28 days of culture. Graph shows mean +/- SD. * = p<0.05, by t-test. N=3 cell donors.

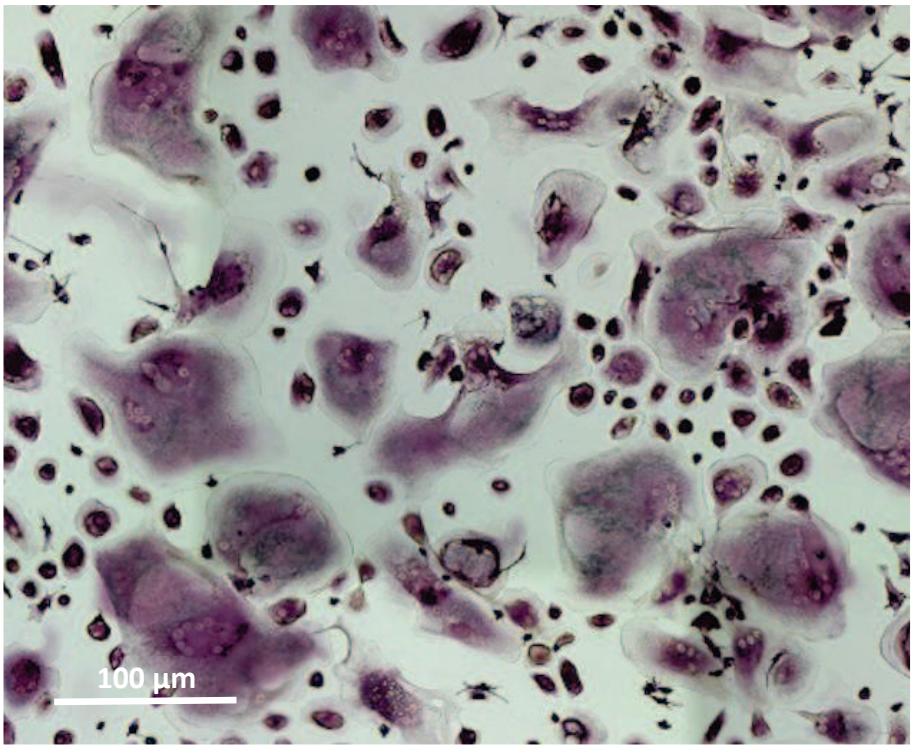

Figure 4:3 TRAP stained co-culture image.
10 x magnification brightfield microscopy image. The purple coloured multinucleated cells are osteoclasts. The osteoclasts are surrounded by smaller TRAP positive macrophages. In the co-culture, osteoclasts were typically around the periphery of the well, whereas MSCs/osteoblasts were more prolific in the central regions. It is not clear why this pattern was present, but was found to be the case in all samples. Previous studies did not find any significant differences in nanoscale displacement across the surface of the well that would account for this (Tsimbouri PM et al, 2017a). It potentially occurred due to the co-culture method requiring HSCs to be seeded several days after the MSCs had adhered to the well. This could potentially lead to the HSCs spreading out towards the periphery of the well if MSCs were already adhering to the centre.

4.3.2 AlamarBlue cell viability assessment

Given the observed differences in osteoclast number between the two groups, cell viability was assessed through use of alamarBlue to determine whether increased cell death or reduced metabolic activity was a factor. This was performed at day 7, 14 and 21. Although no difference was observed at day 7 or 21, a significant increase in alamarBlue reduction was found at day 14 (Figure 4:4, p=0.0056) in the nanokick group. This therefore indicates that increased cell death or reduced metabolic activity is not responsible for the reduction in osteoclast numbers observed in this group.

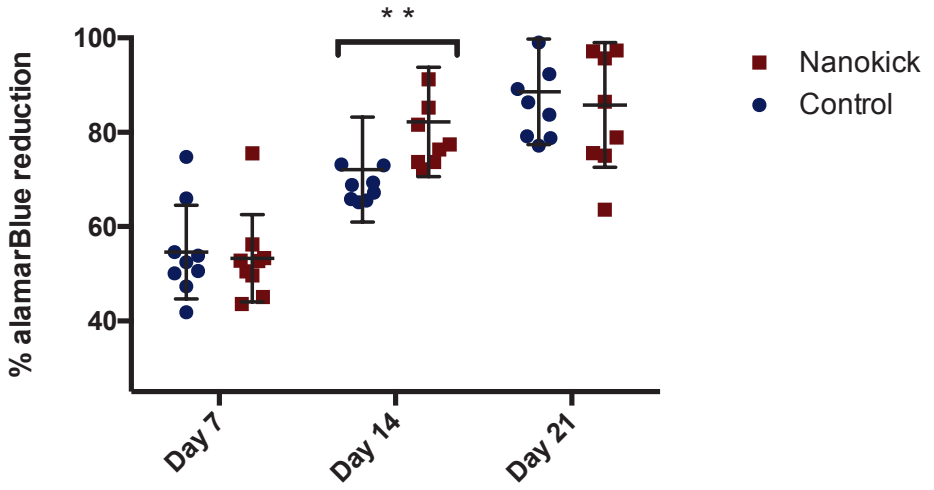

Figure 4:4 alamarBlue cell viability assay of co-culture.
Cell metabolic activity and viability was assessed via the alamarBlue assay at day 7, 14 and 21. A significant increase in alamarBlue reduction was measured in the nanokick group at day 14. No difference was found at day 7 or 21. Graph shows mean +/- SD. ** = p<0.01, by t-test. N=3 cell donors.

4.3.3 Cell viability in 3D collagen gel

Prior to experiments being conducted in 3D collagen gels, an assessment of the ability of the co-culture cells to survive was required. Live-dead staining was performed to visualise and measure the proportion of living cells in the 3D culture. This demonstrated >99% living cells present in the culture after seven days incubation (Figure 4:5). This therefore confirmed the 3D technique was able to support this cell culture.

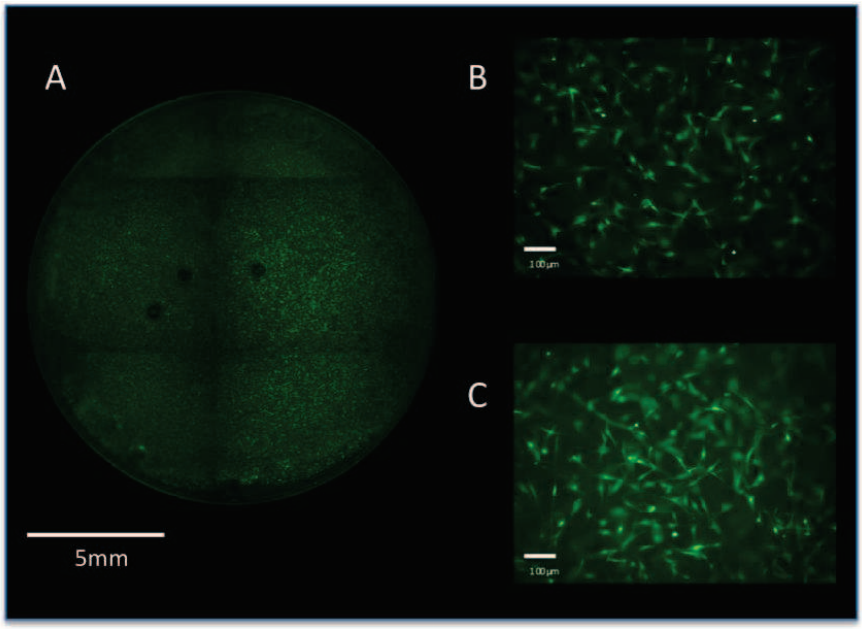

Figure 4:5 Live/dead stain microscopy images of 3D co-culture.
A – 2 x magnification with green/red light composite images of entire well in 24 well plate. B & C – 10 x magnification with green/red light composite images of selected areas of 3D collagen gel. >99% of cells were living in the gel. Green cells = live, red cells = dead.

4.3.4 Immunostaining

In Chapter 1.18, it was highlighted that previous studies involving nanoscale vibration of MSCs found features suggestive of increased cytoskeleton tension. Immunostaining was therefore performed in this study to determine whether this would still be the case when macrophages and osteoclasts were present in the culture.

A significant increase in vimentin (p=0.01) and tubulin (p=0.03) staining intensity was found in the nanokick group (Figure 4:6 and 4:7). Given that both of these proteins are key components of the cytoskeleton, being responsible for tensile stiffness (Fletcher DA and Mullins RD, 2010), it can be postulated that greater cytoskeleton tension was present in the nanokick group.

No difference was found in vinculin staining intensity (Figure 4:8). This is perhaps not surprising, however. Other authors found vinculin dispersion to be altered following nanoscale vibration, with movement from the periphery to the cells base and projections (Nikukar H et al, 2013). This suggests there may be no difference in the quantity of vinculin present, just its location within the cell. A similar appearance was present in this study, as demonstrated in Figure 4:9. The distribution is present throughout the cell in the nanokick group, rather than being focused towards the periphery. Furthermore, the nanokick cells took on a more elongated appearance, compared to the relatively round/square composition of the control. In being elongated, or “stretched’, it is possible this reflects the greater cellular tension that is present. Given the alterations in these surrogate markers of cytoskeleton tension, this infers the current study is in keeping with the finding of other authors. As such, the presence of macrophages and osteoclasts does not significantly affect the observable changes in cytoskeleton tension.

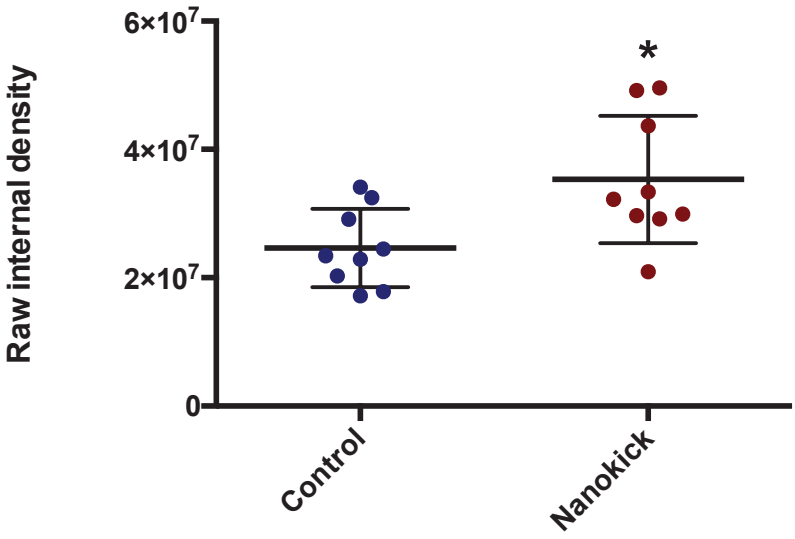

Figure 4:6 Vimentin staining intensity.
Vimentin staining intensity was significantly increased in the nanokick group. Staining was performed after 28 days stimulation. Graph shows mean +/- SD. * = p<0.05, by t-test. N=3 cell donors.

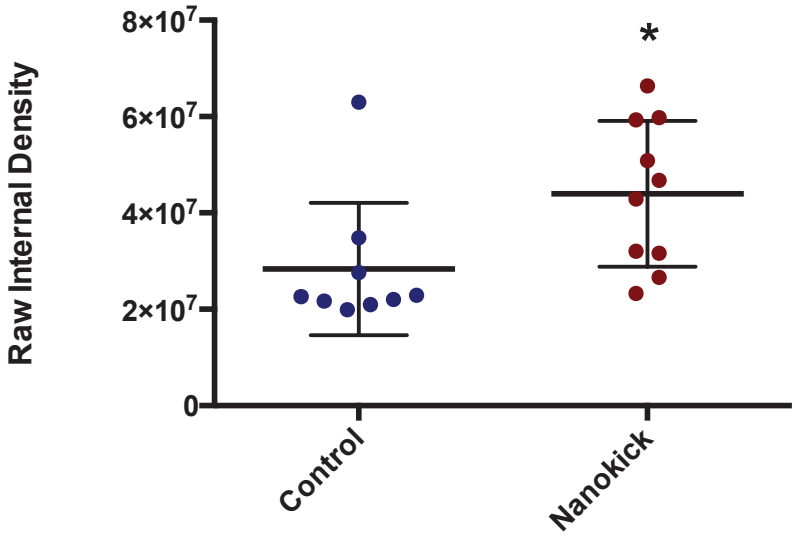

Figure 4:7 Tubulin staining intensity.
Vimentin staining intensity was significantly increased in the nanokick group. Staining was performed after 28 days stimulation. Taken alongside the vimentin result above, this suggests increased cytoskeleton tension was present in the nanokick group. Increased cytoskeleton tension is associated with the promotion of osteogenesis in MSCs. Graph shows mean +/- SD. * = p<0.05, by t-test. N=3 cell donors.

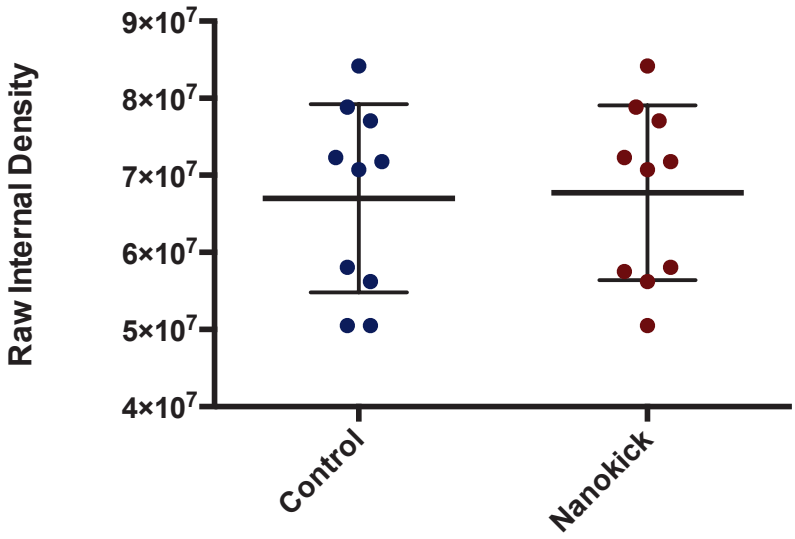

Figure 4:8 Vinculin staining intensity.
There was no difference in vinculin staining intensity between the two groups following 28 days of stimulation. There were changes in the distribution of vinculin, however, as seen in the figure below. Graph shows mean +/- SD. N=3 cell donors.

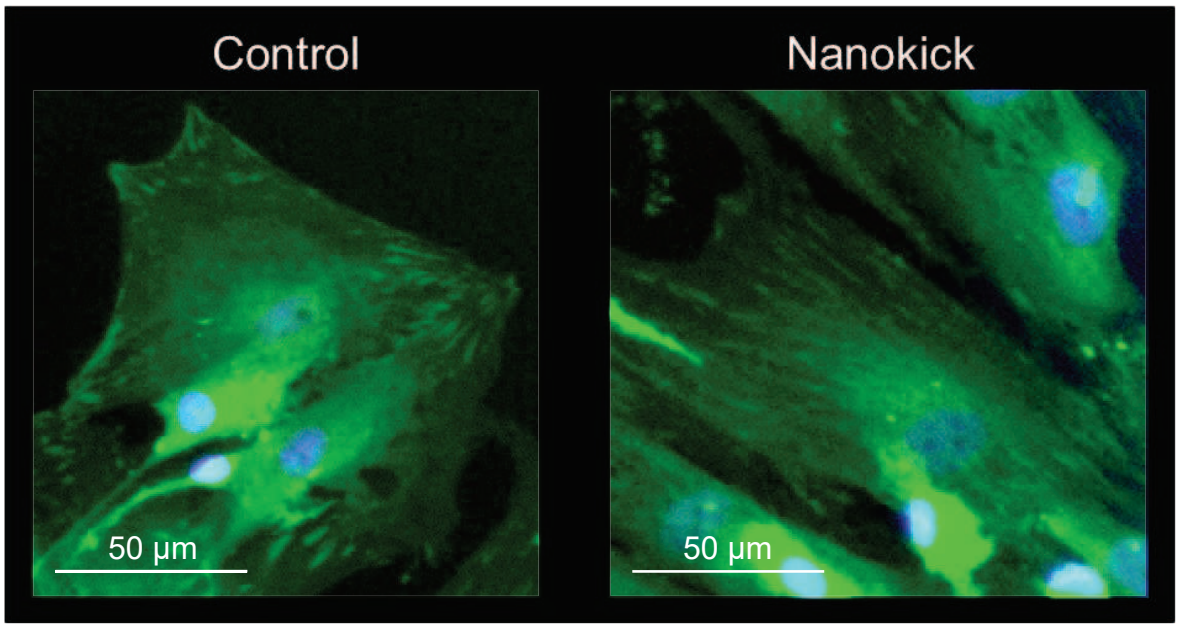

Figure 4:9 Vinculin staining of co-culture.
10 x magnification immunofluorescence images of co-culture demonstrating differences in distribution if vinculin between the control and nanokick group following 28 days culture. Vinculin can be seen located predominantly at the periphery of the control cells, compared to throughout the nanokick cells. The cell shapes also differed, with more elongation noted in the nanokick group. Vinculin = green, DAPI stained nucleus = blue.

Staining for the presence of an actin ring was subsequently undertaken. An actin ring is an indicator of mature osteoclastogenesis. This was therefore undertaken to provide evidence the co-culture technique could support the development of this cell type. Both the control and nanokick groups stained positively for an actin ring (Figure 4:10), thus supporting the use of this culture technique.

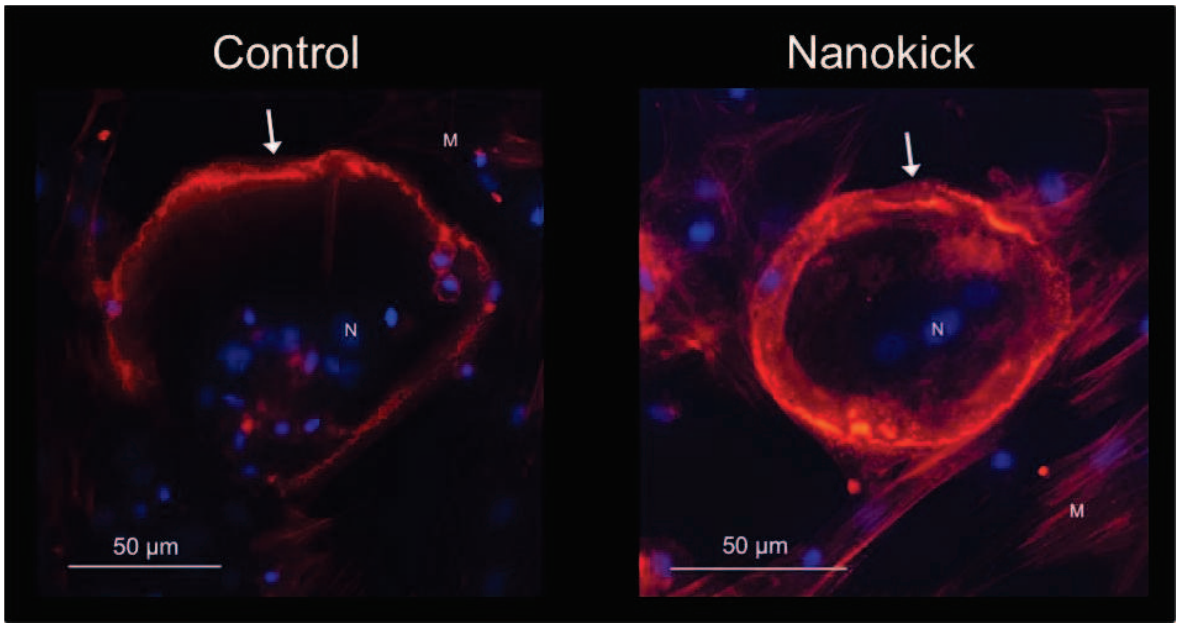

Figure 4:10 Actin ring staining of osteoclasts in co-culture.
Both images demonstrate the presence of an actin ring in the osteoclasts; a feature indicative of mature osteoclast formation. The white arrows point to the actin ring. N = an osteoclast nuclei, stained with DAPI. M = MSC present alongside the osteoclast as part of the co-culture.

4.3.5 Scanning electron microscopy

TRAP staining had demonstrated a reduction in osteoclast numbers and area, and immunostaining identified possible alterations in cytoskeleton tension. SEM was therefore undertaken to identify any potential morphological changes between the control and nanokick group when viewed in more detail. Cells were cultured for 14 days and prepared for SEM as per Chapter 2.9.

The microscopic appearance of the control and nanokick groups was broadly similar. Osteoclasts were observed in close relation to MSCs, with the characteristic filopodia being identified on the periphery of the osteoclasts. Filopodia play an important role in cell migration (Mattila PK and Lappalainen P, 2008). The length and number of filopodia between the two groups was grossly similar. However, in the control group the occasional significantly larger osteoclast was observed (as depicted in Figure 4:11, A). No osteoclasts of a similar size were found in the nanokick group (Figure 4:12). This observation conforms with the TRAP staining result, where a greater mean osteoclast size was found in the control group.

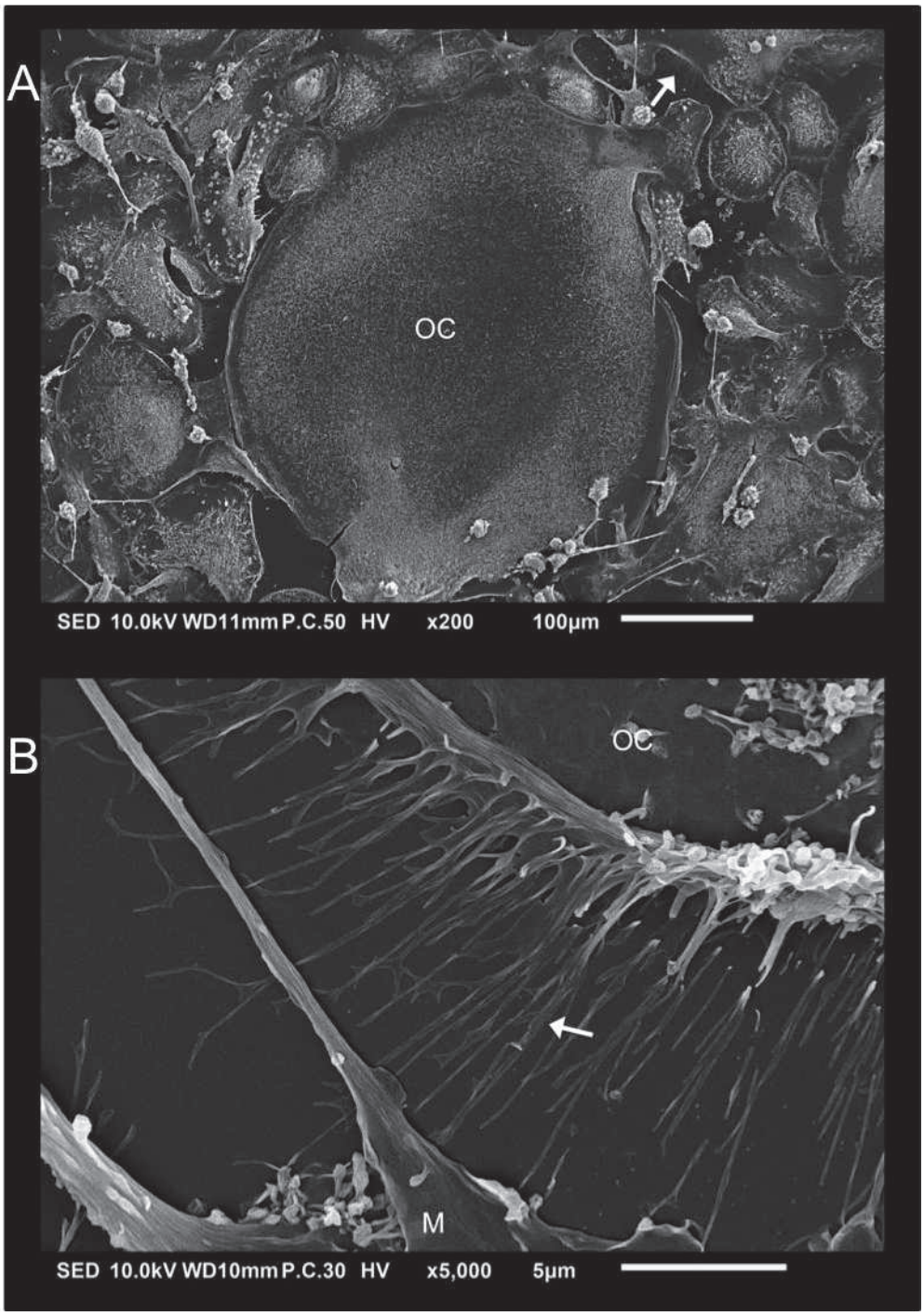

Figure 4:11 SEM images of co-culture control.
A – 200 x magnification displaying a large osteoclast surrounded by smaller osteoclasts. The image potentially illustrates fusion occurring given the close proximity of the cells. B – 5000 x magnification image of osteoclast filopodia and an adjacent MSC. OC = osteoclast; M = MSC; arrow = filopodia.

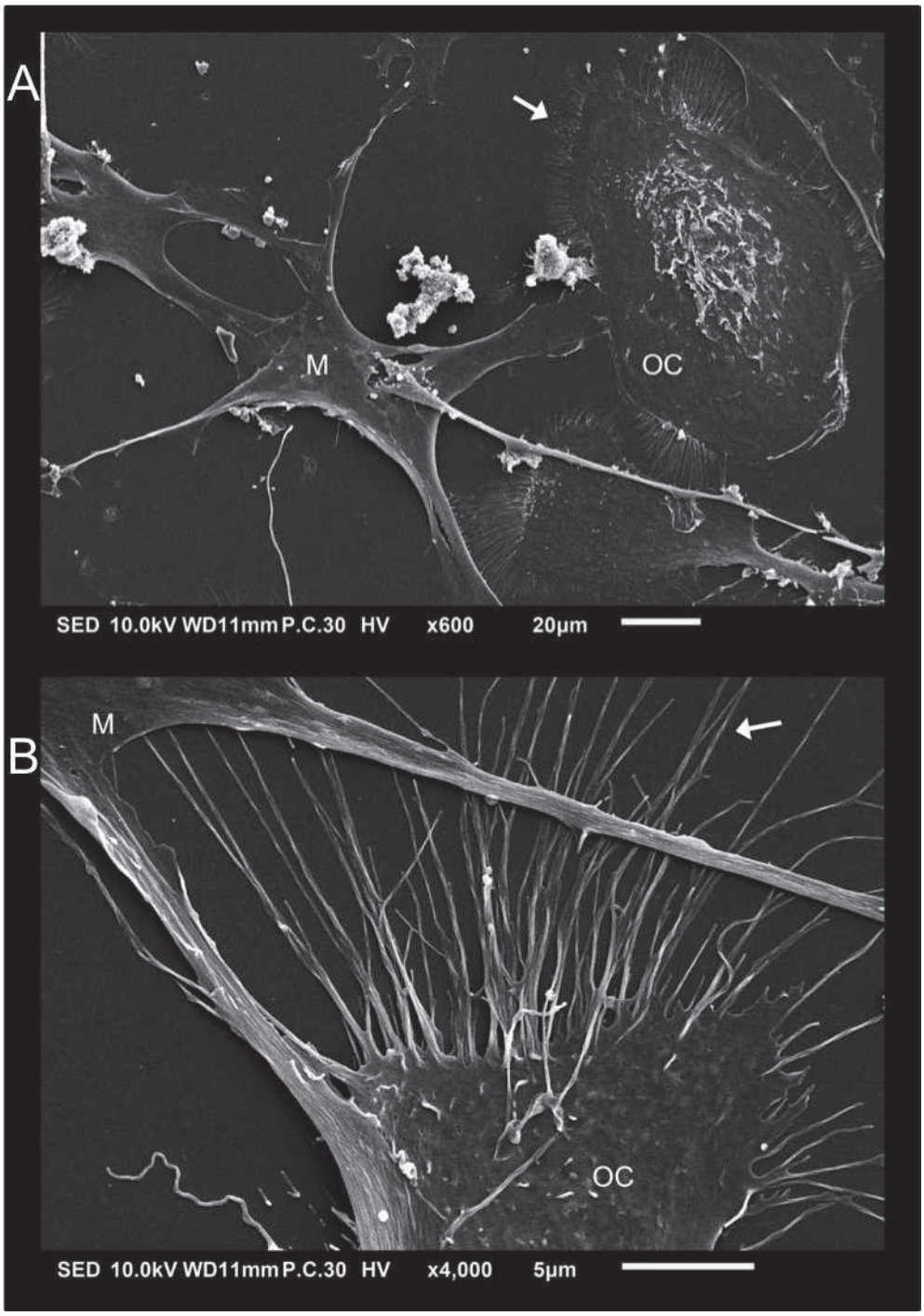

Figure 4:12 SEM images of co-culture following nanoscale vibration.
A – 600 x magnification image of osteoclast and MSC. B – 4000 x magnification image displaying filopodia in greater detail. OC = osteoclast; M = MSC; arrow = filopodia.

4.3.6 Mineralisation analysis

4.3.6.1 2D monoculture Von Kossa stain

Von Kossa staining facilitates measurement of bone mineralisation. This measurement is therefore pertinent to this study as ultimately the aim of the Nanokick bioreactor is to stimulate osteogenesis and bone development. Other authors demonstrated greater levels of mineralisation for MSCs cultured in

isolation (i.e. no osteoclasts or other cell types were present) (Tsimbouri PM et al, 2017b, Childs PG et al, 2016). To confirm this effect, Stro-1+ cells (a more primitive subset of MSCs (Ning H et al, 2011)) were isolated and cultured for 28 days. The entire well was imaged and the surface area with mineralisation present measured. A significant increase in mineralisation was found in the nanokick group (p=0.01, Figure 4:13). This corroborated the evidence presented by other authors and so Von Kossa analysis was then performed on the co-culture.

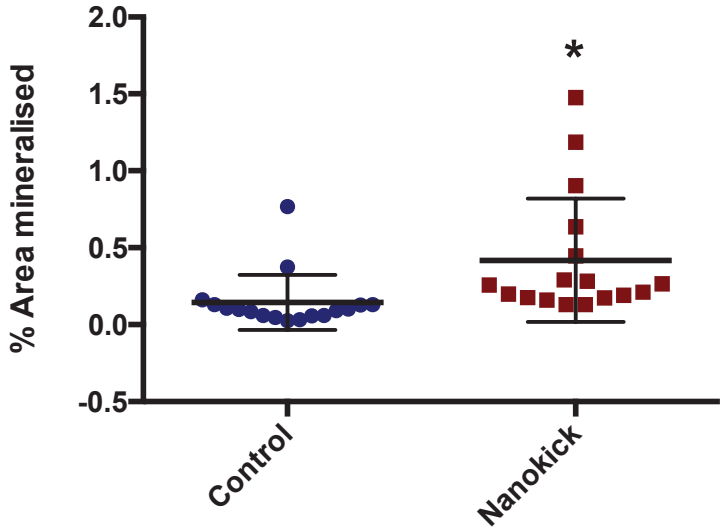

Figure 4:13 Von Kossa staining of Stro-1+ MSC culture.
The nanokick group had a significant increase in the percentage area of the well mineralised (0.14% *cf* 0.42%). Graph shows mean +/- SD. * = p<0.05, by t-test. N=3 cell donors.

4.3.6.2 2D co-culture Von Kossa

Nanoscale vibration produced a significant increase in mineralisation in the 2D co-culture (Figure 4:14). The increased was of a similar proportion to the monoculture illustrated above (i.e. 3-fold change for Stro-1+ MSC culture, 2-fold change in co-culture). This suggests that the presence of macrophages and osteoclasts does not significantly interfere with the ability of osteoblasts to form bone when exposed to vibration.

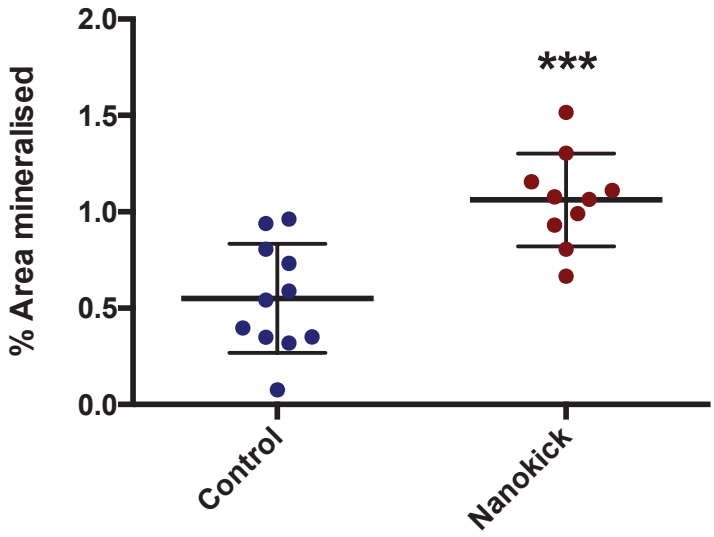

Figure 4:14 Von Kossa stain analysis of 2D co-culture.
A significant increase in mineralisation was found in the nanokick group (0.55% *cf* 1.06%). Graph shows mean +/- SD. *** = $p<0.001$, by t-test. N=3 cell donors.

4.3.6.3 3D co-culture Von Kossa

Collagen gels were seeded with the co-culture and stained with Von Kossa after 28 days. A significant increase in mineralisation was found in the nanokick group (Figure 4:15), in keeping with the 2D data. Although the change was statistically significant, the absolute difference was comparatively small when viewed alongside the 2D results. It is possible that this is related to difficulties in assessing the quantity of mineralisation in collagen gels. In 2D, discrete nodules of mineralisation were present on the surface of the well that are measured and taken as a percentage of the surface area. In 3D, the collagen gels would reduce in size with time due to the contractile nature of MSCs. The degree of contraction was frequently greater in the nanokick group (Figure 4:16), which conforms to the increased cytoskeleton tension evidenced earlier in Chapter 4.3.4. Given the difference in size of the gels between groups, and the limitations of viewing 3D structures with microscopy, measuring the size of mineralised material as a percentage of the well surface area was not appropriate. Instead, mineralisation was measured and calculated as a percentage of the total size of the gel.

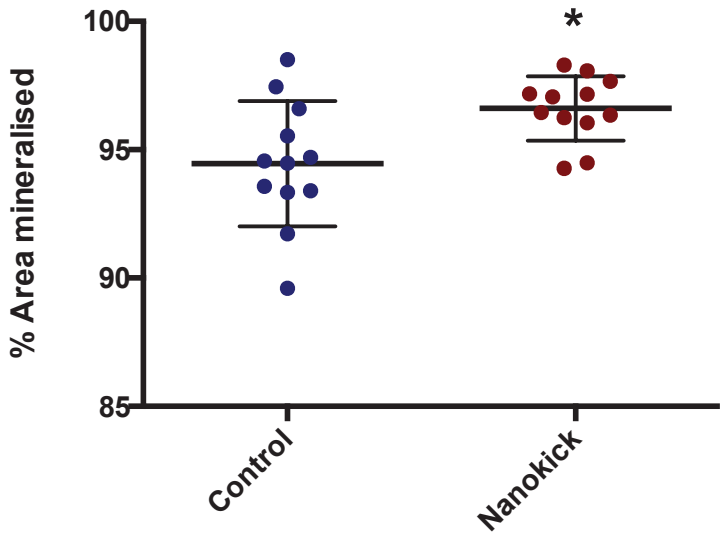

Figure 4:15 Von Kossa staining results of 3D co-culture.
A significant increase in mineralisation was found in the nanokick group compared to the control. Graph shows mean +/- SD. * = p<0.05, by t-test. N=3 cell donors.

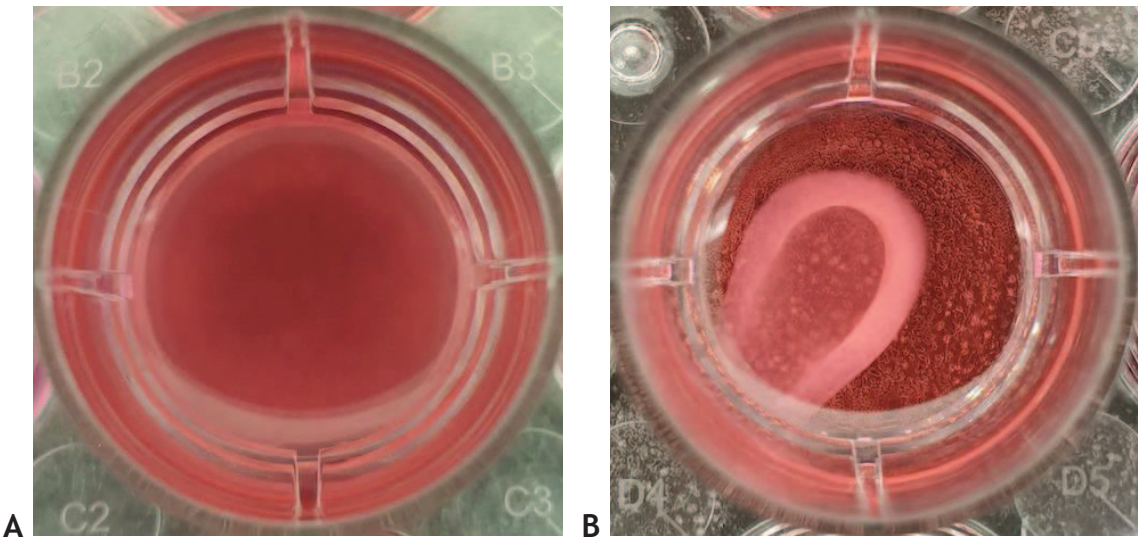

Figure 4:16 Images of 3D co-culture of control and nanokick groups.
Figure A shows the control group, while B displays the nanokick group. Both images are of a single well in a 24 well plate after 14 days culture. As discussed in the 3D Von Kossa section, there was a visual difference in the size of the collagen gels between the two groups as the culture progressed. In Figure A there is minimal change in the appearance of the gel, with only slight contraction of the gel at the lower edge being visible. Conversely, in Figure B significant contraction of the gel can be seen, with the thick white oval shape representing the outer edge of the gel that initially occupied the entirety of the well.

4.3.7 Gene expression

RT-qPCR was performed to assess for differences in gene expression between the control and the nanokick group. This was performed in an effort to better understand the mechanism leading the aforementioned changes produced through nanoscale vibration. Cells were cultured as previously described, both in 2D and 3D, and RNA extracted at days 7, 14, 21 and 28. The different approaches to RNA

extraction for the 2D and 3D culture are detailed in Chapter 2.12. A range of primers was chosen to provide adequate insight into osteoclastogenesis.

4.3.7.1 2D co-culture RT-qPCR

A significant reduction in IL-6 expression was observed in the nanokick group at day 14 (Figure 4:18, p=0.001). IL-6 is a pro-inflammatory cytokine that is crucial for the development of mature osteoclasts (Wu Q et al, 2017). OSCAR was also significantly reduced in the nanokick group (Figure 4:19, p=0.05). OSCAR plays an important role in osteoclast differentiation and maturation (Nemeth K et al, 2011), and therefore reduced levels of this gene links to the lower number of osteoclasts observed through TRAP staining. Although not statistically significant, there appeared to be a trend towards higher production of OPG at days 7 and 14. OPG can limit bone resorption by inhibiting the action of RANKL, which drives osteoclast differentiation (Boyce BF and Xing L, 2007). Similar to the IL-6 and OSCAR findings, these results align themselves with the earlier findings of increased bone mineralisation and reduced osteoclast numbers. The heatmaps displayed below (Figure 4:17) highlight the trends in gene expression. Statistically significant changes are highlighted with independent graphs.

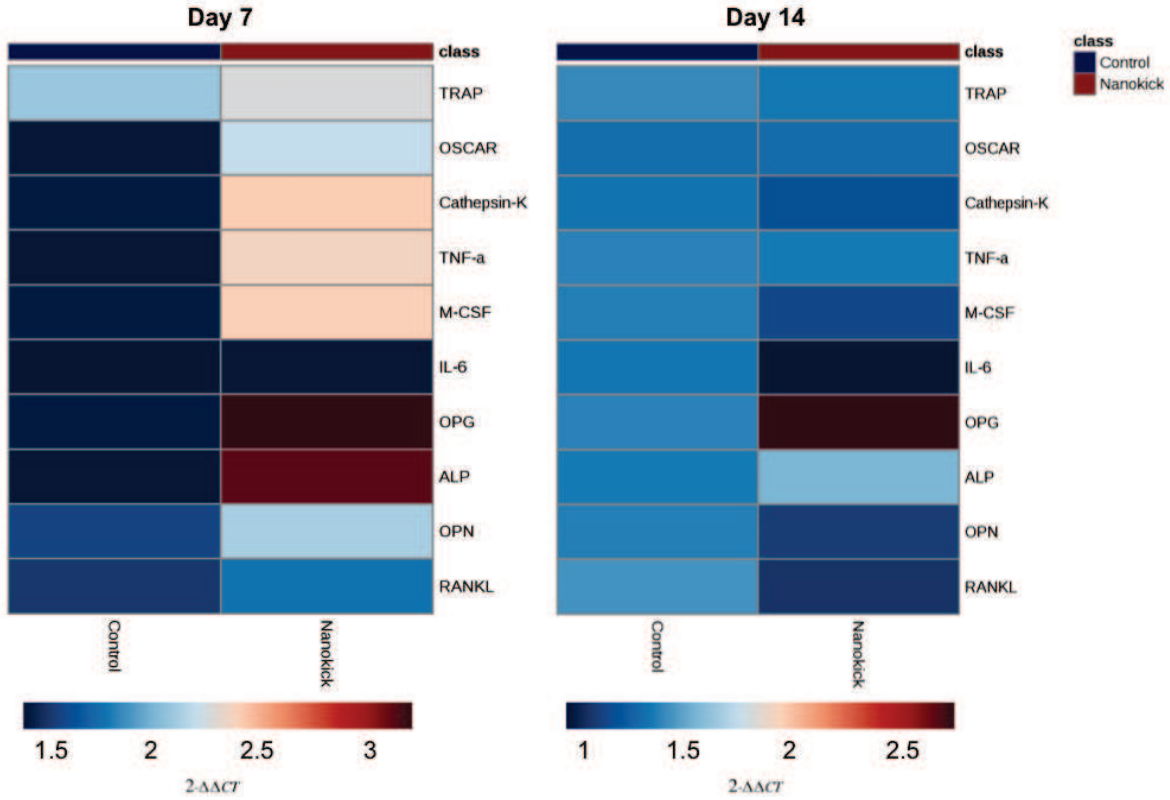

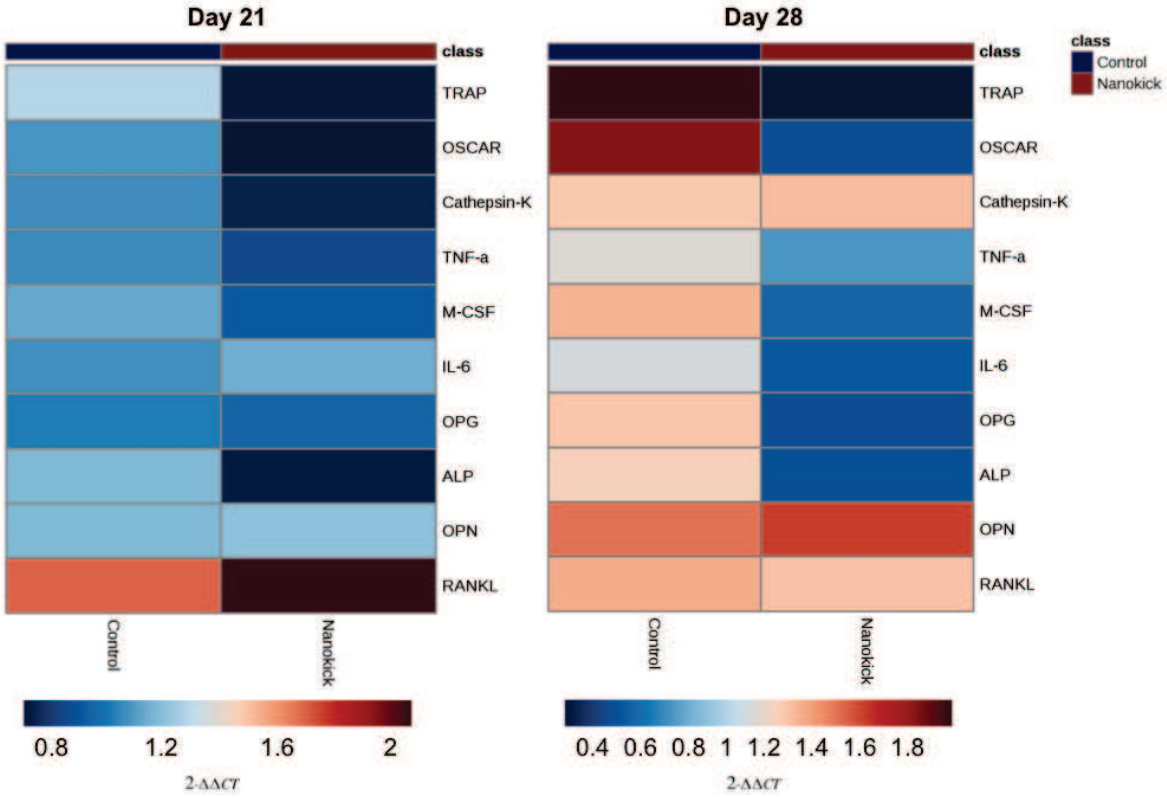

Figure 4:17 RT-qPCR heatmap of 2D co-culture.
Day 7 - There were a number of differences in gene expression at this time point. OPG (an inhibitor of osteoclastogenesis) and ALP (an osteogenic gene) had the greatest upregulation in the nanokick group compared to the control. There was no statistically significant difference between either of the groups however. N=1 cell donor. Day 14 - There was a statistically significant reduction in IL-6 production in the nanokick group at this time point. A number of other changes which did not reach statistical significance were also noted, including an increase in the osteoclast inhibitory gene OPG (also noted at day 7), and a reduction in pro-osteoclast gene RANKL. N=3 cell donors. Day 21 – there was a general trend towards a reduction in gene expression in the nanokick group. A statistically significant reduction in pro-osteoclast gene OSCAR was identified. N=3 cell donors. Day 28 - The overall trend by day 28 was a reduction in gene expression in the nanokick group, although none of these differences reached statistical significance. The greatest difference was noted in the reduction of osteoclast markers TRAP and OSCAR in the nanokick group. N=1 cell donor.

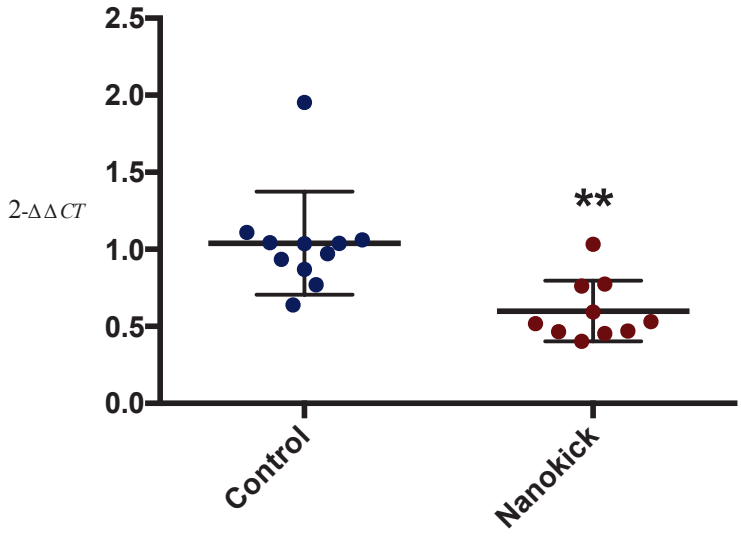

Figure 4:18 IL-6 RT-qPCR result of 2D co-culture at day 14.
IL-6 proved to be the only statistically significant gene difference at day 14. The pro-inflammatory cytokine was reduced in the nanokick group. Graph shows mean +/- SD. ** = p<0.01, by t-test. N=3 cell donors.

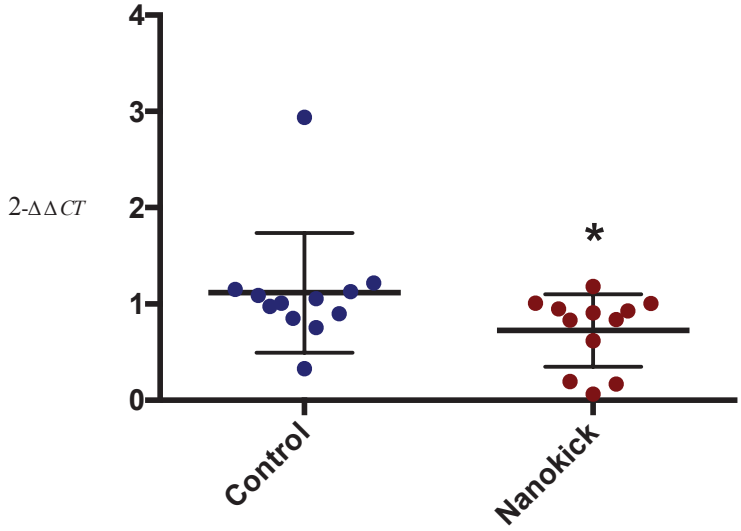

Figure 4:19 OSCAR RT-qPCR result of 2D co-culture at day 21.
The pro-osteoclast gene OSCAR was significant reduced in the nanokick group. OSCAR is important in osteoclast differentiation and maturation (Nemeth K et al, 2011). Graph shows mean +/- SD. * = $p<0.05$, by t-test. N=3 cell donors.

4.3.7.2 3D co-culture RT-qPCR

There were two statistically significant changes in gene expression identified in the 3D co-culture: cathepsin-K (Figure 4:21) and OPN (Figure 4:22) were both increased in the nanokick group at day 7 ($p<0.001$ in both genes). Cathepsin-K is an enzyme responsible for the degradation of type 1 collagen, and therefore, bone resorption (Saftig P et al, 2000). The role of OPN is more complex. While some authors have shown OPN promotes bone formation during mechanical stress (Morinobu M et al, 2003a), others have found it inhibits mineralisation, prevents ectopic calcification and inhibits vascular calcification (Lund SA et al, 2009). Although not statistically significant beyond day 7, cathepsin-K and OPN remained elevated at days 14 and 21, whilst the majority of other genes were reduced in the nanokick group. This reversed by day 28, however, with the majority of genes being increased in the nanokick group, with the exception of pro-osteoclast markers OSCAR and cathepsin-K (Figure 4:20). As noted, these changes did not reach statistical significance.

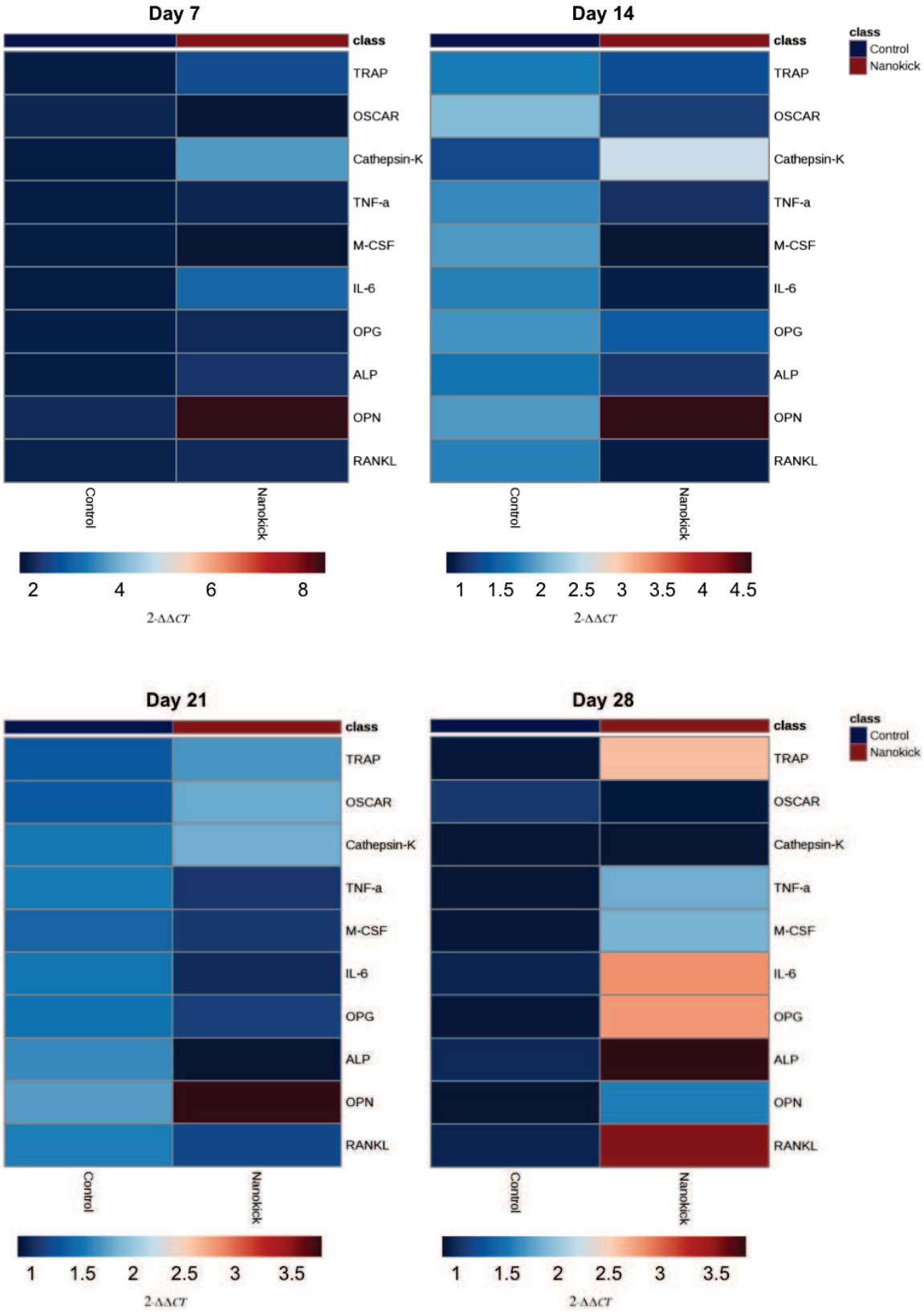

Figure 4:20 RT-qPCR heatmaps of 3D co-culture.
Day 7 - there were two statistically significant changes at this time point: an increased in both cathepsin-K and OPN in the nanokick group. Cathepsin-K is a pro-osteoclast gene, being involved in bone resorption, and conversely OPN is crucial to bone formation. N=2 cell donors. Day 14 - no statistically significant difference was found between any of the genes. N=4 cell donors. Day 21 - no statistically significant difference was observed between any genes at this time point, although there were similar trends to the day 14 results. N=4 cell donors. Day 28 – there was no statistically significant difference between any genes at this time point. There was a trend towards increases in gene expression in the nanokick group (with the exception of pro-osteoclast genes OSCAR and cathepsin-K), with the largest increase being observed in osteoblast marker ALP. N=2 cell donors.

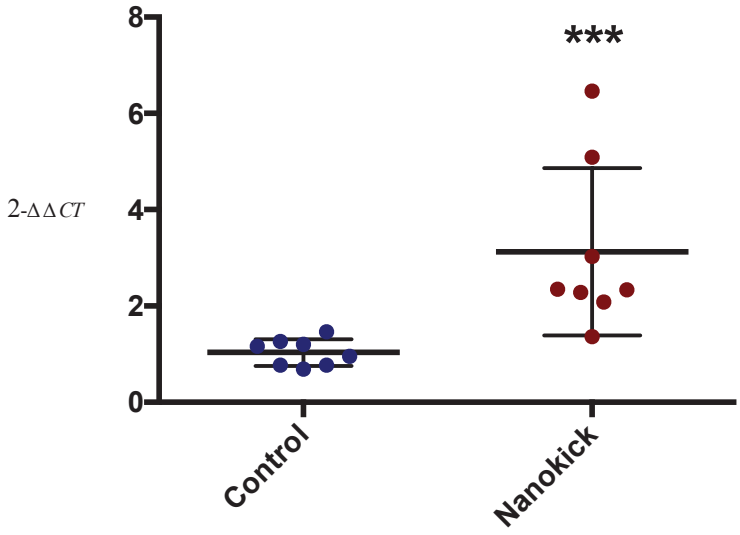

Figure 4:21 Cathepsin-K RT-qPCR results of 3D co-culture at day 7.
As highlighted in the heatmap above, cathepsin-K was significantly increased in the nanokick group. Graph shows mean +/- SD. *** = p<0.001, by t-test. N=2 cell donors.

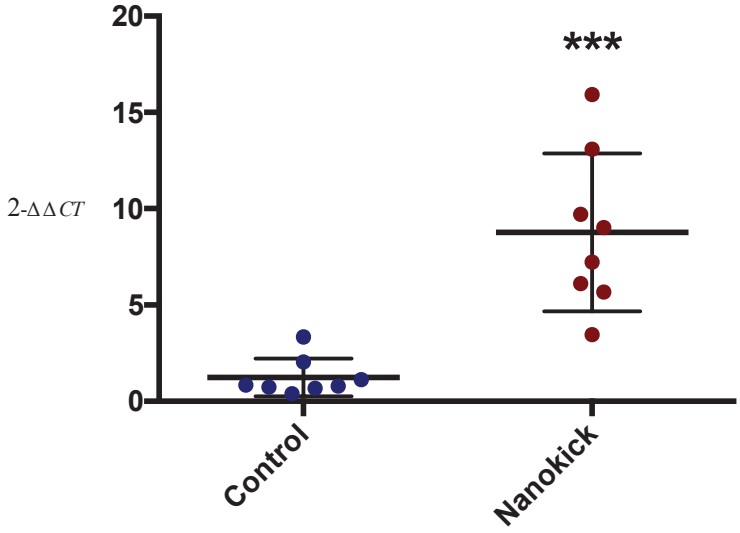

Figure 4:22 OPN RT-qPCR results of 3D co-culture at day 7.
OPN was also significantly increased in the nanokick group at day 7. Graph shows mean +/- SD. *** = p<0.001, by t-test. N=2 cell donors.

4.3.8 Protein assay

RT-qPCR had demonstrated alterations at a gene level. An assessment of protein production by the cell cultures was next undertaken to determine whether they correlated with the gene changes. Three proteins were examined: IL-6, TNF-α (both osteoclast stimulatory) and OPG (osteoclast inhibitory). The ELISA experiments were performed as detailed in Chapter 2.13. Two times points were assessed: day 14 and 21. Both times points were conducted in 2D and 3D.

4.3.8.1 2D ELISA

There were no significant differences in protein levels identified at day 14 (Figure 4:23). However, IL-6 was noted to be slightly lower in the nanokick group (1606 *cf* 1384 pg/ml). When comparing each of the three individual donors, one was significantly lower in the nanokick group (1435 *cf* 960 pg/ml, p=0.01). On review of the three OPG donors, one was found to have significantly higher levels in the nanokick group (4186 *cf* 5173, *p*=0.007).

Moving on to day 21, a significant reduction in IL-6 was found in the nanokick group (Figure 4:24). The lower level of IL-6 ties in with the similarly significant reduction in this gene identified in the RT-qPCR analysis at day 14. As with the day 14 ELISA data, further analysis of each individual donor revealed one had a significant increase in OPG (7989 *cf* 9279 pg/ml, *p*=0.02).

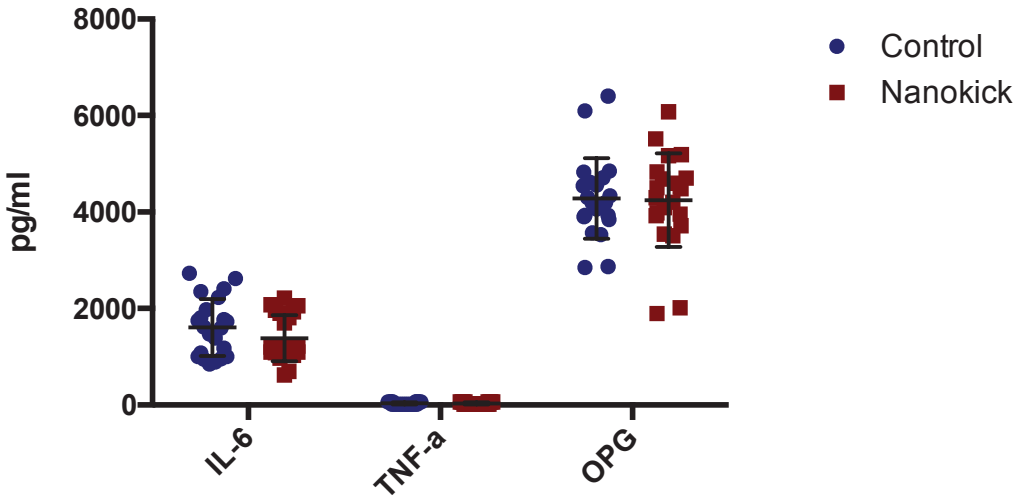

Figure 4:23 ELISA result of 2D co-culture at day 14.
No significant difference was found in any of the protein levels at this time point. IL-6 levels were lower but this was no statistically significant. Graph shows mean +/- SD. N=3 cell donors.

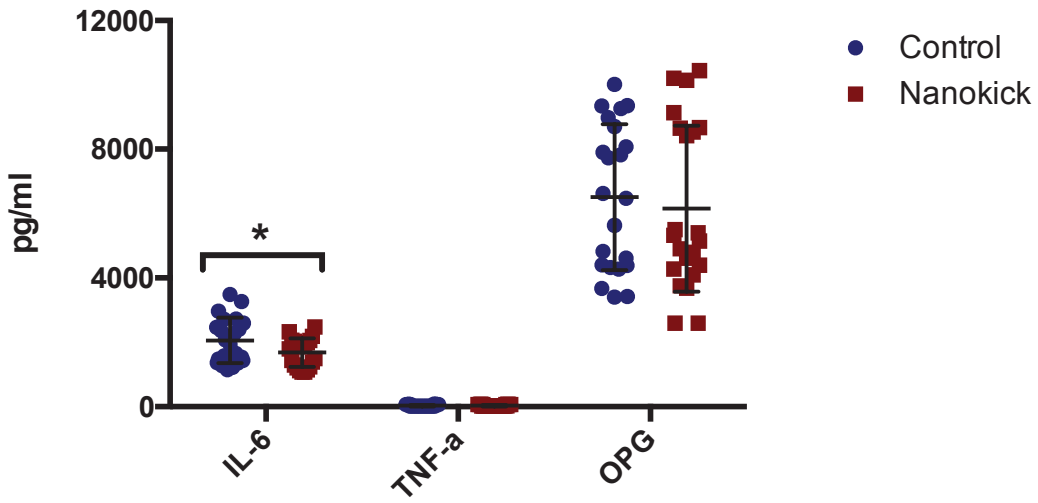

Figure 4:24 ELISA result of 2D co-culture at day 21.
A significant reduction in IL-6 was observed in the nanokick group (2059 *cf* 1681 pg/ml). There was no difference in TNF- α and OPG production. Graph shows mean +/- SD. * = $p<0.05$, by t-test. N=3 cell donors.

4.3.8.2 3D ELISA

At day 14, no significant differences were identified between the two groups (Figure 4:25). The same picture was present at day 21 (Figure 4:26). However, when each individual donor was examined, a significant reduction in IL-6 was found in all three in the nanokick group (Figure 4:27). The wide disparity between the donors resulted in a non-significant result when combined. It is not surprising that there will be differences found between individuals, but regardless of inherent disparities nanoscale vibration produced a reduction in the secretion of IL-6. This conforms to the 2D ELISA and RT-qPCR results.

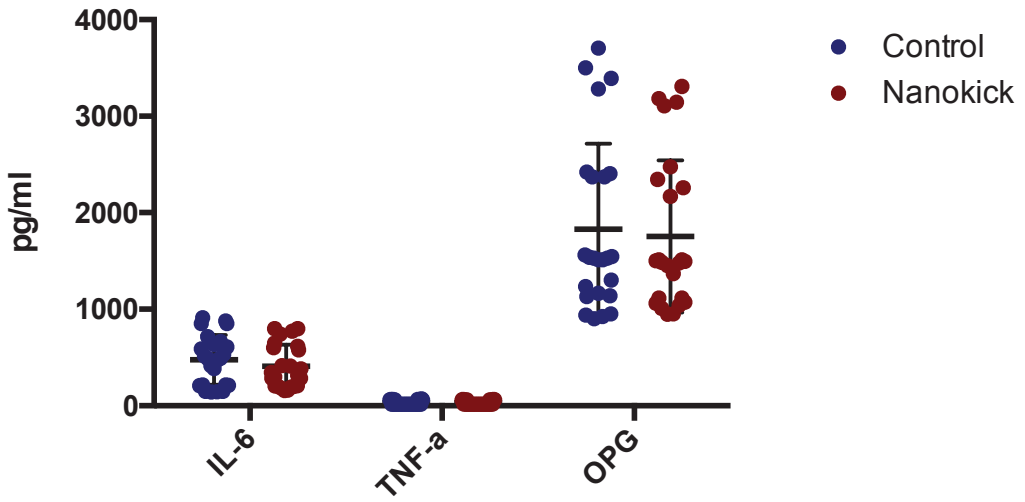

Figure 4:25 ELISA results of 3D co-culture at day 14.
There was no significant difference between any of the assays at day 14. Graph shows mean +/- SD. N=3 cell donors.

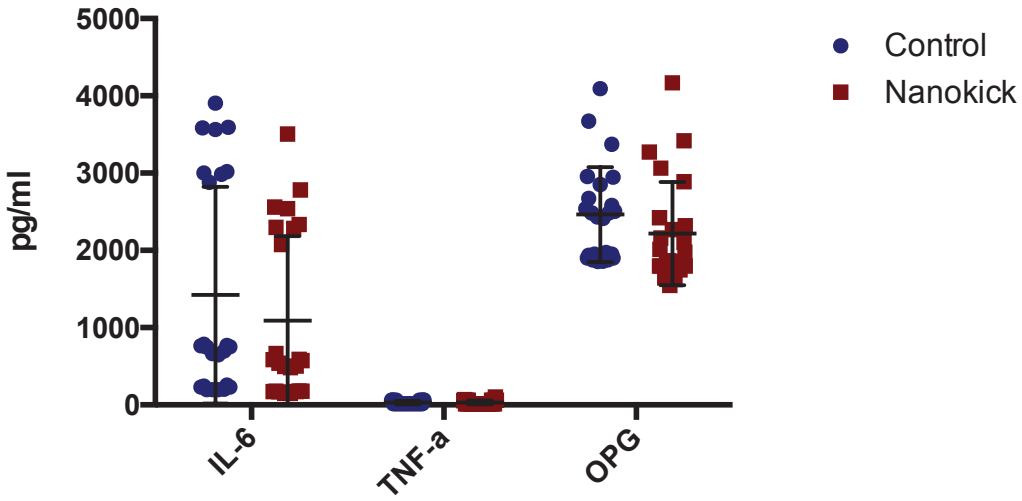

Figure 4:26 ELISA results of 3D co-culture at day 21.
Although there was no difference in any of the assays at day 14, all three of the IL-6 results when analysed independently showed a significant reduction in the nanokick group. This is highlighted in Figure 4:27. Graph shows mean +/- SD. N=3 cell donors.

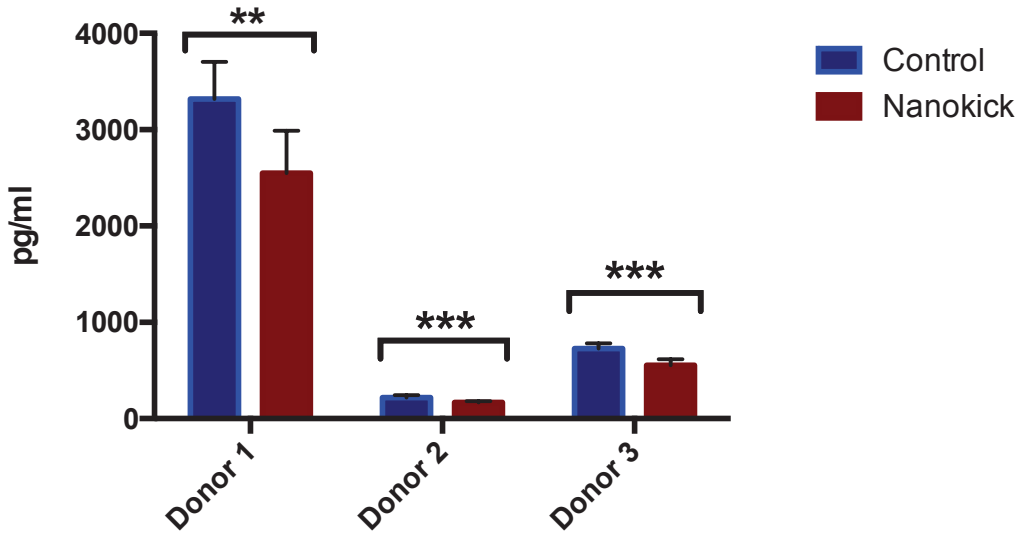

Figure 4:27 ELISA IL-6 result of 3D co-culture at day 21.
When each donor was examined independently, all were found to have a significant reduction in the nanokick group. The variation between donors highlights the natural disparity that can be present when comparing individuals. Donor 1 – 3316 *cf* 2547 pg/ml. Donor 2 – 220 *cf* 169 pg/ml. Donor 3 – 729 *cf* 555 pg/ml. Graph shows mean +/- SD. ** = $p<0.01$, *** = $p<0.001$, by t-test.

4.3.9 Metabolomics

4.3.9.1 2D co-culture

Metabolites were extracted from the 2D and 3D cultures at day 14 and 21. Experiments were performed as detailed in Chapter 2.15. IPA was used to analyse the data and produce graphs of the highest scoring pathways and networks.

At both day 14 and 21, the majority of significant changes observed in the pathway analysis were in relation to amino acid synthesis (Figure 4:28). On review of the

literature, some of these amino acids have been found to play significant roles in bone formation and osteoclastogenesis. Proline is a key constituent of collagen (Barbul A, 2008), one of the most abundant components in bone (Tzaphlidou M, 2008), and was increased in the nanokick group. Conversely, both glutamine and serine were reduced. Glutamine is essential for osteoclast differentiation (Indo Y et al, 2013), and serine is required for NFAT2 induction by RANKL as discussed in the CD14+ metabolomics results section (Ogawa T et al, 2006, Pollari S et al, 2011). The antioxidant glutathione was also reduced in the nanokick group. Although previously thought to inhibit osteoclastogenesis, it has since been shown to accelerates osteoclast differentiation by promoting TNF-α stimulated osteoclast formation (Fujita H et al, 2019).

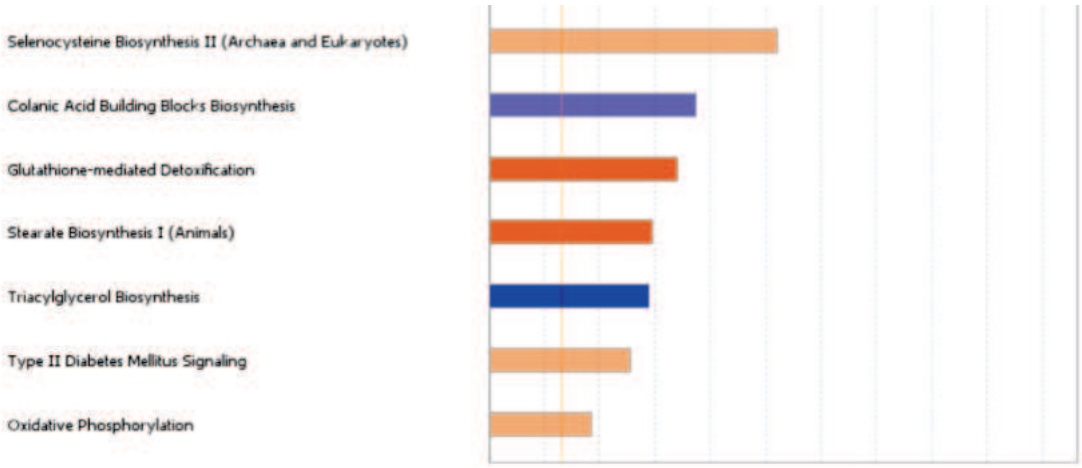
Selenocysteine Biosynthesis II (Archaea and Eukaryotes)
Colanic Acid Building Blocks Biosynthesis
Glutathione-mediated Detoxification
Stearate Biosynthesis I (Animals)
Triacylglycerol Biosynthesis
Type II Diabetes Mellitus Signaling
Oxidative Phosphorylation

B

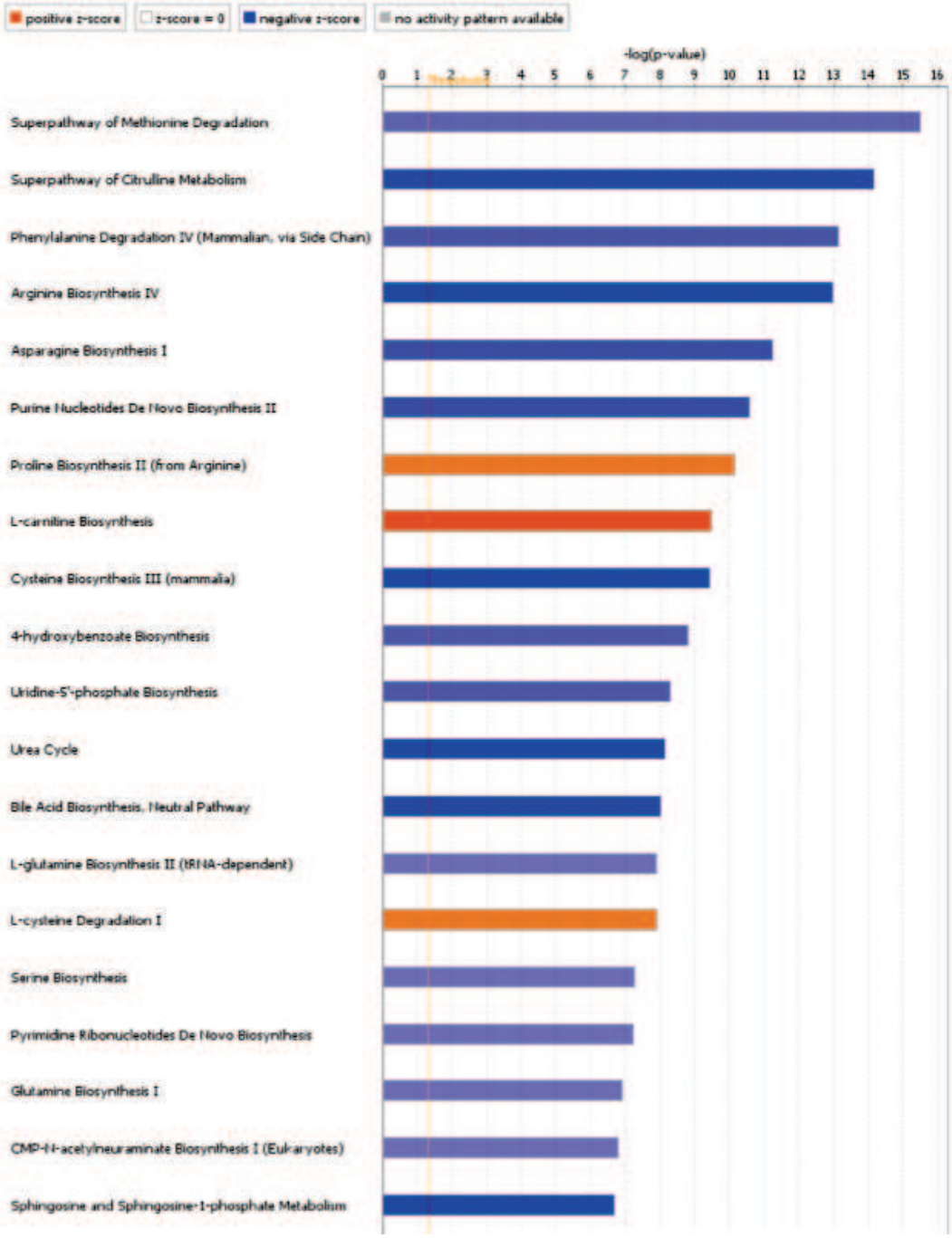
positive z-score
z-score = 0
negative z-score
no activity pattern available
-log(p-value)
0 1 2 3 4 5 6 7 8 9 10 11 12 13 14 15 16
Superpathway of Methionine Degradation
Superpathway of Citrulline Metabolism
Phenylalanine Degradation IV (Mammalian, via Side Chain)
Arginine Biosynthesis IV
Asparagine Biosynthesis I
Purine Nucleotides De Novo Biosynthesis II
Proline Biosynthesis II (from Arginine)
L-carnitine Biosynthesis
Cysteine Biosynthesis III (mammalia)
4-hydroxybenzoate Biosynthesis
Uridine-5'-phosphate Biosynthesis
Urea Cycle
Bile Acid Biosynthesis, Neutral Pathway
L-glutamine Biosynthesis II (tRNA-dependent)
L-cysteine Degradation I
Serine Biosynthesis
Pyrimidine Ribonucleotides De Novo Biosynthesis
Glutamine Biosynthesis I
CMP-N-acetylneuraminate Biosynthesis I (Eukaryotes)
Sphingosine and Sphingosine-1-phosphate Metabolism

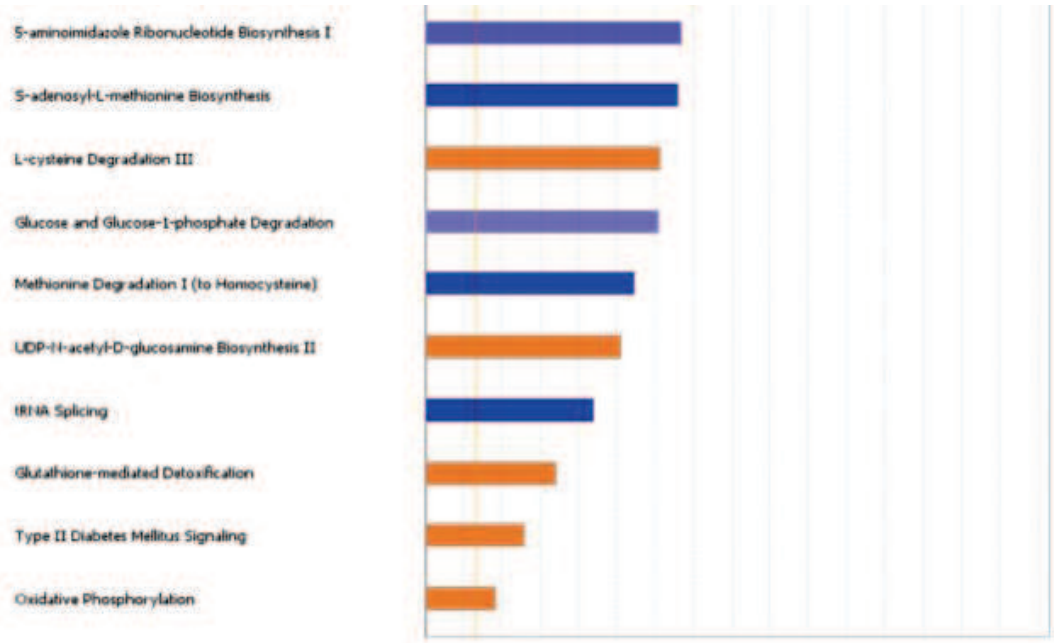

Figure 4:28 Metabolomics pathway analysis of 2D co-culture.
Metabolite analysis with IPA identified a number of significant changes between the control and nanokick group. Figure A = day 14, figure B = day 21. There was a trend towards reductions in amino acid metabolism at both time points in the nanokick group, including glutamine, serine and arginine. Some potentially significant amino acids, such as proline which is a key constituent of collagen, were increased. Glutathione, an antioxidant that plays a role in promoting osteoclast differentiation, was reduced at day 14. The threshold for significance is p <0.05 with Fisher's exact test. N=3 cell donors.

The top scoring networks were then analysed. At day 14, a number of important complexes were predicted to be inhibited in the nanokick group (Figure 6:3). Several of these were also found to be inhibited in the CD14+ culture and, as discussed in Chapter 3.3.9, play a role in promoting osteoclastogenesis. These included NADPH oxidase, IL-1, JNK, PARP and NF-κB. Unlike the CD14+ culture, LDL – a stimulator of osteoclastogenesis (Luegmayr E et al, 2004) – was inhibited. Other factors found to be inhibited were hypoxia-inducible factor 1 (HIF1) and CCAAT/enhancer binding protein (C-EBP), both of which are required for osteoclast differentiation and activation (Chen W et al, 2018, Miyauchi Y et al, 2013). There were also increases in osteoblast stimulatory markers. These included AMPK and ALP. AMPK both promotes the survival of osteoblasts and negatively impacts osteoclast differentiation by suppressing RANKL (Lee YS et al, 2010). Table 4:1 highlights the key complexes that were altered. The full network analysis is presented in the Appendices.

Moving on to the day 21 network, there were similarities observed. In particular, there was a predicted reduction in many of the inflammatory and osteoclast stimulatory pathways, including IL-1, JNK, LDL, C/EBP and NF-κB. Additional new complexes with similar function were also identified (Figure 6:4). TNF was found

to be inhibited; a feature noted in the CD14+ metabolomics results. In contract to the CD14+ results, however, AhR was found to be inhibited – a transcription factor that is activated by RANKL to promote osteoclast formation (Izawa T et al, 2016). Ras-proximate-1 (Rap1) was also inhibited. A previous study found when this protein was reduced, osteoclast mediated resorption was impaired due to cytoskeleton changes that prevent adhesion to bone (Zou W et al, 2013). The pathway for integrin subunit alpha M (ITGAM) was found to be inhibited. This integrin that is upregulated by TNF is expressed by pre-osteoclasts derived from the bone marrow niche, and ITGAM silencing leads to impaired osteoclast differentiation and function (Yang G et al, 2017, Hayashi H et al, 2008). Table 4:2 highlights the key complexes that were altered. The full network analysis is presented in the Appendices.

Table 4:1 Selected complexes activated and inhibited in metabolomics network analysis of nanokick 2D day 14 co-culture group

Inhibition	Activation
HIF1	ALP
NF-κB	AMPK
NADPH oxidase	
IL-1	
C/EBP	
PARP	
JNK	
LDL	
ERK	

Table 4:2 Selected complexes activated and inhibited in metabolomics network analysis of nanokick 2D day 21 co-culture group

Inhibition	Activation
TNF	ALP
NF-κB	
IL-1	
C/EBP	
PLA2	
JNK	
LDL	
AhR	
Rap1	
ITGAM	
IL-13	

4.3.9.2 3D co-culture

Metabolites were extracted from 3D gels at day 14 and 21 using the same methods detailed in Chapter 2.15. IPA was again used to analyse the data and produce charts of the top scoring networks and pathways.

On analysis of the top scoring pathways, the overall trend observed was a reduction in amino acid synthesis, similar to that of the 2D culture. There were specific changes that aligned with the 2D culture, for example reductions in glutamine, serine and glutathione. All of these compounds have been found to stimulate osteoclastogenesis (Indo Y et al, 2013, Takarada T et al, 2012, Fujita H et al, 2019). There were some notable differences observed, however. In contrast to the 2D culture, proline was found to be reduced in the nanokick group. As previously noted, this amino acid is a key component of collagen and, therefore, bone. The significance of this result given the cells were cultured in collagen is difficult to determine. tRNA charging was also increased in the nanokick group at day 21 (Figure 4:31). tRNAs play a role in amino acid transport and protein synthesis (Lodish H et al, 2000), and so this is interesting given the observed trend towards lower amino acid levels. However, given that there are both MSCs and BMHCs in this culture, and nanoscale vibration has been shown to have differing effects on these cell lines, it is perhaps not surprising that there are conflicting patterns present.

On analysis of the top scoring networks there were several similarities with the preceding experiments. At day 14, the nanokick group was found to have inhibition of multiple inflammatory and osteoclast stimulatory factors, including TNF, JNK, IL-1, NADPH oxidase, pro-inflammatory cytokine, AhR, HIF1, ITGAM and interferon- ϒ (IFN-ϒ) (Figure 6:5). IFN-ϒ stimulates osteoclast formation and bone resorption by promoting increases in RANKL and TNF-α (Gao Y et al, 2007). The osteogenic marker ALP was increased. A similar pattern was present at day 21, with the additional inhibition of osteoclast stimulatory factors epidermal growth factor receptor (EGFR) and C-X-C chemokine receptor type 2 (CXCR2). EGFR promotes osteoclast differentiation by upregulating RANKL signalling pathways. CXCR2 is a chemokine that promotes inflammation and stimulates osteoclast differentiation and function (Hardaway AL et al, 2015). However, in contrast to previous cultures there was an increase in some pro-osteoclast markers, namely

HIF1, LDL and NADPH oxidase (Figure 6:6). This therefore presents a more ambiguous picture compared to the prior conditions that predicted a widespread inhibition of inflammatory complexes. Tables 4:3 and 4:4 highlights the key complexes that were altered. The full network analyses are presented in the Appendices.

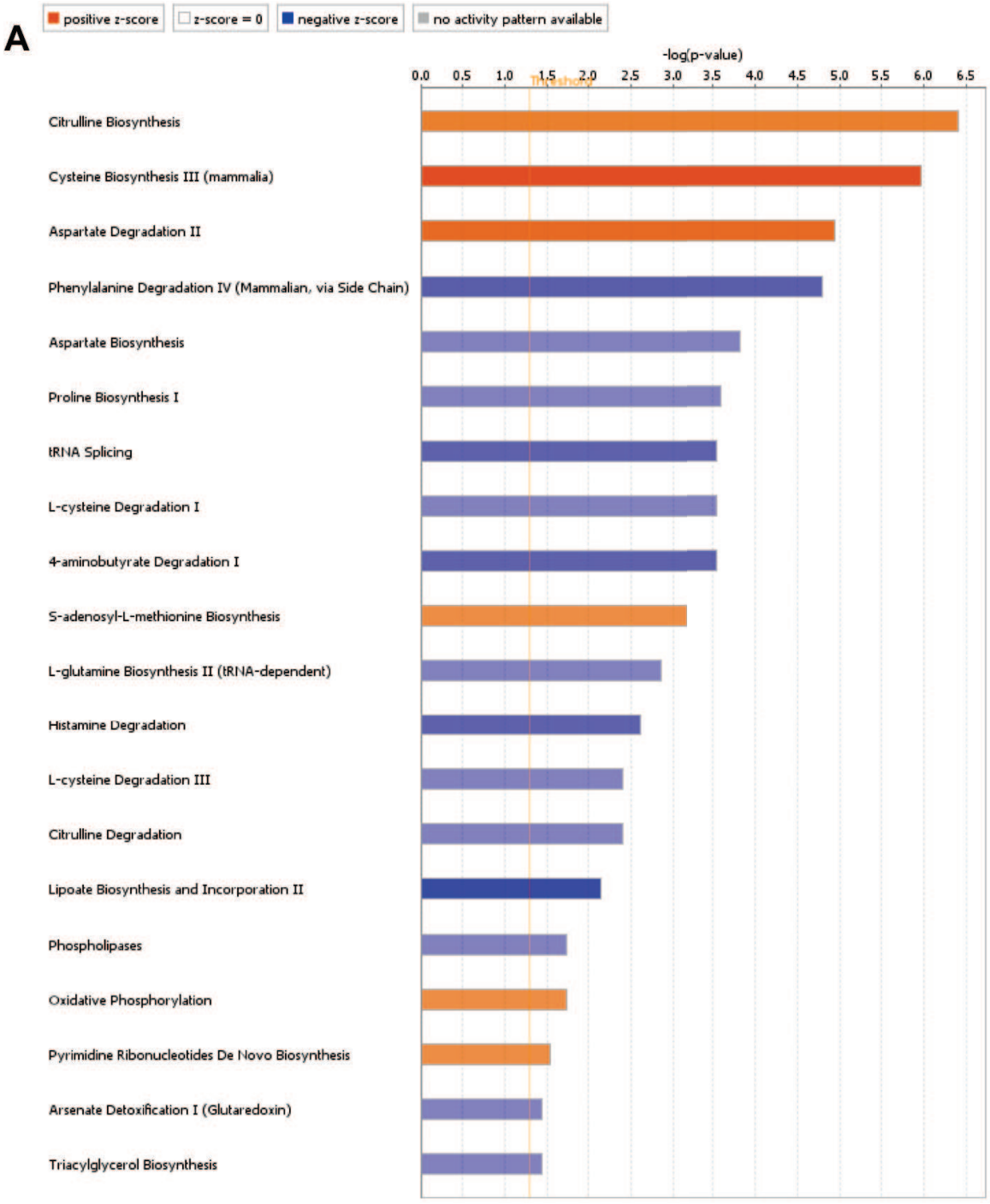

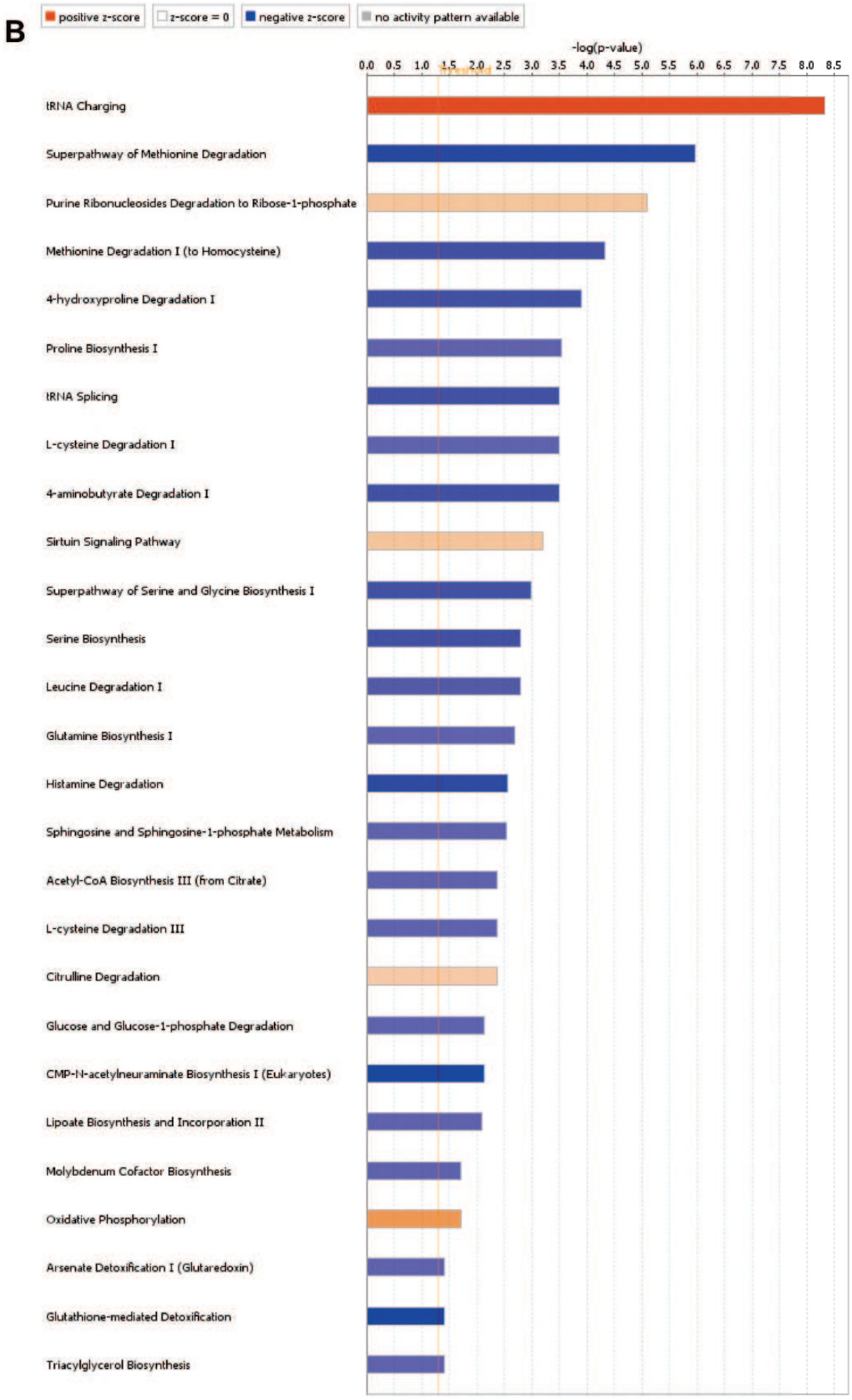
B
positive z-score
z-score = 0
negative z-score
no activity pattern available
-log(p-value)
0.0 0.5 1.0 1.5 2.0 2.5 3.0 3.5 4.0 4.5 5.0 5.5 6.0 6.5 7.0 7.5 8.0 8.5
tRNA Charging
Superpathway of Methionine Degradation
Purine Ribonucleosides Degradation to Ribose-1-phosphate
Methionine Degradation I (to Homocysteine)
4-hydroxyproline Degradation I
Proline Biosynthesis I
tRNA Splicing
L-cysteine Degradation I
4-aminobutyrate Degradation I
Sirtuin Signaling Pathway
Superpathway of Serine and Glycine Biosynthesis I
Serine Biosynthesis
Leucine Degradation I
Glutamine Biosynthesis I
Histamine Degradation
Sphingosine and Sphingosine-1-phosphate Metabolism
Acetyl-CoA Biosynthesis III (from Citrate)
L-cysteine Degradation III
Citrulline Degradation
Glucose and Glucose-1-phosphate Degradation
CMP-N-acetylneuraminate Biosynthesis I (Eukaryotes)
Lipoate Biosynthesis and Incorporation II
Molybdenum Cofactor Biosynthesis
Oxidative Phosphorylation
Arsenate Detoxification I (Glutaredoxin)
Glutathione-mediated Detoxification
Triacylglycerol Biosynthesis

Figure 4:29 Metabolomics pathway analysis of 3D co-culture.
Metabolite analysis with IPA identified a number of significant changes between the control and nanokick group. Figure A = day 14, figure B = day 21. There was a trend towards reductions in amino acids at both time points. Conversely, tRNA – which plays a role in amino acid transport and protein synthesis – was found to be increased. The osteoclast-stimulatory antioxidant glutathione was reduced. The threshold for significance is p <0.05 with Fisher's exact test. N=3 cell donors.

Table 4:3 Selected complexes activated and inhibited in metabolomics network analysis of nanokick 3D day 14 co-culture group

Inhibition	Activation
TNF	ALP
IL-1	SIRT6
PLA2	AMPK
JNK	
AhR	
ITGAM	
HIF1	
NADPH oxidase	
Pro-inflammatory cytokine	
IFN-ϒ	

Table 4:4 Selected complexes activated and inhibited in metabolomics network analysis of nanokick 3D day 21 co-culture group

Inhibition	Activation
TNF	HIF1
IL-1	LDL
JNK	NADPH oxidase
AhR	
IFN-ϒ	
EGFR	
CXCR2	
C/EBP	

4.4 Discussion

In the CD14+ results chapter, the effect of nanoscale vibration on an isolated culture of macrophages and osteoclasts was discussed. Whilst it was beneficial to examine this area, these cell types ultimately do not exist in isolation. Rather, they form but one component of the bone marrow niche. As detailed in the introduction chapter, osteoclasts have a co-dependent relationship with osteoblasts, both in terms of their function and survival. Specifically, factors produced by osteoblasts can stimulate or inhibit osteoclast function (Marino S et al, 2014). One of the primary objectives of the Nanokick bioreactor – and other tissue engineering technologies – is to stimulate bone development and eventually be used in a clinical context. Therefore, examining what effect nanoscale

vibration has on a co-culture of osteoblasts and osteoclasts that is representative of the *in vivo* environment provided valuable new insights.

Firstly, osteoclast numbers were determined following stimulation. Similar to the CD14+ culture, a significant reduction in osteoclasts was observed in the nanokick group. Interestingly, this reduction was of a similar proportion to the CD14+ culture, i.e. approximately 30%. This suggests the effect of vibration is not enhanced or inhibited by the presence of MSCs and osteoblasts. Osteoclast size was also reduced in the nanokick group. This was noted objectively with measurement of TRAP stained cells, but also subjectively with SEM where the occasional significantly larger osteoclast was noted in the control but not the nanokick group. There were no other morphological differences noted between groups on SEM, however, and immunofluorescence confirmed the presence of an actin ring in both cultures – a feature consistent with mature osteoclast formation. Although a reduction in osteoclasts may be beneficial when attempting to stimulate bone growth, it is important that functioning osteoclasts are present. Otherwise the normal remodelling process will not occur, leading to abnormal bone production. Just as with the CD14+ culture, alamarBlue assay revealed an increase in cell metabolic activity and viability in the nanokick group, suggesting cell death is not the cause of the reduced osteoclast numbers.

An assessment of the MSCs and osteoblasts in the co-culture was then undertaken. Prior studies demonstrated increases in osteogenesis when MSCs were exposed to nanoscale vibration (Tsimbouri PM et al, 2017b, Nikukar H et al, 2013, Pemberton GD et al, 2015). It was uncertain whether osteoclasts would ultimately negate this effect. Firstly, immunostaining was performed. This identified increases in vimentin and tubulin staining intensity; a feature suggestive of increased cytoskeleton tension. Tubulin is a key component of microtubules, one of the most rigid components of the cytoskeleton (Fletcher DA and Mullins RD, 2010). Microtubules help control cell shape and mechanics, particularly long extensions, and bear loads to stabilise the cytoskeleton (Brangwynne CP et al, 2006). Vinculin is a crucial protein in focal adhesions (FA) (Chang CW and Kumar S, 2013). FA are mechanosensitive structure which engage with the ECM and interact with stress fibres to generate tension (Rikitake Y and Takai Y, 2011). MSCs have been shown to have greater cytoskeleton tension when differentiating down an osteogenic route compare to adipogenic or chondrogenic (Mathieu PS and Loboa EG, 2012).

This result therefore suggests nanoscale vibration promotes osteogenesis via cytoskeleton changes. Related to increased cytoskeleton tension, contraction of the collagen gels was notably more significant in the nanokick group, suggesting greater contractility of the MSCs in this culture. Von Kossa staining was then performed to analyse mineralisation. In both the 2D and 3D cultures, a significant increase in mineralisation was identified in the nanokick group. This confirmed that osteogenesis can be stimulated through nanoscale vibration when osteoclasts are present.

As with the CD14+ culture, RT-qPCR was undertaken in an attempt to better understand the underlying mechanism responsible for the observed changes detailed above. In the 2D culture, significant reductions in IL-6 and OSCAR were found. IL-6 promotes osteoclast differentiation by enhancing expression of RANKL (Wu Q et al, 2017). OSCAR also stimulates osteoclast differentiation, and has been implicated in diseases such as rheumatoid arthritis and osteoporosis (Nemeth K et al, 2011). Reductions in these genes therefore conforms to the lower number of osteoclasts observed. In the 3D culture, however, cathepsin-K and OPN were found to be significantly elevated in the nanokick group at day 7. Cathepsin-K is a protease that promotes bone degradation, and is stimulated by cytokines such as RANKL (Troen BR, 2006). Interestingly, there was no increase in RANKL noted at this time point. The significance of the raise OPN level is less clear. OPN has been shown to play a role in the formation of osteoclast podosomes (Duong LT et al, 2000), as well as their survival (Singh A et al, 2018) and motility (Chellaiah MA and Hruska KA, 2003). Equally, however, OPN is produced by osteoblasts and osteocytes in response to mechanical stimulation as a positive factor for bone formation (Morinobu M et al, 2003b). OPN was also found to be elevated during distraction osteogenesis, with the hypothesis that early expression (similar to the raised level at day 7 noted in this study) may facilitate pre-osteoblast proliferation and migration (Perrien DS et al, 2002). In a separate study involving nanoscale vibration of MSCs, OPN was also found to be increased at day 7. It is interesting to note this consistent finding even when HSCs are present in the culture (Tsimbouri PM et al, 2017a).

Following the RT-qPCR results, ELISA was undertaken. In the 2D culture, a significant reduction in IL-6 was found. In 3D, although IL-6 was not significantly reduced when the data were pooled, each of the three donors had a significant

reduction in the nanokick group. The cumulative result did not reach statistical significance due to variation in IL-6 levels between donors. This does demonstrate, however, that irrespective of donor differences, IL-6 was reduced by nanoscale vibration. This result also aligns with the significant reduction in IL-6 found with RT-qPCR, albeit at a different time point.

Metabolite analysis was then performed to gain further insight into the biological process driving the reduction in osteoclast numbers. Reassuringly, a similar picture appeared to that of the CD14+ culture, suggesting there may be a shared underlying mechanism. The common theme that emerged was of an inhibition in inflammatory pathways, many of which promote osteoclastogenesis. For example, TNF, IL-1 and JNK appeared to be consistently inhibited across all conditions, to name a selected few. Overlaying the IL-6 pathway (presented in the Appendices) also demonstrated inhibition of a number of complexes which is of interest given the RT-qPCR and ELISA result. There are few studies performing metabolomic analysis of mechanically stimulated MSCs/HSCs, however other authors have used RT-PCR to find ALP is increased with nanoscale vibration of MSCs (Tsimbouri PM et al, 2017a) which mirrors the metabolomics result of this study. As with the CD14+ result, the metabolomics results are potentially promising but confirmation is required by conducting further experiments to validate the observations.

Chapter 5 General discussion

5.1 Introduction

The ability to influence stem cell fate represent one of the primary goals of cell engineering. This is frequently with the aim of developing methods to produce replacement human tissue for either medical research or novel treatments (Mali P and Cheng L, 2012). With the ageing population, in whom degenerative and pathological conditions are more prolific, the demand for tissue and organs has never been higher (Wang W and Yeung KWK, 2017, White SL et al, 2014, Olson JL et al, 2011). Bone represents the second most commonly transplanted tissue and as such has been subject to extensive research (Amini AR et al, 2013). Additionally, there are well-evidenced disadvantages to the current graft options which has prompted investigation into new technologies. The current "gold standard" approach involves harvesting bone graft from the same patient (i.e. autologous), at sites such as the iliac crest (Dimitriou R et al, 2011). This has the advantage of being osteoinductive (growth factors and osteoprogenitor cells) and osteoconductive (bone scaffold) (Bauer TW and Muschler GF, 2000). However, in addition to significant pain this procedure is associated with a number of potential complications, including damage to blood vessels and nerves, pelvic fracture and herniation of abdominal contents (Ahlmann E et al, 2002, Dimitriou R et al, 2011).

Current alternatives to autograft are also not without their own drawbacks. Allograft – i.e. tissue from another individual – requires irradiation or freeze-drying, leading to the loss of osteoinductive factors (Delloye C et al, 2007). And growth factors used to stimulate new bone development, such as BMP-2, have been associated with cancer (Carragee EJ et al, 2013, Raida M et al, 2005). Tissue engineering aims to overcome these shortfalls by producing lab grown bone that does not require additional surgical procedures or potentially harmful growth factors, yet stimulates healing and can meet the increase in demand (Olson JL et al, 2011).

Crucial to this goal is developing an understanding of the mechanisms that drive bone growth, and how they can be utilised to guide stem cell fate. One such mechanism is mechanical stimulation. The concept of force having an impact on bone formation is not new. It is well established that athletes involved in physical

activity increase their bone mass, whilst immobility and low gravity environments reduce bone quality (Amin S, 2010). Utilising mechanical stimulation in tissue engineering is therefore a logical progression. This has the benefit of avoid growth factors and their potential problems.

Varying techniques have been described within the literature to exert mechanical force on cells. These include, but are not limited to, compressive stress (Wang YK and Chen CS, 2013), tensile stress (Tang N et al, 2012) and vibration (Tsimbouri PM et al, 2017b). One technique that previously received significant attention with regard to bone healing was low intensity pulsed ultrasound (LIPUS). In 2008, 21% of Canadian trauma surgeons prescribed LIPUS for tibial fracture (Busse JW et al, 2008). This non-invasive technique utilises acoustic energy to exert mechanical stress at the fracture site (Mundi R et al, 2009). A frequency of 1.5 MHz is typically utilised (Claes L and Willie B, 2007). It is believed that this produces movement at the fracture ends, with a range of 0.15 nm (Pounder NM and Harrison AJ, 2008) to 2 mm (Claes L and Willie B, 2007) bone end displacement being reported. This movement was thought to result in increases in osteogenic gene expression (Sena K et al, 2005), alterations in the cell cytoskeleton via integrins (Yang RS et al, 2005) and recruitment of osteoprogenitor cells (Mundi R et al, 2009). Despite this, a range of outcomes were reported in the literature. The size of the surrounding soft tissue mass was reported as a potential reason for failure of treatment. Greater success was reported in superficial bones, such as the tibia and ulna, compared to deeper structures, such as the femur (Mayr E et al, 2000). However, when multiple studies were pooled in a systematic review, no difference was found in return to work or number of subsequent operations. There was a possible reduction in days to full weight bearing, pain and radiographic union. However, when trials at high risk of bias were excluded, these benefits were no longer present (Schandelmaier S et al, 2017). As such, the use of LIPUS is no longer advocated (Poolman RW et al, 2017). It is tempting to draw similarities between LIPUS and nanoscale vibration given the fundamental principle of mechanical stimulation. However, given the different frequency, amplitude and external application of the stimulus such conclusions are not appropriate.

In this thesis, nanoscale vibration has been investigated as a method of influencing stem cell differentiation and osteoclastogenesis. This bioreactor utilised the reverse piezo effect, whereby electrical energy is used to generate mechanical

force. Interestingly, the piezo effect can be observed in bone. When an electrical current is applied to bone, it causes mechanical deformation. Equally, mechanical stress produces polarisation (Reinish GB and Nowick AS, 1975).

Electrical polarisation of bone has been suggested as one means by which bone remodelling occurs, with bone resorption taking place in positively charged areas and formation at negatively charged regions (Cerrolaza M et al, 2017b). Negative charge can be found in areas of compression (Fernández JR et al, 2012) and as such this conforms to Wolff's law which states that mechanical loading leads to remodelling that will better equip the bone to deal with similar loads (Frost HM, 2004). Vibration in the micrometre and millimetre range as a means of stimulating osteogenesis has previously been investigated by other authors and has been shown to promote osteogenesis (Zhou Y et al, 2011, Zhang C et al, 2012, Prè D et al, 2011). Given that many cell interactions occur on the nanoscale (Nikukar H et al, 2016), it was a logical progression to develop a bioreactor that delivers nanoscale vibration. Although a relatively recent innovation, the Nanokick bioreactor has shown promising results, with upregulation of osteogenesis in MSCs (Nikukar H et al, 2016, Nikukar H et al, 2013, Pemberton GD et al, 2015, Tsimbouri PM et al, 2017b).

In the bone marrow niche, however, MSCs and osteoblasts do not exist in isolation. They live in a co-dependent relationship with a range of other cells, with one of the most significant of these being osteoclasts. The interplay between osteoblasts and osteoclasts is crucial to normal bone development, homeostasis and remodelling after injury. Any imbalance in this dynamic, particularly with regard to osteoclast function, can lead to pathological conditions, such as osteoporosis (Tang P et al, 2014, Mizuno A et al, 1998) and osteopetrosis (Saftig P et al, 1998, Naito A et al, 1999). The effect of nanoscale vibration on osteoclasts was hitherto not known. When considering this new technology as a means of producing lab grown bone graft, or even potentially using implantable vibration devices to stimulate osteogenesis, this information is crucial. The aim of this MD thesis was therefore to examine what response is elicited from osteoclasts following stimulation with the Nanokick bioreactor.

5.2 Osteoclastogenesis and osteoblastogenesis following nanoscale vibration

In this study, a reduction in osteoclast number and size was observed following exposure to nanoscale vibration. Although these are the first reported outcomes in this area, some research has been performed utilising microscale vibration. 20 μm displacements at 4 Hz reduced osteoclast differentiation and fusion in mouse cells, potentially through the suppression of dendritic cell-specific transmembrane protein (DC-STAMP), a regulator of osteoclast differentiation (Kulkarni RN et al, 2013) that is stimulated by RANKL (Kukita T et al, 2004). With vibration at 45 Hz and 50 μm Xie *et al* found mice tibia had a 30% reduction in osteoclast numbers – a similar proportion to what was found in this study. The authors also noted a 25% reduction in osteoclast-mediated resorption (Xie L et al, 2006).

Frequency also plays an important role. In a study which examined the correlation between frequency and expression of COX-2 – a prostaglandin essential for bone healing (Simon AM et al, 2002) – increases in frequency (5 – 100 Hz) were found to produce a linear increase in COX-2. A similar effect was found with nitric oxide (NO), which supports bone growth (Diwan AD et al, 2000) partly by detaching osteoclasts and inhibiting resorption (Mancini L et al, 1998). Conversely, increasing frequency resulted in lower levels of prostaglandin E_2 (PGE_2). PGE_2 stimulates osteoclast differentiation and resorption (Kaji H et al, 1996) and so taken alongside the increases in COX-2 and NO further confirms the importance of higher frequency vibration in osteogenesis (Bacabac RG et al, 2006). The Nanokick bioreactor delivers a frequency of 1000 Hz. This was based on prior studies which identified this as the most conductive to osteogenesis with MSC cultures (Pemberton GD et al, 2015, Nikukar H et al, 2016). The results of this thesis support the continued use of this frequency given the combination of increases in osteogenesis and reduction in osteoclastogenesis observed.

Osteocytes, one of the most abundant cells in bone, have also been shown to be mechanosensitive. This is important given their role in cell signalling and orchestration of osteogenesis. In a separate study, vibration of mouse osteocytes at 10 μm was found to negatively influence osteoclastogenesis (Lau E et al, 2010). This was through a reduction in RANKL and PGE_2 and increases in COX-2. Not only

were cell numbers reduced, but the size of the osteoclasts also. The number of nuclei is linked to an osteoclasts resorptive ability (Lees RL et al, 2001), with larger cells resorbing greater amounts of bone. Given the smaller size of osteoclasts observed in the nanokick group of this study, it can be surmised that their activity would be similarly reduced. Indeed, this was borne out in the functional assessment of Chapter 3.3.5, as the nanokick group had a significant reduction in resorption.

The initial experiment performed in this study was TRAP staining, with the aim of identifying any differences in osteoclast differentiation following nanoscale vibration. Once the inhibitory effect was established, the underlying mechanism was initially investigated through RT-qPCR and ELISA. Some evidence was found to support the changes observed in TRAP staining and resorption analysis. At certain time points, M-CSF, TNF-α and IL-6 were found to be reduced; factors which would inhibit osteoclastogenesis. For example, IL-6 is involved in a number of pathological resorptive conditions, including rheumatoid arthritis, osteoporosis (Edwards CJ and Williams E, 2010) and primary hyperparathyroidism (Grey A et al, 1996). However, cathepsin-K, OSCAR and OPG were both increased and decreased at different time points, which made a definitive interpretation of the results challenging. It is possible the inhibitory factors were of greater significance to osteoclast stimulation and differentiation. Equally, it may be that an examination of different genes and cytokines would have yielded more conclusive information. A broad range of markers was investigated in this study to cast a wide net, but it is certainly possible that a significant factor was missed. Given the complexity of the cellular process and multiple steps involved this is perhaps not surprising. Following the RT-qPCR and ELISA results, a metabolomic analysis was performed. This technique has been performed in MSC tissue engineering studies previously (Tsimbouri PM et al, 2017b). It has the benefit of obtaining a large volume of data, providing valuable insight into a range of biological processes. Equally, data overload can be an issue with this technique (Daviss B, 2005), leading to difficulties determining what results are both relevant and significant. In analysing the data from this study, only the top scoring networks and pathways deemed relevant to the cell culture were examined.

The common theme that emerged across all experimental conditions was an inhibition of inflammatory pathways. Multiple complexes and cytokines were

consistently downregulated, such as TNF, JNK and NF-κB. Given the significance of these factors in the stimulation of osteoclastogenesis – and their correlation with the lower levels of TNF-α and IL-6 seen in the RT-qPCR and ELISA results – they represent a promising process through which nanoscale vibration may exert an effect on osteoclast differentiation and function. To conclude that inhibition of inflammatory factors is the underlying biological process that downregulates osteoclastogenesis based on these observations would be premature, however. Further metabolomic experiments are required to validate these results.

While a reduction in osteoclast numbers, size and resorptive ability was demonstrated, it was also important to assess whether osteogenesis was influenced by the presence of cells from the HSC lineage. Following nanoscale vibration, alternations in MSC shape and cytoskeleton features were found. Specifically, cells were elongated with increases in vimentin and tubulin which suggests increases in cytoskeleton tension. Cellular tension is important in the determination of stem cell fate. Other authors have demonstrated that greater tension is associated with cells of an osteoblast lineage, compared to adipogenic cell lines which have lower tension (Robertson SN et al, 2018, Dalby MJ et al, 2007, Kilian KA et al, 2010b). It has been suggested that the cytoskeleton plays an important role in the transfer of mechanical force to the nucleus. When a force is transmitted through the ECM, it is detected by surface-adhesion receptors, such as integrins. Integrins are attached to the cytoskeleton, which are in turn integrated with the nuclear scaffold, nuclei and DNA of the cell. It is therefore possible that forces transmitted from outside the cell result in gene level changes via the cytoskeleton (Wang N et al, 2009). Figure 5.1 demonstrates a tensegrity model, illustrating that the cell cytoskeleton and nucleus alter in response to external stresses.

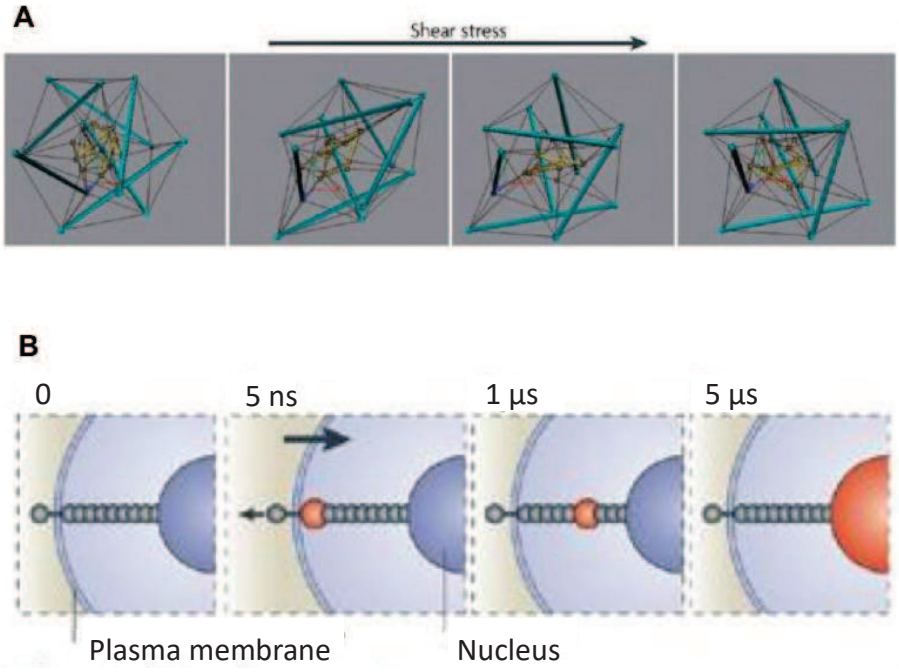

Figure 5:1 Mechanical force propagation.
A – a computer stimulation of a cell tensegrity model, illustrating the connections between the cytoskeleton and nucleus that rearrange in response to sheer stress. B – a graphic representation of force (red dot) being detected by integrins on the cell surface and then transmitted through the cytoskeleton to the nucleus. It takes approximately 5 µs for forces to propagate from integrins to the nucleus. Images presented with permission from Springer Nature (Wang N et al, 2009).

Bone mineralisation was also altered, with significant increases in the nanokick group in both 2D and 3D. The same technique was also performed on an isolated culture of MSCs. Although the increase in mineralisation was greater than the co-culture (3-fold *cf* 2-fold increase) it suggests the presence of osteoclasts does not significantly impair bone formation. This is potentially a highly significant result. Whilst the current literature on nanoscale vibration confirmed increases in mineralisation in MSCs, it did not provide insight into what response vibration would elicit *in vivo*. The use of a co-culture method therefore provides useful information for any future studies involving whole marrow samples or implantable devices.

5.3 Limitations

There are several limitations to this work. Firstly, the number of donors per experiment could have been higher. This would have helped with the statistical analysis and as such provide more robust conclusions. In this study, the aim was to provide three donors per experiment as this would be in line with other research papers in the field (Tsimbouri PM et al, 2017a). However, this was not

achieved in all cases as a result of restrictions on donor sample availability, bioreactor space and, ultimately, time.

Despite examining a number of genes, the RT-qPCR experiments did not yield a definitive answer. Specifically, there was not a common gene the was consistently up- or downregulated in response to nanoscale vibration that would explain the observed changes in osteoclast differentiation. It is possible selecting a different set of genes to analyse would have provided more certainty. Equally, the complexity of the cellular processes may mean that there is not one individual gene that we can attribute responsibility to. Taken alongside the ELISA and metabolomics data, however, the RT-qPCR results do appear to support the observed trend towards a state of lower inflammation.

There are potentially factors that may have influenced the results which we could not examine for within the scope of this study. For example, electric fields have been shown to influence cell differentiation and growth (Taghian T et al, 2015). It is possible that the Nanokick bioreactor produces an electric field that alters cell biology. In an effort to mitigate this and similar issues, all cell cultures – both control and nanoscale vibration groups – were placed in the same incubator in close proximity. Therefore, all cell conditions are more likely to be located a similar distance from any electric field produced. Linked with this, a magnetic field will be in close proximity to the nanokick group given the coupling of culture ware to the bioreactor. However, there is no evidence that even strong magnetic fields influence cell growth, survival or differentiation (Miyakoshi J, 2005).

5.4 Future work

This thesis highlighted the observed effect of nanoscale vibration on osteoclasts and a co-culture. Whilst morphological changes were undoubtedly present, the underlying mechanism is still not fully understood. Specifically, what gene changes drive the inhibition of osteoclastogenesis. RT-qPCR, ELISA and metabolomics suggested inhibition of a number of inflammatory and osteoclast stimulatory factors. Exploring additional genes through RT-qPCR could further our understanding of osteoclast biology. Additionally, inhibiting integrins and determining what effect this has on inflammatory pathways could provide valuable

insights. Conversely, supplementing the culture with inflammatory cytokines and assessing the response of both osteoblasts and osteoclasts would further develop our understanding of the role of inflammation in osteogenesis.

As noted, microscale displacements and alternate frequencies were found to inhibit osteoclastogenesis in other studies. It may therefore be beneficial to explore different parameters with the Nanokick bioreactor and determine whether any significant difference is observed in osteoclast and MSC cultures. Equally, exploring whether the cells have a "memory" by providing intermittent or short-term stimulation would be beneficial as it would confirm whether the observed effects last when vibration is removed. This is of particular importance when considering transplantation of tissue-engineered graft.

Finally, methods to optimise the delivery of primed cells to patients should be explored. This could include osteogenic scaffolds into which cells can be seeded. Such methods should be sterile, customisable and easy to work with in order to facilitate the safe and effective intra-operative delivery of osteogenic components. Furthermore, equipment that allows the volume of cells being stimulated to be upscaled, either through cultureware or bioreactor size, could be developed to meet the demands of clinical application.

5.5 Conclusions

In this thesis, the effects of nanoscale vibration on osteoclasts and a co-culture of osteoblasts and osteoclasts were discussed. A novel technology – the Nanokick bioreactor – was utilised to deliver the vibration. Without the addition of growth factors or complex techniques, the Nanokick bioreactor was found to inhibit osteoclastogenesis and stimulate osteogenesis. Despite these early promising results, further work is still required. A greater understanding of the underlying mechanisms driving the inhibition of osteoclastogenesis would be beneficial not just for this study, but also in considering potential therapeutic targets for conditions such as osteoporosis. It is hoped that with continued research and development, the Nanokick bioreactor will be utilised in the future to produce tissue-engineered bone graft for both clinical use and pharmacological research. Looking further still, wearable or implantable devices that can deliver localised

stimulation may be considered to enhance the treatment of musculoskeletal disease.

List of References

Abbott BD *et al* 2009. LIGO: the laser Interferometer gravitational-wave observatory. *Rep Prog Phys,* 72**,** 076901.

Ahlmann E, Patzakis M, Roidis N, Shepherd L & Holtom P 2002. Comparison of anterior and posterior iliac crest bone graft in terms of harvest-site morbidity and functional outcomes. *J Bone Joint Surg Am,* 84**,** 716 - 20.

Alberts B, Johnson A, Lewis J, Raff M, Roberts K & Walter P 2002. *Molecular Biology of the Cell,* New York, Gartland Science.

Allard-Chamard H, Haroun S & de Brum-Fernandes AJ 2014. Secreted phospholipase A2 type II is present in Paget's disease of bone and modulates osteoclastogenesis, apoptosis and bone resorption of human osteoclasts independently of its catalytic activity in vitro. *Prostaglandins Leukot Essent Fatty Acids,* 90**,** 39 - 45.

Amin S 2010. Mechanical factors and bone health: effects of weightlessness and neurologic injury. *Curr Rheumatol Rep,* 12**,** 170 - 6.

Amini AR, Laurencin CT & Nukavarapu SP 2013. Bone tissue engineering: recent advances and challenges. *Crit Rev Biomed Eng,* 40**,** 363 - 408.

Arai F, Miyamoto T, Ohneda O, Inada T, Sudo T, Brasel K, Miyata T, Anderson DM & Suda T 1999. Commitment and differentiation of osteoclast precursor cells by the sequential expression of c-Fms and receptor activator of nuclear factor kappaB (RANK) receptors. *J Exp Med,* 190**,** 1741 - 54.

Asagiri M, Sato K, Usami T, Ochi S, Nishina H, Yoshida H, Morita I, Wagner EF, Mak TW, Serfling E & Takayanagi H 2005. Autoamplification of NFATc1 expression determines its essential role in bone homeostasis. *J Exp Med,* 202**,** 1261 - 9.

Bacabac RG, Smit TH, Van Loon JJ, Doulabi BZ, Helder M & Klein-Nulend J 2006. Bone cell responses to high-frequency vibration stress: does the nucleus oscillate within the cytoplasm? *FASEB J,* 20**,** 858 - 64.

Back SA, Khan R, Gan X, Rosenberg PA & Volpe JJ 1999. A new Alamar Blue viability assay to rapidly quantify oligodendrocyte death. *J Neurosci Methods,* 91**,** 47 - 54.

Barbul A 2008. Proline precursors to sustain Mammalian collagen synthesis. *J Nutr,* 138**,** 2021S - 2024S.

Bauer TW & Muschler GF 2000. Bone graft materials. An overview of the basic science. *Clin Orthop Relat Res,* 371**,** 10 - 27.

Bellido T, Plotkin LI & Bruzzaniti A 2014. *Basic and Applied Bone Biology*, Academic Press.

Beranger GE, Momier D, Rochet N, Quincey D, Guigonis JM, Samson M, Carle GF & Scimeca JC 2006. RANKL treatment releases the negative regulation

of the poly(ADP-ribose) polymerase-1 on Tcirg1 gene expression during osteoclastogenesis. *J Bone Miner Res,* 21**,** 1757 - 69.

Berthiaume F, Maguire TJ & Yarmush ML 2011. Tissue engineering and regenerative medicine: history, progress, and challenges. *Annu Rev Chem Biomol Eng,* 2**,** 403 - 30.

Bjerre L, Bünger C, Baatrup A, Kassem M & Mygind T 2011. Flow perfusion culture of human mesenchymal stem cells on coralline hydroxyapatite scaffolds with various pore sizes. *J Biomed Mater Res A,* 97**,** 251 - 63.

Blair HC, Teitelbaum SL, Ghiselli R & Gluck S 1989. Osteoclastic bone resorption by a polarized vacuolar proton pump. *Science,* 245**,** 855 - 7.

Boyce BF & Xing L 2007. The RANKL/RANK/OPG pathway. *Curr Osteoporos Rep,* 5**,** 98 - 104.

Boyce BF & Xing L 2008. Functions of RANKL/RANK/OPG in bone modeling and remodeling. *Arch Biochem Biophys,* 473**,** 139 - 46.

Brangwynne CP, MacKintosh FC, Kumar S, Geisse NA, Talbot J, Mahadevan L, Parker KK, Ingber DE & Weitz DA 2006. Microtubules can bear enhanced compressive loads in living cells because of lateral reinforcement. *J Cell Biol,* 173**,** 733 - 41.

Buckwalter JA, Glimcher MJ, Cooper RR & Recker R 1996. Bone biology. I: Structure, blood supply, cells, matrix, and mineralization. *J Bone Joint Surg Am,* 77**,** 1256 - 75.

Busse JW, Morton E, Lacchetti C, Guyatt GH & Bhandari M 2008. Current management of tibial shaft fractures: a survey of 450 Canadian orthopedic trauma surgeons. *Acta Orthop,* 79**,** 689 - 94.

Calvi LM, Adams GB, Weibrecht KW, Weber JM, Olson DP, Knight MC, Martin RP, Schipani E, Divieti P, Bringhurst FR, Milner LA, Kronenberg HM & Scadden DT 2003. Osteoblastic cells regulate the haematopoietic stem cell niche. *Nature,* 425**,** 841 - 6.

Campsie P, Childs PG, Robertson SN, Cameron K, Hough J, Salmerán-Sánchez M, Tsimbouri MP, Vichare P, Dalby MJ & Reid S 2019. Design, construction and characterisation of a novel nanovibrational bioreactor and cultureware for osteogenesis. *bioRxiv 543660*.

Carragee EJ, Chu G, Rohatgi R, Hurwitz EL, Weiner BK, Yoon ST, Comer G & Kopjar B 2013. Cancer risk after use of recombinant bone morphogenetic protein-2 for spinal arthrodesis. *J Bone Joint Surg Am,* 95**,** 1537 - 45.

Cerrolaza M, Duarte V & Garzón-Alvarado D 2017a. Analysis of bone remodeling under piezoelectricity effects using boundary elements *J Bionic Eng,* 14**,** 659 - 71.

Cerrolaza M, Duarte V & Garzón-Alvaradod D 2017b. Analysis of Bone Remodeling Under Piezoelectricity Effects Using Boundary Elements. *J Bionic Eng,* 14**,** 659 - 71.

Chang CW & Kumar S 2013. Vinculin tension distributions of individual stress fibers within cell-matrix adhesions. *J Cell Sci,* 126**,** 3021 - 30.

Chellaiah MA & Hruska KA 2003. The integrin alpha(v)beta(3) and CD44 regulate the actions of osteopontin on osteoclast motility. *Calcif Tissue Int,* 72**,** 197 - 205.

Chen W, Zhu G, Tang J, Zhou HD & Li YP 2018. C/ebpα controls osteoclast terminal differentiation, activation, function, and postnatal bone homeostasis through direct regulation of Nfatc1. *J Pathol,* 244**,** 271 - 82.

Chen X, Wang Z, Duan N, Zhu G, Schwarz EM & Xie C 2018. Osteoblast-osteoclast interactions. *Connect Tissue Res,* 59**,** 99 - 107.

Chenu C, Colucci S, Grano M, Zigrino P, Barattolo R, Zambonin G, Baldini N, Vergnaud P, Delmas PD & Zallone AZ 1994. Osteocalcin induces chemotaxis, secretion of matrix proteins, and calcium-mediated intracellular signaling in human osteoclast-like cells. *J Cell Biol,* 127**,** 1149 - 58.

Childs PG, Boyle CA, Pemberton GD, Nikukar H, Curtis ASG, Henriquez FL, Dalby MJ & Reid S 2016. Use of nanoscale mechanical stimulation for control and manipulation of cell behaviour. *Acta Biomater,* 34**,** 159 - 68.

Chung ST, Geerts D, Roseman K, Renaud A & Connelly L 2017. Osteoprotegerin mediates tumor-promoting effects of Interleukin-1beta in breast cancer cells. *Mol Cancer,* 16**,** https://doi.org/10.1186/s12943-017-0606-y.

Claes L & Willie B 2007. The enhancement of bone regeneration by ultrasound. *Prog Biophys Mol Biol,* 93**,** 384 - 98.

Clish CB 2015. Metabolomics: an emerging but powerful tool for precision medicine. *Cold Spring Harb Mol Case Stud,* 1**,** a000588.

Coste B, Xiao B, Santos JS, Syeda R, Grandl J, Spencer KS, Kim SE, Schmidt M, Mathur J, Dubin AE, Montal M & Patapoutian A 2012. Piezo proteins are pore-forming subunits of mechanically activated channels. *Nature,* 483**,** 176 - 81.

Coyer SR, Singh A, Dumbauld DW, Calderwood DA, Craig SW, Delamarche E & García AJ 2012. Nanopatterning reveals an ECM area threshold for focal adhesion assembly and force transmission that is regulated by integrin activation and cytoskeleton tension. *J Cell Sci,* 125**,** 5110 - 23.

Crippes BA, Engleman VW, Settle SL, Ornberg RL, Helfrich MH, Horton MA & Nickols GA 1994. Antibody to β3 integrin inhibits the calcemic response to PTHrP in the thyroparathyroidectomized rat. *J Bone Miner Res,* 9**,** S178.

Dalby MJ, Gadegaard N & Oreffo RO 2014. Harnessing nanotopography and integrin-matrix interactions to influence stem cell fate. *Nat Mater,* 13**,** 558 - 69.

Dalby MJ, Gadegaard N, Tare R, Andar A, Riehle MO, Herzyk P, Wilkinson CD & Oreffo RO 2007. The control of human mesenchymal cell differentiation using nanoscale symmetry and disorder. *Nat Mater,* 6**,** 997 - 1003.

Darnay BG, Haridas V, Ni J, Moore PA & Aggarwal BB 1998. Characterization of the intracellular domain of receptor activator of NFkappaB (RANK). Interaction with tumor necrosis factor receptor-associated factors and activation of NF-kappab and c-Jun N-terminal kinase. *J Biol Chem,* 273**,** 20551 - 5.

Daviss B 2005. Growing pains for metabolomics. *The Scientist,* 19**,** 25 - 9.

Delloye C, Cornu O, Druez V & Barbier O 2007. Bone allografts: What they can offer and what they cannot. *J Bone Joint Surg Br,* 89**,** 574 - 9.

Dimitriou R, Mataliotakis GI, Angoules AG, Kanakaris NK & Giannoudis PV 2011. Complications following autologous bone gra harvesting from the iliac crest and using the RIA: a systematic review. *Injury,* 42**,** S3 - S15.

Diwan AD, Wang MX, Jang D, Zhu W & Murrell GA 2000. Nitric oxide modulates fracture healing. *J Bone Miner Res,* 15**,** 342 - 51.

Dominici M, Le Blanc K, Mueller I, Slaper-Cortenbach I, Marini F, Krause D, Deans R, Keating A, Prockop Dj & Horwitz E 2006. Minimal criteria for defining multipotent mesenchymal stromal cells. The International Society for Cellular Therapy position statement. *Cytotherapy,* 8**,** 315 - 7.

Dong L, Wang SJ, Zhao XR, Zhu YF & Yu JK 2017. 3D- Printed Poly(ε-caprolactone) Scaffold Integrated with Cell-laden Chitosan Hydrogels for Bone Tissue Engineering. *Sci Rep,* 7**,** 13412.

Duong LT, Lakkakorpi P, Nakamura I & Rodan GA 2000. Integrins and signaling in osteoclast function. *Matrix Biol,* 19**,** 97 - 105.

Ebraheim NA, Elgafy H & Xu R 2001. Bone-graft harvesting from iliac and fibular donor sites: techniques and complications. *J Am Acad Orthop Surg,* 9**,** 210 - 8.

Edwards CJ & Williams E 2010. The role of interleukin-6 in rheumatoid arthritis-associated osteoporosis. *Osteoporos Int,* 21**,** 1287 - 93.

Engler AJ, Sen S, Sweeney HL & Discher DE 2006. Matrix elasticity directs stem cell lineage specification. *Cell,* 126**,** 677 - 89.

Etheridge ML, Campbell SA, Erdman AG, Haynes CL, Wolf SM & McCullough J 2013. The big picture on nanomedicine: the state of investigational and approved nanomedicine products. *Nanomedicine,* 9**,** 1 - 14.

Everts V, Delaissé JM, Korper W, Jansen DC, Tigchelaar-Gutter W, Saftig P & Beertsen W 2002. The bone lining cell: its role in cleaning Howship's lacunae and initiating bone formation. *J Bone Miner Res,* 17**,** 77 - 90.

Fernández JR, García-Aznar JM & Martínez R 2012. Piezoelectricity could predict sites of formation/resorption in bone remodelling and modelling. *J Theor Biol,* 292**,** 86 - 92.

Fiehn O 2002. Metabolomics--the link between genotypes and phenotypes. *Plant Mol Biol,* 48**,** 155 - 71.

Fletcher DA & Mullins RD 2010. Cell mechanics and the cytoskeleton. *Nature,* 463**,** 485 - 92.

Franchimont N, Wertz S & Malaise M 2005. Interleukin-6: An osteotropic factor influencing bone formation? *Bone,* 37**,** 601 - 6.

Frost HM 1994. Wolff's Law and bone's structural adaptations to mechanical usage: an overview for clinicians. *Angle Orthod,* 64**,** 175 - 88.

Frost HM 2004. A 2003 update of bone physiology and Wolff's Law for clinicians. *Angle Orthod,* 74**,** 3 - 15.

Fujihara S, Yokozeki M, Oba Y, Higashibata Y, Nomura S & Moriyama K 2006. Function and regulation of osteopontin in response to mechanical stress. *J Bone Miner Res,* 21**,** 956-64.

Fujita H, Ochi M, Ono M, Aoyama E, Ogino T, Kondo Y & Ohuchi H 2019. Glutathione accelerates osteoclast differentiation and inflammatory bone destruction. *Free Radic Res,* 53**,** 226 - 36.

Fuller K, Owens JM, Jagger CJ, Wilson A, Moss R & Chambers TJ 1993. Macrophage colony-stimulating factor stimulates survival and chemotactic behavior in isolated osteoclasts. *J Exp Med,* 178**,** 1733 - 44.

Galbraith CG, Yamada KM & Sheetz MP 2002. The relationship between force and focal complex development. *J Cell Biol,* 159**,** 695 - 705.

Gao Y, Grassi F, Ryan MR, Terauchi M, Page K, Yang X, Weitzmann MN & Pacifici R 2007. IFN-gamma stimulates osteoclast formation and bone loss in vivo via antigen-driven T cell activation. *J Clin Invest,* 117**,** 122 - 32.

Gardel LS, Serra LA , Reis RL & Gomes ME 2014. Use of perfusion bioreactors and large animal models for long bone tissue engineering. *Tissue Engineering Part B: Reviews,* 20**,** 126 - 46.

Gaur T, Lengner CJ, Hovhannisyan H, Bhat RA, Bodine PV, Komm BS, Javed A, van Wijnen AJ, Stein JL, Stein GS & Lian JB 2005. Canonical WNT signaling promotes osteogenesis by directly stimulating Runx2 gene expression. *J Biol Chem,* 280**,** 33132 - 40.

Gerstenfeld LC, Cho TJ, Kon T, Aizawa T, Tsay A, Fitch J, Barnes GL, Graves DT & Einhorn TA 2003. Impaired fracture healing in the absence of TNF-alpha signaling: the role of TNF-alpha in endochondral cartilage resorption. *J Bone Miner Res,* 18**,** 1584 - 92.

Giannoudis PV, Chris Arts JJ, Schmidmaier G & Larsson S 2011. What should be the characteristics of the ideal bone graft substitute? . *Injury,* 42**,** S1-S2.

Glass GE, Chan JK, Freidin A, Feldmann M, Horwood NJ & Nanchahal J 2011. TNF-alpha promotes fracture repair by augmenting the recruitment and differentiation of muscle-derived stromal cells. *Proc Natl Acad Sci U S A,* 108**,** 1585 - 90.

Goldmann WH 2012. Mechanotransduction and focal adhesions. *Cell Biol Int,* 36**,** 649 - 52.

Goldstein AS, Juarez TM, Helmke CD, Gustin MC & Mikos AG 2001. Effect of convection on osteoblastic cell growth and function in biodegradable polymer foam scaffolds. *Biomaterials,* 22**,** 1279 - 88.

Green H, Kehinde O & Thomas J 1979. Growth of cultured human epidermal cells into multiple epithelia suitable for grafting. *Proc Natl Acad Sci U S A,* 76**,** 5665 - 8.

Greenwald AS, Boden SD, Goldberg VM, Khan Y, Laurencin CT, Rosier RN, American Academy of Orthopaedic Surgeons & The Committee on Biological Implants 2001. Bone-graft substitutes: facts, fictions, and applications. *J Bone Joint Surg Am,* 83-A**,** 98 - 103.

Grey A, Mitnick MA, Shapses S, Ellison A, Gundberg C & Insogna K 1996. Circulating levels of interleukin-6 and tumor necrosis factor-alpha are elevated in primary hyperparathyroidism and correlate with markers of bone resorption--a clinical research center study. *J Clin Endocrinol Metab,* 81**,** 3450 - 4.

Håkansson B, Brandt A, Carlsson P & Tjellström A 1994. Resonance frequencies of the human skull in vivo. *J Acoust Soc Am,* 95**,** 1474 - 81.

Hardaway AL, Herroon MK, Rajagurubandara E & Podgorski I 2015. Marrow adipocyte-derived CXCL1 and CXCL2 contribute to osteolysis in metastatic prostate cancer. *Clin Exp Metastasis,* 32**,** 353 - 68.

Harre U, Georgess D, Bang H, Bozec A, Axmann R, Ossipova E, Jakobsson PJ, Baum W, Nimmerjahn F, Szarka E, Sarmay G, Krumbholz G, Neumann E, Toes R, Scherer HU, Catrina AI, Klareskog L, Jurdic P & Schett G 2012. Induction of osteoclastogenesis and bone loss by human autoantibodies against citrullinated vimentin. *J Clin Invest,* 122**,** 1791 - 802.

Haug JS, He XC, Grindley JC, Wunderlich JP, Gaudenz K, Ross JT, Paulson A, Wagner KP, Xie Y, Zhu R, Yin T, Perry JM, Hembree MJ, Redenbaugh EP, Radice GL, Seidel C & Li L 2008. N-cadherin expression level distinguishes reserved versus primed states of hematopoietic stem cells. *Cell Stem Cell,* 2**,** 367 - 79.

Hayashi H, Nakahama K, Sato T, Tuchiya T, Asakawa Y, Maemura T, Tanaka M, Morita M & Morita I 2008. The role of Mac-1 (CD11b/CD18) in osteoclast differentiation induced by receptor activator of nuclear factor-kappaB ligand. *FEBS Lett,* 582**,** 3243 - 8.

Hayman AR 2008. Tartrate-resistant acid phosphatase (TRAP) and the osteoclast/immune cell dichotomy. *Autoimmunity,* 41**,** 218 - 23.

He L & Montell D 2012. A cellular sense of touch. *Nat Cell Biol,* 14**,** 902 - 3.

Hodge JM, Kirkland MA & Nicholson GC 2007. Multiple roles of M-CSF in human osteoclastogenesis. *J Cell Biochem,* 102**,** 759 - 68.

Hofbauer LC, Lacey DL, Dunstan CR, Spelsberg TC, Riggs BL & Khosla S 1999. Interleukin-1beta and tumor necrosis factor-alpha, but not interleukin-6, stimulate osteoprotegerin ligand gene expression in human osteoblastic cells. *Bone,* 25**,** 255 - 9.

Hoffman BD, Grashoff C & Schwartz MA 2011. Dynamic molecular processes mediate cellular mechanotransduction. *Nature,* 475**,** 316 - 23.

Ikeda F, Matsubara T, Tsurukai T, Hata K, Nishimura R & Yoneda T 2008. JNK/c-Jun signaling mediates an anti-apoptotic effect of RANKL in osteoclasts. *J Bone Miner Res,* 23**,** 907 - 14.

Indo Y, Takeshita S, Ishii KA, Hoshii T, Aburatani H, Hirao A & Ikeda K 2013. Metabolic regulation of osteoclast differentiation and function. *J Bone Miner Res,* 28**,** 2392 - 9.

Izawa T, Arakaki R, Mori H, Tsunematsu T, Kudo Y, Tanaka E & Ishimaru N 2016. The Nuclear Receptor AhR Controls Bone Homeostasis by Regulating Osteoclast Differentiation via the RANK/c-Fos Signaling Axis. *J Immunol,* 197**,** 4639 - 50.

Jacquin C, Gran DE, Lee SK, Lorenzo JA & Aguila HL 2006. Identification of multiple osteoclast precursor populations in murine bone marrow. *J Bone Miner Res,* 21**,** 67 - 77.

Janmey PA & Miller RT 2011. Mechanisms of mechanical signaling in development and disease. *J Cell Sci,* 124**,** 9 - 18.

Jiang G, Giannone G, Critchley DR, Fukumoto E & Sheetz MP 2003. Two-piconewton slip bond between fibronectin and the cytoskeleton depends on talin. *Nature,* 424**,** 337 - 7.

Jimi E, Nakamura I, Duong LT, Ikebe T, Takahashi N, Rodan GA & Suda T 1999. Interleukin 1 induces multinucleation and bone-resorbing activity of osteoclasts in the absence of osteoblasts/stromal cells. *Exp Cell Res,* 247**,** 84 - 93.

Jurdic P, Saltel F, Chabadel A & Destaing O 2006. Podosome and sealing zone: specificity of the osteoclast model. *Eur J Cell Biol,* 85**,** 195 - 202.

Kaji H, Sugimoto T, Kanatani M, Fukase M, Kumegawa M & Chihara K 1996. Prostaglandin E2 stimulates osteoclast-like cell formation and bone-resorbing activity via osteoblasts: role of cAMP-dependent protein kinase. *J Bone Miner Res,* 11**,** 62 - 71.

Kameyama S, Yoshimura Y, Kameyama T, Kikuiri T, Matsuno M, Deyama Y, Suzuki K & Iida J 2013. Short-term mechanical stress inhibits osteoclastogenesis via suppression of DC-STAMP in RAW264.7 cells. *Int J Mol Med,* 31**,** 292 - 8.

Kanchanawong P, Shtengel G, Pasapera AM, Ramko EB, Davidson MW, Hess HF & Waterman CM 2010. Nanoscale architecture of integrin-based cell adhesions. *Nature,* 468**,** 580 - 4.

Kang IS & Kim C 2016. NADPH oxidase gp91phox contributes to RANKL-induced osteoclast differentiation by upregulating NFATc1. *Sci Rep,* 6**,** 38014.

Kang JH, Ko HM, Moon JS, Yoo HI, Jung JY, Kim MS, Koh JT, Kim WJ & Kim SH 2014. Osteoprotegerin expressed by osteoclasts: an autoregulator of osteoclastogenesis. *J Dent res,* 93**,** 1116 - 23.

Katsumi A, Orr AW, Tzima E & Schwartz MA 2004. Integrins in mechanotransduction. *J Cell Biol,* 279**,** 12001 - 4.

Kearns AE, Khosla S & Kostenuik PJ 2008. Receptor activator of nuclear factor kappaB ligand and osteoprotegerin regulation of bone remodeling in health and disease. *Endocr Rev,* 29**,** 155 - 92.

Kilian KA, Bugarija B, BT L & M M 2010a. Geometric cues for directing the differentiation of mesenchymal stem cells. *Proc. Natl Acad. Sci. USA,* 107**,** 4972 - 7.

Kilian KA, Bugarija B, Lahn BT & Mrksich M 2010b. Geometric cues for directing the differentiation of mesenchymal stem cells. *Proc Natl Acad Sci U S A,* 107**,** 4872 - 7.

Kim JH & Kim N 2016. Signaling Pathways in Osteoclast Differentiation. *Chonnam Medical Journal,* 52**,** 12 - 17.

Kim K, Kim JH, Lee J, Jin HM, Lee SH, Fisher DE, Kook H, Kim KK, Choi Y & Kim N 2005. Nuclear factor of activated T cells c1 induces osteoclast-associated receptor gene expression during tumor necrosis factor-related activation-induced cytokine-mediated osteoclastogenesis. *J Biol Chem,* 280**,** 35209-16.

Kobayashi N, Kadono Y, Naito A, Matsumoto K, Yamamoto T, Tanaka S & Inoue J 2001. Segregation of TRAF6-mediated signaling pathways clarifies its role in osteoclastogenesis. *EMBO J,* 20**,** 1271 - 80.

Kong YY, Yoshida H, Sarosi I, Tan HL, Timms E, Capparelli C, Morony S, Oliveira-dos-Santos AJ, Van G, Itie A, Khoo W, Wakeham A, Dunstan CR, Lacey DL, Mak TW, Boyle WJ & Penninger JM 1999. OPGL is a key regulator of osteoclastogenesis, lymphocyte development and lymph-node organogenesis. *Nature,* 397**,** 315 - 23.

Korin N, Bransky A, Dinnar U & Levenberg S 2009. Periodic "flow-stop" perfusion microchannel bioreactors for mammalian and human embryonic stem cell long-term culture. *Biomed Microdevices,* 11**,** 87 - 94.

Kuipers AJ, Middelbeek J & van Leeuwen FN 2012. Mechanoregulation of cytoskeletal dynamics by TRP channels. *Eur J Cell Biol,* 91**,** 834 - 46.

Kukita T, Wada N, Kukita A, Kakimoto T, Sandra F, Toh K, Nagata K, Iijima T, Horiuchi M, Matsusaki H, Hieshima K, Yoshie O & Nomiyama H 2004. RANKL-induced DC-STAMP is essential for osteoclastogenesis. *J Exp Med,* 200**,** 941 - 6.

Kulkarni RN, Voglewede PA & Liu D 2013. Mechanical vibration inhibits osteoclast formation by reducing DC-STAMP receptor expression in osteoclast precursor cells. *Bone,* 57**,** 493 - 8.

Kulkarni RP 2007. Nano-Bio-Genesis: tracing the rise of nanotechnology and nanobiotechnology as 'big science'. *J Biomed Discov Collab,* 2**,** 3.

Landgraeber S, Jäger M, Jacobs JJ & Hallab NJ 2014. The Pathology of Orthopedic Implant Failure Is Mediated by Innate Immune System Cytokines. *Mediators of Inflammation,* 2014**,** 9.

Langdahl B, Ferrari S & Dempster DW 2016. Bone modeling and remodeling: potential as therapeutic targets for the treatment of osteoporosis. *Ther Adv Musculoskelet Dis,* 8**,** 225 - 35.

Lau E, Al-Dujaili S, Guenther A, Liu D, Wang L & You L 2010. Effect of low-magnitude, high-frequency vibration on osteocytes in the regulation of osteoclasts. *Bone,* 46**,** 1508 - 15.

Lee W, Leddy HA, Chen Y, Lee SH, Zelenski NA, McNulty AL, Wu J, Beicker KN, Coles J, Zauscher S, Grandl J, Sachs F, Guilak F & Liedtke WB 2014. Synergy between Piezo1 and Piezo2 channels confers high-strain mechanosensitivity to articular cartilage. *Proc Natl Acad Sci U S A,* 111**,** E5114 - 22.

Lee YS, Kim YS, Lee SY, Kim GH, Kim BJ, Lee SH, Lee KU, Kim GS, Kim SW & Koh JM 2010. AMP kinase acts as a negative regulator of RANKL in the differentiation of osteoclasts. *Bone,* 47**,** 926 - 37.

Lees RL, Sabharwal VK & Heersche JN 2001. Resorptive state and cell size influence intracellular pH regulation in rabbit osteoclasts cultured on collagen-hydroxyapatite films. *Bone,* 28**,** 187 - 94.

Li P, Ma YC, Sheng XY, Dong HT, Han H, Wang J & Xia YY 2012. Cyclic fluid shear stress promotes osteoblastic cells proliferation through ERK5 signaling pathway. *Mol Cell Biochem,* 364**,** 321 - 7.

Lian JB, Stein GS, Bortell R & Owen TA 1991. Phenotype suppression: a postulated molecular mechanism for mediating the relationship of proliferation and differentiation by Fos/Jun interactions at AP-1 sites in steroid responsive promoter elements of tissue-specific genes. *J Cell Biochem,* 45**,** 9 - 14.

Lin FH, Chang JB, McGuire MH, Yee JA & Brigman BE 2010. Biphasic effects of interleukin-1beta on osteoblast differentiation in vitro. *J Orthop Res,* 28**,** 958 - 64.

Linder S & Aepfelbacher M 2003. Podosomes: adhesion hot-spots of invasive cells. *Trends Cell Biol,* 13**,** 376 - 85.

Liu P, Huang G, Wei T, Gao J, Huang C, Sun M, Zhu L & Shen W 2018. Sirtuin 3-induced macrophage autophagy in regulating NLRP3 inflammasome activation. *Biochim Biophys Acta Mol Basis Dis,* 1864**,** 764 - 77.

Lodish H, Berk A, Zipursky L, Matsudaira P, Baltimore D & Darnell J 2000. *Molecular Cell Biology,* New York, W.H. Freeman.

Lomas R, Chandrasekar A & Board TN 2013. Bone allograft in the U.K.: perceptions and realities. *Hip Int,* 23**,** 427 - 33.

Lorenzo JA, Sousa S, Alander C, Raisz LG & Dinarello CA 1987. Comparison of the bone-resorbing activity in the supernatants from phytohemagglutinin

stimulated human peripheral blood mononuclear cells with that of cytokines through the use of an antiserum to interleukin 1. *Endocrinology,* 121**,** 1164 - 70.

Luegmayr E, Glantschnig H, Wesolowski GA, Gentile MA, Fisher JE, Rodan GA & Reszka AA 2004. Osteoclast formation, survival and morphology are highly dependent on exogenous cholesterol/lipoproteins. *Cell Death Differ,* 11**,** 108 - 18.

Lund SA, Giachelli CM & Scatena M 2009. The role of osteopontin in inflammatory processes. *J Cell Commun Signal,* 3**,** 311 - 22.

Lv FJ, Tuan RS, Cheung KM & Leung VY 2014. Concise review: the surface markers and identity of human mesenchymal stem cells. *Stem Cells,* 32**,** 1408 - 19.

Mali P & Cheng L 2012. Concise review: Human cell engineering: cellular reprogramming and genome editing. *Stem Cells,* 30**,** 75 - 81.

Mancini L, Moradi-Bidhendi N, Brandi ML & MacIntyre I 1998. Nitric oxide superoxide and peroxynitrite modulate osteoclast activity. *Biochem Biophys Res Commun,* 243**,** 785 - 90.

Marino S, Logan JG, Mellis D & Capulli M 2014. Generation and culture of osteoclasts. *Bonekey Rep,* 3**,** 570.

Martin TJ & Sims NA 2005. Osteoclast-derived activity in the coupling of bone formation to resorption. *Trends Mol Med,* 11**,** 76 - 81.

Masuyama R, Vriens J, Voets T, Karashima Y, Owsianik G, Vennekens R, Lieben L, Torrekens S, Moermans K, Vanden Bosch A, Bouillon R, Nilius B & Carmeliet G 2008. TRPV4-mediated calcium influx regulates terminal differentiation of osteoclasts. *Cell Metab,* 8**,** 257 - 65.

Mathieu PS & Loboa EG 2012. Cytoskeletal and focal adhesion influences on mesenchymal stem cell shape, mechanical properties, and differentiation down osteogenic, adipogenic, and chondrogenic pathways. *Tissue Eng Part B Rev,* 18**,** 436 - 44.

Matsumoto M, Kogawa M, Wada S, Takayanagi H, Tsujimoto M, Katayama S, Hisatake K & Nogi Y 2004. Essential role of p38 mitogen-activated protein kinase in cathepsin K gene expression during osteoclastogenesis through association of NFATc1 and PU.1. *J Biol Chem,* 279**,** 45969-79.

Mattila PK & Lappalainen P 2008. Filopodia: molecular architecture and cellular functions. *Nat Rev Mol Cell Biol,* 9**,** 446 - 54.

Mayr E, Frankel V & Rüter A 2000. Ultrasound--an alternative healing method for nonunions? *Arch Orthop Trauma Surg,* 120**,** 1 - 8.

McBeath R, Pirone DM, Nelson CM, Bhadriraju K & Chen CS 2004. Cell shape, cytoskeletal tension, and RhoA regulate stem cell lineage commitment. *Dev Cell,* 6**,** 483 - 95.

McMurray RJ, Gadegaard N, Tsimbouri PM, Burgess KV, McNamara LE, Tare R, Murawski K, Kingham E, Oreffo RO & Dalby MJ 2011. Nanoscale Surfaces for the Long-Term Maintenance of Mesenchymal Stem Cell Phenotype and Multipotency. *Nat Mater,* 10**,** 637 - 44.

McNamara LE, Sjöström T, Meek RM, Oreffo RO, Su B, Dalby MJ & Burgess KE 2012. Metabolomics: a valuable tool for stem cell monitoring in regenerative medicine. *J R Soc Interface,* 9**,** 1713 - 24.

Miller SC, de Saint-Georges L, Bowman BM & Jee WS 1989. Bone lining cells: structure and function. *Scanning Microsc,* 3**,** 953 - 60.

Mills CD 2012. M1 and M2 Macrophages: Oracles of Health and Disease. *Crit Rev Immunol,* 32**,** 463 - 88.

Miyakoshi J 2005. Effects of static magnetic fields at the cellular level. *Prog Biophys Mol Biol,* 87**,** 213 - 23.

Miyauchi Y, Sato Y, Kobayashi T, Yoshida S, Mori T, Kanagawa H, Katsuyama E, Fujie A, Hao W, Miyamoto K, Tando T, Morioka H, Matsumoto M, Chambon P, Johnson RS, Kato S, Toyama Y & Miyamoto T 2013. HIF1α is required for osteoclast activation by estrogen deficiency in postmenopausal osteoporosis. *Proc Natl Acad Sci U S A,* 110**,** 16568 - 73.

Mizuno A, Amizuka N, Irie K, Murakami A, Fujise N, Kanno T, Sato Y, Nakagawa N, Yasuda H, Mochizuki S-I, Gomibuchi T, Yano K, Shima N, Washida N, Tsuda E, Morinaga T, Higashio K & Ozawa H 1998. Severe osteoporosis in mice lacking osteoclastogenesis inhibitory factor/osteoprotegerin. *Biochem Biophys Res Commun,* 247**,** 610 - 5.

Morinobu M, Ishijima M, Rittling SR, Tsuji K, Yamamoto H, Nifuji A, Denhardt DT & Noda M 2003a. *J Bone Miner Res,* 18**,** 1706 - 15.

Morinobu M, Ishijima M, Rittling SR, Tsuji K, Yamamoto H, Nifuji A, Denhardt DT & Noda M 2003b. Osteopontin expression in osteoblasts and osteocytes during bone formation under mechanical stress in the calvarial suture in vivo. *J Bone Miner Res,* 18**,** 1706 - 15.

Mundi R, Petis S, Kaloty R, Shetty V & Bhandari M 2009. Low-intensity pulsed ultrasound: Fracture healing. *Indian J Orthop,* 43**,** 132 - 40.

Murakami T, Yamamoto M, Yamamoto M, Ono K, Nishikawa M, Nagata N, Motoyoshi K & Akatsu T 1998. Transforming growth factor-β1 increases mRNA levels of osteoclastogenesis inhibitory factor in osteoblastic/stromal cells and inhibits the survival of murine osteoclast-like cells. *Biochem Biophys Res Commun,* 252**,** 747 - 52.

Nagy P, Bisgaard HC, Santoni-Rugiu E & Thorgeirsson SS 1996. In vivo infusion of growth factors enhances the mitogenic response of rat hepatic ductal (oval) cells after administration of 2-acetylaminofluorene. *Hepatology,* 23**,** 71 - 9.

Naito A, Azuma S, Tanaka S, Miyazaki T, Takaki S, Takatsu K, Nakao K, Nakamura K, Katsuki M, Yamamoto T & Inoue J 1999. Severe

osteopetrosis, defective interleukin-1 signalling and lymph node organogenesis in TRAF6-deficient mice. *Genes Cells,* 4**,** 353 - 62.

Nakamura I, Lipfert L, Rodan GA & Le T Duong 2001. Convergence of alpha(v)beta(3) integrin- and macrophage colony stimulating factor-mediated signals on phospholipase Cgamma in prefusion osteoclasts. *J Cell Biol,* 152**,** 361 - 73.

Nemeth K, Schoppet M, Al-Fakhri N, Helas S, Jessberger R, Hofbauer LC & Goettsch C 2011. The role of osteoclast-associated receptor in osteoimmunology. *J Immunol,* 186**,** 13 - 8.

Nesbitt SA & Horton MA 1997. Trafficking of matrix collagens through bone-resorbing osteoclasts. *Science,* 276**,** 266 - 9.

Neve A, Corrado A & Cantatore FP 2011. Osteoblast physiology in normal and pathological conditions. *Cell Tissue Res,* 343**,** 289 - 302.

Nguyen BB, Moriarty RA, Kamalitdinov T, Etheridge JM & Fisher JP 2017. Collagen hydrogel scaffold promotes mesenchymal stem cell and endothelial cell coculture for bone tissue engineering. *J Biomed Mater Res A,* 105**,** 1123 - 31.

Nikukar H, PG C, Curtis AS, Martin IW, Riehle MO, Dalby MJ & Reid S 2016. Production of nanoscale vibration for stimulation of human mesenchymal stem cells. *J Biomed Nanotechnol,* 12**,** 1478 - 88.

Nikukar H, Reid S, Tsimbouri PM, Riehle MO, Curtis AS & Dalby MJ 2013. Osteogenesis of mesenchymal stem cells by nanoscale mechanotransduction. *ACS Nano,* 7**,** 2758 - 67.

Ning H, Lin G, Lue TF & Lin CS 2011. Mesenchymal stem cell marker Stro-1 is a 75 kd endothelial antigen. *Biochem Biophys Res Commun,* 413**,** 353 - 7.

Noble BS, Peet N, Stevens HY, Brabbs A, Mosley JR, Reilly GC, Reeve J, Skerry TM & Lanyon LE 2003. Mechanical loading: biphasic osteocyte survival and targeting of osteoclasts for bone destruction in rat cortical bone. *Am J Physiol Cell Physiol,* 284**,** C934 - 43.

Novack DV, Yin L, Hagen-Stapleton A, Schreiber RD, Goeddel DV, Ross FP & Teitelbaum SL 2003. The IkappaB function of NF-kappaB2 p100 controls stimulated osteoclastogenesis. *J Exp Med,* 198**,** 771 - 81.

O'Brien CA, Nakashima T & Takayanagi H 2013. Osteocyte control of osteoclastogenesis. *Bone,* 54**,** 258 - 63.

Ogawa T, Ishida-Kitagawa N, Tanaka A, Matsumoto T, Hirouchi T, Akimaru M, Tanihara M, Yogo K & Takeya T 2006. A novel role of L-serine (L-Ser) for the expression of nuclear factor of activated T cells (NFAT)2 in receptor activator of nuclear factor kappa B ligand (RANKL)-induced osteoclastogenesis in vitro. *J Bone Miner Metab,* 24**,** 373 - 9.

Olson JL, Atala A & Yoo JJ 2011. Tissue engineering: current strategies and future directions. *Chonnam Med J,* 47**,** 1 - 13.

Ostlund C, Folker ES, Choi JC, Gomes ER, Gundersen GG & Worman HJ 2009. Dynamics and molecular interactions of linker of nucleoskeleton and cytoskeleton (LINC) complex proteins. *J Cell Sci,* 122**,** 4099 - 108.

Parameswaran N & Patial S 2010. Tumor necrosis factor-α signaling in macrophages. *Crit Rev Eukaryot Gene Expr,* 20**,** 87 - 103.

Park J, Berthiaume F, Toner M, Yarmush ML & Tilles AW 2005. Microfabricated grooved substrates as platforms for bioartificial liver reactors. *Biotechnol Bioeng,* 90**,** 632 - 44.

Park JH, Lee NK & Lee SY 2017. Current Understanding of RANK Signaling in Osteoclast Differentiation and Maturation. *Mol Cells,* 40**,** 706 - 13.

Partap S, O'Brien FJ & Plunkett NA 2010. *Bioreactors in tissue engineering*, INTECH Open Access Publisher.

Pemberton GD, Childs P, Reid S, Nikukar H, Tsimbouri PM, Gadegaard N, Curtis AS & Dalby MJ 2015. Nanoscale stimulation of osteoblastogenesis from mesenchymal stem cells: nanotopography and nanokicking. *Nanomedicine (Lond),* 10**,** 547 - 60.

Perrien DS, Brown EC, Aronson J, Skinner RA, Montague DC, Badger TM & Lumpkin CK Jr 2002. Immunohistochemical study of osteopontin expression during distraction osteogenesis in the rat. *J Histochem Cytochem,* 50**,** 567 - 74.

Pittenger MF, Mackay AM, Beck SC, Jaiswal RK, Douglas R, Mosca JD, Moorman MA, Simonetti DW, Craig S & Marshak DR 1999. Multilineage potential of adult human mesenchymal stem cells. *Science,* 284**,** 143 - 7.

Pollack SR, Meaney DF, Levine EM, Litt M & Johnston ED 2000. Numerical model and experimental validation of microcarrier motion in a rotating bioreactor. *Tissue Eng,* 6**,** 519 - 30.

Pollari S, Käkönen SM, Edgren H, Wolf M, Kohonen P, Sara H, Guise T, Nees M & Kallioniemi O 2011. Enhanced serine production by bone metastatic breast cancer cells stimulates osteoclastogenesis. *Breast Cancer Res Treat,* 125**,** 421 - 30.

Pongkitwitoon S, Weinheimer-Haus EM, Koh TJ & Judex S 2016. Low-intensity vibrations accelerate proliferation and alter macrophage phenotype in vitro. *J Biomech,* 49**,** 793 - 6.

Poolman RW, Agoritsas T, Siemieniuk RA, Harris IA, Schipper IB, Mollon B, Smith M, Albin A, Nador S, Sasges W, Schandelmaier S, Lytvyn L, Kuijpers T, van Beers LW, Verhofstad MH & Vandvik PO 2017. Low intensity pulsed ultrasound (LIPUS) for bone healing: a clinical practice guideline. *BMJ,* 356**,** j576.

Pounder NM & Harrison AJ 2008. Low intensity pulsed ultrasound for fracture healing: a review of the clinical evidence and the associated biological mechanism of action. *Ultrasonics,* 48**,** 330 - 8.

Prè D, Ceccarelli G, Gastaldi G, Asti A, Saino E, Visai L, Benazzo F, Cusella De Angelis MG & Magenes G 2011. The differentiation of human adipose-derived stem cells (hASCs) into osteoblasts is promoted by low amplitude, high frequency vibration treatment. *Bone,* 49**,** 295 - 303.

Raggatt LJ & Partridge NC 2010. Cellular and Molecular Mechanisms of Bone Remodeling. *J Biol Chem,* 285**,** 25103 - 8.

Raida M, Clement JH, Leek RD, Ameri K, Bicknell R, Niederwieser D & Harris AL 2005. Bone morphogenetic protein 2 (BMP-2) and induction of tumor angiogenesis. *J Cancer Res Clin Oncol,* 131**,** 741 - 50.

Rao AJ, Gibon E, Ma T, Yao Z, Smith RL & Goodman SB 2012. Revision joint replacement, wear particles, and macrophage polarization. *Acta Biomater,* 8**,** 2815 - 23.

Reinholt FP, Hultenby K, Oldberg A & Heinegård D 1990. Osteopontin--a possible anchor of osteoclasts to bone. *Proc Natl Acad Sci U S A,* 87**,** 4473 - 5.

Reinish GB & Nowick AS 1975. Piezoelectric properties of bone as functions of moisture content. *Nature,* 253**,** 626 - 27.

Renema N, Navet B, Heymann MF, Lezot F & Heymann D 2016. RANK-RANKL signalling in cancer. *Biosci Rep,* 36**,** e00366.

Rikitake Y & Takai Y 2011. *International Review of Cell and Molecular Biology*, Academic Press.

Robertson SN, Campsie P, Childs PG, Madsen F, Donnelly H, Henriquez FL, Mackay WG, Salmerón-Sánchez M, Tsimbouri MP, Williams C, Dalby MJ & Reid S 2018. Control of cell behaviour through nanovibrational stimulation: nanokicking. *Philos Trans A Math Phys Eng Sci,* 28**,** 2120.

Robling AG, Niziolek PJ, Baldridge LA, Condon KW, Allen MR, Alam I, Mantila SM, Gluhak-Heinrich J, Bellido TM, Harris SE & Turner CH 2008. Mechanical stimulation of bone in vivo reduces osteocyte expression of Sost/sclerostin. *J Biol Chem,* 283**,** 5866 - 75.

Roodman GD 1999. Cell biology of the osteoclast. *Exp Hematol,* 27**,** 1229 - 41.

Saftig P, Hunziker E, Everts V, Jones S, Boyde A, Wehmeyer O, Suter A & von Figura K 2000. Functions of cathepsin K in bone resorption. Lessons from cathepsin K deficient mice. *Adv Exp Med Biol,* 477**,** 293 - 303.

Saftig P, Hunziker E, Wehmeyer O, Jones S, Boyde A, Rommerskirch W, Moritz JD, Schu P & von Figura K 1998. Impaired osteoclastic bone resorption leads to osteopetrosis in cathepsin-K-deficient mice. *Proc Natl Acad Sci U S A,* 95**,** 13453 - 8.

Saltel F, Destaing O, Bard F, Eichert D & Jurdic P 2004. Apatite-mediated actin dynamics in resorbing osteoclasts. *Mol Biol Cell,* 15**,** 5231 - 41.

Sampath P, Pritchard DK, Pabon L, Reinecke H, Schwartz SM, Morris DR & Murry CE 2008. A hierarchical network controls protein translation during murine

embryonic stem cell self-renewal and differentiation. *Cell Stem Cell,* 2**,** 448 - 60.

Sargent JF 2014. The National Nanotechnology Initiative: Overview, Reauthorization, and Appropriations Issues *In:* SERVICE, C. R. (ed.).

Sato K, Fujii Y, Asano S, Ohtsuki T, Kawakami M, Kasono K, Tsushima T & Shizume K 1986. Recombinant human interleukin 1 alpha and beta stimulate mouse osteoblast-like cells (MC3T3-E1) to produce macrophage-colony stimulating activity and prostaglandin E2. *Biochem Biophys Res Commun,* 141**,** 285 - 91.

Schaffler MB, Cheung WY, Majeska R & Kennedy O 2014. Osteocytes: master orchestrators of bone. *Calcif Tissue Int,* 94**,** 5 - 24.

Schandelmaier S, Kaushal A, Lytvyn L, Heels-Ansdell D, Siemieniuk RA, Agoritsas T, Guyatt GH, Vandvik PO, Couban R, Mollon B & Busse JW 2017. Low intensity pulsed ultrasound for bone healing: systematic review of randomized controlled trials. *BMJ,* 356**,** j656.

Seeman E & Delmas PD 2006. Bone quality—the material and structural basis of bone strength and fragility. *N Engl J Med,* 354**,** 2250 - 61.

Sena K, Leven RM, Mazhar K, Sumner DR & Virdi AS 2005. Early gene response to low-intensity pulsed ultrasound in rat osteoblastic cells. *Ultrasound Med Biol,* 31**,** 703 - 8.

Shafiee A & Atala A 2017. Tissue Engineering: Toward a New Era of Medicine. *Annu Rev Med,* 14**,** 29 - 40.

Sikavitsas VI, Bancroft GN & Mikos AG 2002. Formation of three-dimensional cell/polymer constructs for bone tissue engineering in a spinner flask and a rotating wall vessel bioreactor. *J Biomed Mater Res,* 62**,** 136 - 48.

Simon AM, Manigrasso MB & O'Connor JP 2002. Cyclo-oxygenase 2 function is essential for bone fracture healing. *J Bone Miner Res,* 17**,** 963 - 76.

Singh A, Gill G, Kaur H, Amhmed M & Jakhu H 2018. Role of osteopontin in bone remodeling and orthodontic tooth movement: a review. *Prog Orthod,* 19**,** 18.

Sohn HS & Oh JK 2019. Review of bone graft and bone substitutes with an emphasis on fracture surgeries. *Biomater Res,* 23**,** doi:10.1186/s40824-019-0157-y.

Somjen D, Binderman I, Berger E & Harell A 1980. Bone remodelling induced by physical stress is prostaglandin E2 mediated. *Biochimica et biophysica acta,* 627**,** 91 - 100.

Song K, Wang H, Zhang B, Lim M, Liu Y & Liu T 2013. Numerical simulation of fluid field and in vitro three-dimensional fabrication of tissue-engineered bones in a rotating bioreactor and in vivo implantation for repairing segmental bone defects. *Cell Stress Chaperones,* 18**,** 193 - 201.

Song RL, Liu XZ, Zhu JQ, Zhang JM, Gao Q, Zhao HY, Sheng AZ, Yuan Y, Gu JH, Zou H, Wang QC & Liu ZP 2014. New roles of filopodia and podosomes

in the differentiation and fusion process of osteoclasts. *Genet Mol Res,* 13**,** 4776 - 87.

St John TA, Vaccaro AR, Sah AP, Schaefer M, Berta SC, Albert T & Hilibrand A 2003. Physical and monetary costs associated with autogenous bone graft harvesting. *Am J Orthop (Belle Mead NJ),* 32**,** 18 - 23.

Stenbeck G 2002. Formation and function of the ruffled border in osteoclasts. *Semin Cell Dev Biol,* 13**,** 285 - 92.

Stier S, Ko Y, Forkert R, Lutz C, Neuhaus T, Grunewald E, Cheng T, Dombkowski D, Calvi LM, Rittling SR & Scadden DT 2005. Osteopontin is a hematopoietic stem cell niche component that negatively regulates stem cell pool size. *J Exp Med,* 201**,** 1781 - 91.

Suda T, Kobayashi K, Jimi E, Udagawa N & Takahashi N 2001. The molecular basis of osteoclast differentiation and activation. *Novartis Found Symp,* 232**,** 235 - 47.

Taghian T, Narmoneva DA & Kogan AB 2015. Modulation of cell function by electric field: a high-resolution analysis. *J R Soc Interface,* 12**,** 20150153.

Takahashi F, Takahashi K, Shimizu K, Cui R, Tada N, Takahashi H, Soma S, Yoshioka M & Fukuchi Y 2004. Osteopontin is strongly expressed by alveolar macrophages in the lungs of acute respiratory distress syndrome. *Lung,* 182**,** 173 - 85.

Takarada T, Takarada-Iemata M, Takahata Y, Yamada D, Yamamoto T, Nakamura Y, Hinoi E & Yoneda Y 2012. Osteoclastogenesis is negatively regulated by D-serine produced by osteoblasts. *J Cell Physiol,* 227**,** 3477 - 87.

Takayanagi H 2007. Osteoimmunology: shared mechanisms and crosstalk between the immune and bone systems. *Nat Rev Immunol,* 7**,** 292 - 304.

Takito J, Inoue S & Nakamura M 2018. The Sealing Zone in Osteoclasts: A Self-Organized Structure on the Bone. *Int J Mol Sci,* 19**,** E984.

Tang N, Zhao Z, Zhang L, Yu Q, Li J, Xu Z & Li X 2012. Up-regulated osteogenic transcription factors during early response of human periodontal ligament stem cells to cyclic tensile strain. *Arch Med Sci,* 8**,** 422 - 30.

Tang P, Xiong Q, Ge W & Zhang L 2014. The role of microRNAs in osteoclasts and osteoporosis. *RNA Biol,* 11**,** 1355 - 63.

Tang Y, Wu X, Lei W, Pang L, Wan C, Shi Z, Zhao L, Nagy TR, Peng X, Hu J, Feng X, Van Hul W, Wan M & Cao X 2009. TGF-beta1-induced migration of bone mesenchymal stem cells couples bone resorption with formation. *Nat Med,* 15**,** 757 - 65.

Tarantino U, Cerocchi I, Scialdoni A, Saturnino L, Feola M, Celi M, Liuni FM, Iolascon G & Gasbarra E 2011. Bone healing and osteoporosis. *Aging Clin Exp Res,* 23**,** 62 - 4.

Tashjian AH Jr, Voelkel EF, Lazzaro M, Goad D, Bosma T & Levine L 1987. Tumor necrosis factor-alpha (Cachectin) stimulates bone resorption in mouse calvaria via a prostaglandinmediated mechanism. *Endocrinology* 120**,** 2029 - 36.

Taylor D, Hazenberg JG & Lee TC 2007. Living with cracks: damage and repair in human bone. *Nat Mater,* 6**,** 263 - 8.

Toyosaki-Maeda T, Takano H, Tomita T, Tsuruta Y, Maeda-Tanimura M, Shimaoka Y, Takahashi T, Itoh T, Suzuki R & Ochi T 2001. Differentiation of monocytes into multinucleated giant bone-resorbing cells: two-step differentiation induced by nurse-like cells and cytokines. *Arthritis Res,* 3**,** 306 - 10.

Tran Van P, Vignery A & Baron R 1982. An electron-microscopic study of the bone-remodeling sequence in the rat. *Cell Tissue Res,* 225**,** 283 - 92.

Troen BR 2006. The regulation of cathepsin K gene expression. *Ann N Y Acad Sci,* 1068**,** 165 - 72.

Tsimbouri PM, Childs PG, Pemberton GD, Yang J, Jayawarna V, Orapiriyakul W, Burgess K, González-García C, Blackburn G, Thomas D, Vallejo-Giraldo C, Biggs MJP, Curtis ASG, Salmerón-Sánchez M, Reid S & Dalby MJ 2017a. Stimulation of 3D osteogenesis by mesenchymal stem cells using a nanovibrational bioreactor. *Nat Biomed Eng,* 1**,** 758 - 70.

Tsimbouri PM, Childs PG, Pemberton GD, Yang J, Jayawarna V, Orapiriyakul W, Burgess K, González-García C, Blackburn G, Thomas D, Vallejo-Giraldo C, Biggs MJP, Curtis ASG, Salmerón-Sánchez M, Reid S & Dalby MJ 2017b. Stimulation of 3D osteogenesis by mesenchymal stem cells using a nanovibrational bioreactor. *Nature Biomedical Engineering,* 1**,** 758 - 70.

Tsimbouri PM, McMurray RJ, Burgess KV, Alakpa EV, Reynolds PM, Murawski K, Kingham E, Oreffo RO, Gadegaard N & Dalby MJ 2012. Using nanotopography and metabolomics to identify biochemical effectors of multipotency. *ACS Nano,* 6**,** 10239 - 49.

Tzaphlidou M 2008. Bone architecture: collagen structure and calcium/phosphorus maps. *J Biol Phys,* 34**,** 39 - 49.

Udagawa N, Takahashi N, Yasuda H, Mizuno A, Itoh K, Ueno Y, Shinki T, Gillespie MT, Martin TJ, Higashio K & Suda T 2000. Osteoprotegerin produced by osteoblasts is an important regulator in osteoclast development and function. *Endocrinology,* 141**,** 3478 - 84.

Väänänen HK & Horton M 1995. The osteoclast clear zone is a specialized cell-extracellular matrix adhesion structure. *J Cell Sci,* 108**,** 2729 - 32.

Väänänen K 2005. Mechanism of osteoclast mediated bone resorption--rationale for the design of new therapeutics. *Adv Drug Deliv Rev,* 57**,** 959 - 71.

Viguet-Carrin S, Garnero P & Delmas PD 2006. The role of collagen in bone strength. *Osteoporos Int,* 17**,** 319 - 36.

Wang N, Tytell JD & Ingber DE 2009. Mechanotransduction at a distance: mechanically coupling the extracellular matrix with the nucleus. *Nat Rev Mol Cell Biol,* 10**,** 75 - 82.

Wang W & Yeung KWK 2017. Bone grafts and biomaterials substitutes for bone defect repair: A review. *Bioact Mater,* 2**,** 224 - 47.

Wang YK & Chen CS 2013. Cell adhesion and mechanical stimulation in the regulation of mesenchymal stem cell differentiation. *J Cell Mol Med,* 17**,** 823 - 32.

White SL, Hirth R, Mahíllo B, Domínguez-Gil B, Delmonico FL, Noel L, Chapman J, Matesanz R, Carmona M, Alvarez M, Núñez JR & Leichtman A 2014. The global diffusion of organ transplantation: trends, drivers and policy implications. *Bull World Health Organ,* 92**,** 826-35.

Wittkowske C, Reilly GC, Lacroix D & Perrault CM 2016. In Vitro Bone Cell Models: Impact of Fluid Shear Stress on Bone Formation. *Front Bioeng Biotechnol,* 15**,** 87.

Wobma H & Vunjak-Novakovic G 2016. Tissue Engineering and Regenerative Medicine 2015: A Year in Review. *Tissue Eng Part B Rev,* 22**,** 101 - 13.

Wong BR, Josien R, Lee SY, Vologodskaia M, Steinman RM & Choi Y 1998. The TRAF family of signal transducers mediates NF-kappaB activation by the TRANCE receptor. *J Biol Chem,* 273**,** 28355 - 9.

Wu JY, Scadden DT & Kronenberg HM 2009. Role of the osteoblast lineage in the bone marrow hematopoietic niches. *J Bone Miner Res,* 24**,** 759 - 64.

Wu Q, Zhou X, Huang D, Ji Y & Kang F 2017. IL-6 Enhances Osteocyte-Mediated Osteoclastogenesis by Promoting JAK2 and RANKL Activity In Vitro. *Cell Physiol Biochem,* 41**,** 1360 - 9.

Xiao G, Jiang D, Gopalakrishnan R & Franceschi RT 2002. Fibroblast growth factor 2 induction of the osteocalcin gene requires MAPK activity and phosphorylation of the osteoblast transcription factor, Cbfa1/Runx2. *J Biol Chem,* 277**,** 36181 - 7.

Xie L, Jacobson JM, Choi ES, Busa B, Donahue LR, Miller LM, Rubin CT & Judex S 2006. Low-level mechanical vibrations can influence bone resorption and bone formation in the growing skeleton. *Bone,* 39**,** 1059 - 66.

Xu Feng 2009. Chemical and Biochemical Basis of Cell-Bone Matrix Interaction in Health and Disease. *Curr Chem Biol,* 3**,** 189 - 96.

Yakar S, Rosen CJ, Beamer WG, Ackert-Bicknell CL, Wu Y, Liu JL, Ooi GT, Setser J, Frystyk J, Boisclair YR & LeRoith D 2002. Circulating levels of IGF-1 directly regulate bone growth and density. *J Clin Invest,* 110**,** 771 - 81.

Yamashita T, Yao Z, Li F, Zhang Q, Badell IR, Schwarz EM, Takeshita S, Wagner EF, Noda M, Matsuo K, Xing L & Boyce BF 2007. NF-kappaB p50 and p52 regulate receptor activator of NF-kappaB ligand (RANKL) and tumor

necrosis factor-induced osteoclast precursor differentiation by activating c-Fos and NFATc1. *J Biol Chem,* 282**,** 18245 - 53.

Yang G, Chen X, Yan Z, Zhu Q & Yang C 2017. CD11b promotes the differentiation of osteoclasts induced by RANKL through the spleen tyrosine kinase signalling pathway. *J Cell Mol Med,* 21**,** 3445 - 52.

Yang RS, Lin WL, Chen YZ, Tang CH, Huang TH, Lu BY & Fu WM 2005. Regulation by ultrasound treatment on the integrin expression and differentiation of osteoblasts. *Bone,* 36**,** 276 - 83.

Yasuda H, Shima N, Nakagawa N, Mochizuki SI, Yano K, Fujise N, Sato Y, Goto M, Yamaguchi K, Kuriyama M, Kanno T, Murakami A, Tsuda E, Morinaga T & Higashio K 1998. Identity of osteoclastogenesis inhibitory factor (OCIF) and osteoprotegerin (OPG): a mechanism by which OPG/OCIF inhibits osteoclastogenesis in vitro. *Endocrinology,* 139**,** 1329 - 37.

You J, Yellowley CE, Donahue HJ, Zhang Y, Chen Q & Jacobs CR 2000. Substrate deformation levels associated with routine physical activity are less stimulatory to bone cells relative to loading- induced oscillatory fluid flow. *J Biomech Eng,* 122**,** 387 - 93.

Young PS, Tsimbouri PM, Gadegaard N, Meek RM & Dalby MJ 2015. Osteoclastogenesis/osteoblastogenesis using human bone marrow-derived cocultures on nanotopographical polymer surfaces. *Nanomedicine,* 10**,** 949 - 57.

Zhang C, Li J, Zhang L, Zhou Y, Hou W, Quan H, Li X, Chen Y & Yu H 2012. Effects of mechanical vibration on proliferation and osteogenic differentiation of human periodontal ligament stem cells. *Arch Oral Biol,* 57**,** 1395 - 407.

Zhang D, Jing J, Lou F, Li R, Ping Y, Yu F, Wu F, Yang X, Xu R, Li F, Wang K, Bai M, Pi C, Xie J, Zheng L, Ye L & Zhou X 2018. Evidence for excessive osteoclast activation in SIRT6 null mice. *Sci Rep,* 8**,** 10992.

Zhang K, Barragan-Adjemian C, Ye L, Kotha S, Dallas M, Lu Y, Zhao S, Harris M, Harris SE, Feng JQ & Bonewald LF 2006. E11/gp38 selective expression in osteocytes: regulation by mechanical strain and role in dendrite elongation. *Mol Cell Biol,* 26**,** 4539 - 52.

Zhang S, Wang X, Li G, Chong Y, Zhang J, Guo X, Li B & Bi Z 2017. Osteoclast regulation of osteoblasts via RANK-RANKL reverse signal transduction in vitro. *Mol Med Rep,* 16**,** 3994 - 4000.

Zhao T, Goh KJ, Ng HH & Vardy LA 2012. A role for polyamine regulators in ESC self-renewal. *Cell Cycle,* 11**,** 4517 - 23.

Zhou Y, Guan X, Zhu Z, Gao S, Zhang C, Li C, Zhou K, Hou W & Yu H 2011. Osteogenic differentiation of bone marrow-derived mesenchymal stromal cells on bone-derived scaffolds: effect of microvibration and role of ERK1/2 activation. *Eur Cell Mater,* 6**,** 12 - 25.

Zou W, Izawa T, Zhu T, Chappel J, Otero K, Monkley SJ, Critchley DR, Petrich BG, Morozov A, Ginsberg MH & Teitelbaum SL 2013. Talin1 and Rap1 are critical for osteoclast function. *Mol Cell Biol,* 33**,** 830-44.

Chapter 6 Appendices

6.1 Metabolomics network analysis

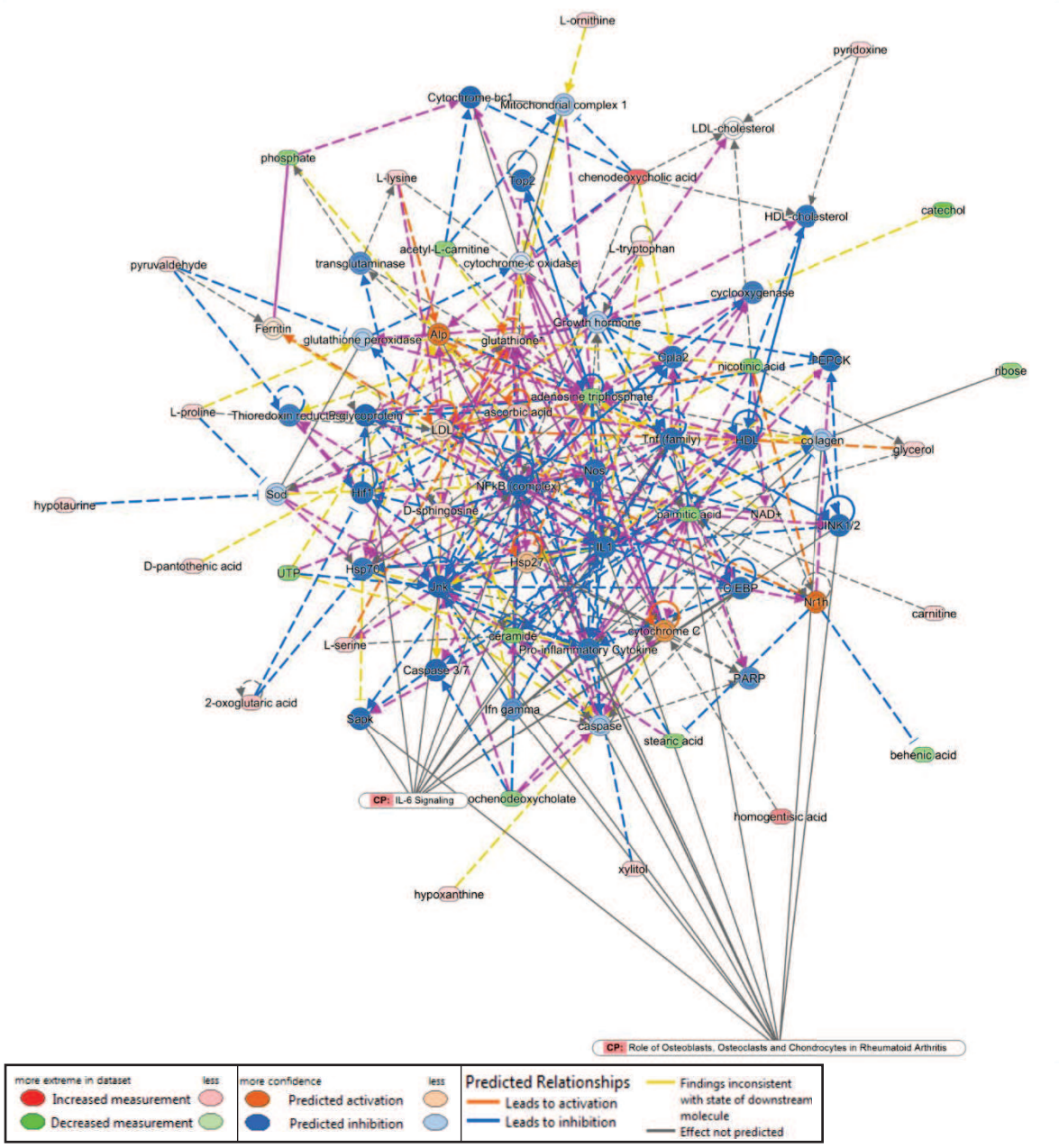

Figure 6:1 Metabolomics network and selected pathways in the M-CSF group
IPA network analysis illustrating the top scoring networks identified. There was a predicted trend towards inhibition of pro-inflammatory cytokines in the nanokick group. Potentially significant complexes that were inhibited include IL-1, TNF, NF-κB, JNK and pro-inflammatory cytokine. These complexes are indicated by the canonical pathway arrows for IL-6 and role of osteoblasts, osteoclasts and chondrocytes in rheumatoid arthritis. Blue = inhibition, orange = upregulation. CP = canonical pathway. N=3 cell donors.

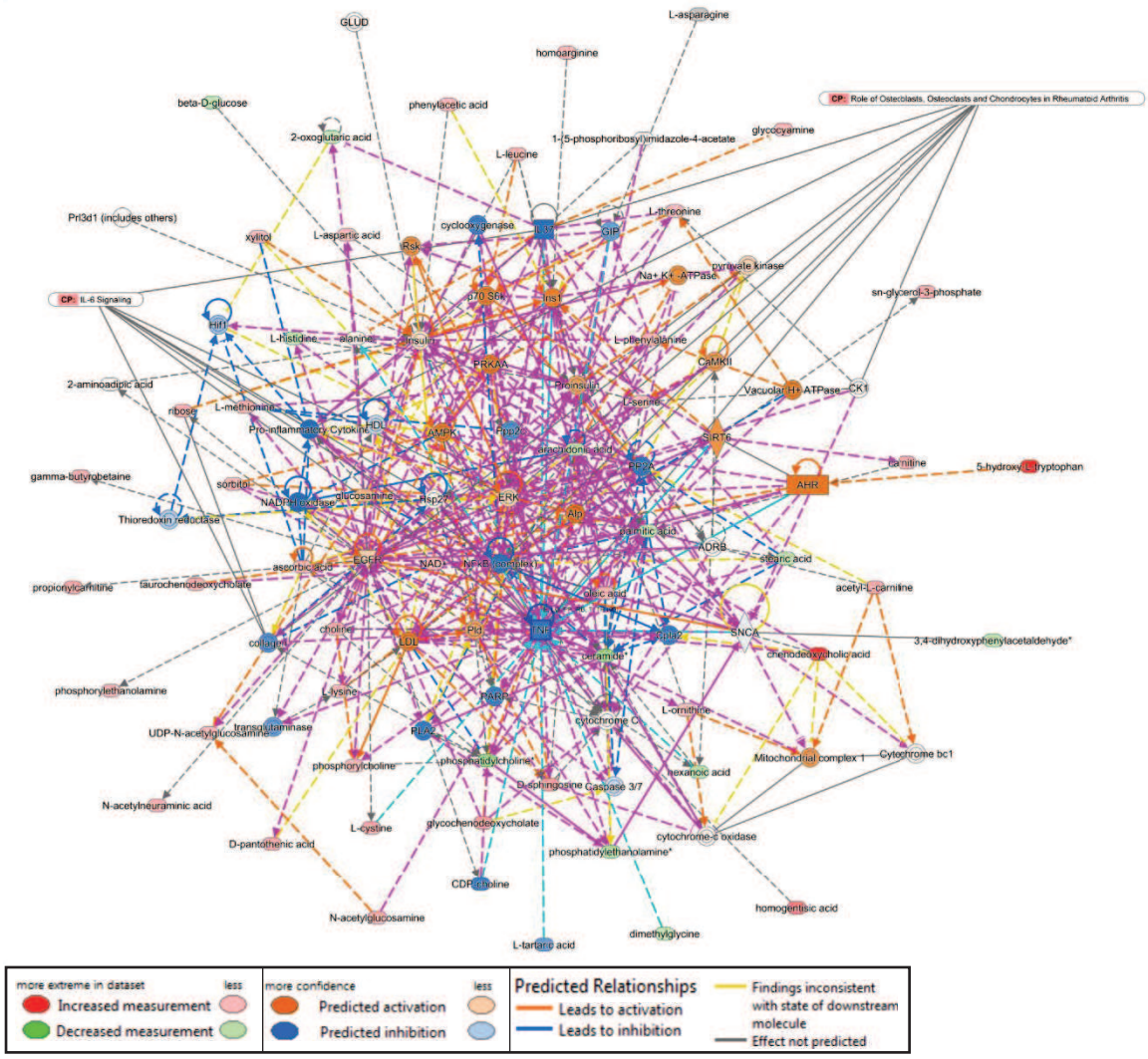

Figure 6:2 Metabolomics network and selected pathways for +RANKL group.
IPA network analysis illustrating some of the common networks identified. The overall predicted trend was an anti-inflammatory and osteoclast inhibitory change. Specifically, this occurred through alterations in TNF, NF-κB, pro-inflammatory cytokine, PARP, NADHP oxidase, PLA2, AMPK and SIRT6. However, there were also increases in LDL and AhR which conflicted with this trend. These potentially significant complexes are indicated by the canonical pathway arrows for IL-6 and role of osteoblasts, osteoclasts and chondrocytes in rheumatoid arthritis. Blue = inhibition, orange = upregulation. CP = canonical pathway. N=3 cell donors.

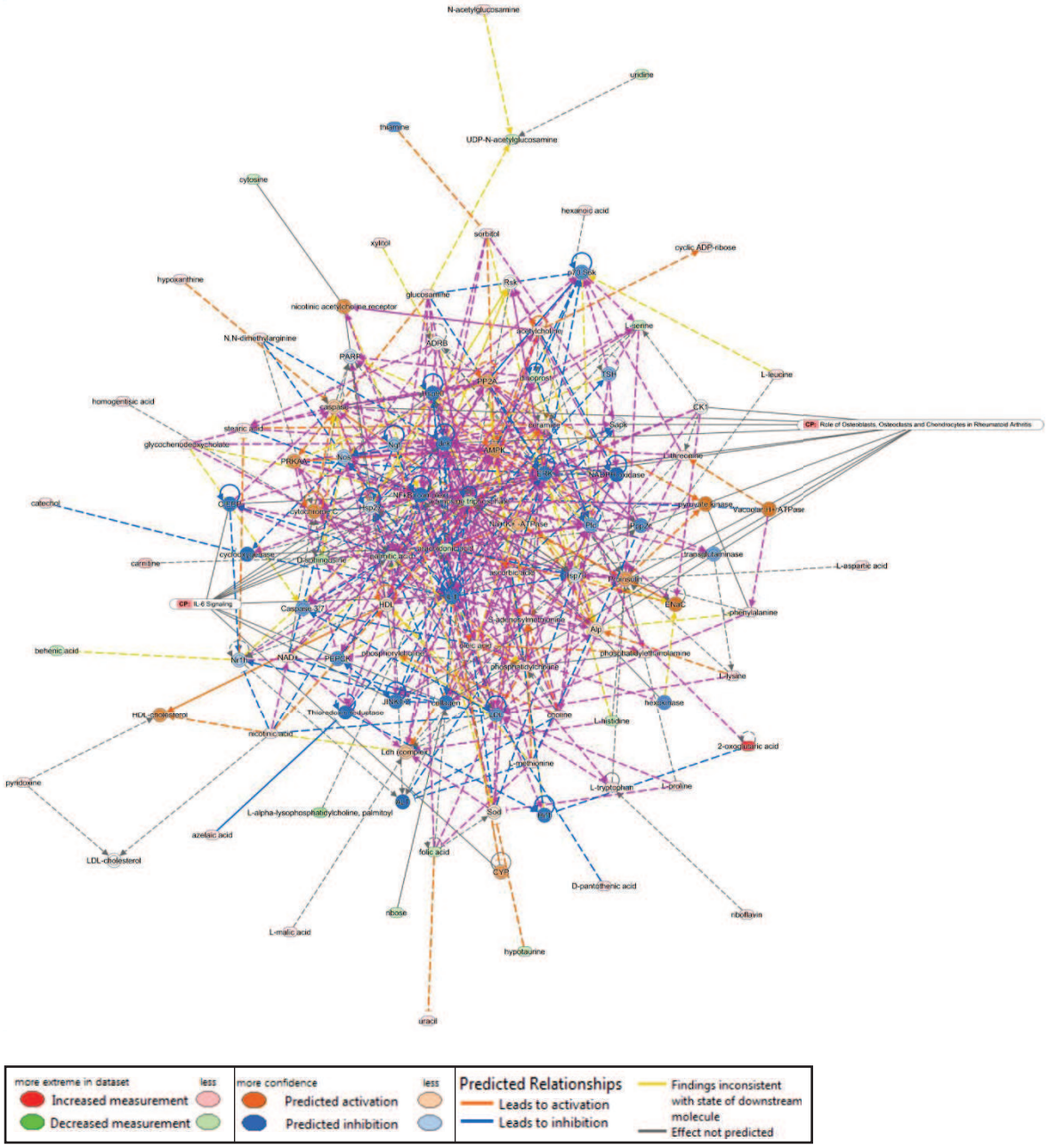

Figure 6:3 Metabolomics network and selected pathways for 2D day 14 co-culture.
IPA network analysis illustrating the top scoring networks identified. A number of pathways that play a role in osteoclast differentiation were predicted to be inhibited in the nanokick group. The overall picture was similar to that of the CD14+ culture. Potentially significant complexes included JNK, NADPH oxidase, IL-1, NF-κB, LDL, C/EBP and HIF1. Osteoblast stimulatory factors were found to be increased, including ALP and AMPK. These complexes are indicted by the canonical pathway arrows for IL-6 and role of osteoblasts and osteoclasts in rheumatoid arthritis. These pathways were chosen given the significant reduction in IL-6 identified in RT-qPCR and ELISA and the relevance of osteoblast/osteoclast imbalance to this study. Blue = inhibition, orange = upregulation. CP = canonical pathway. N=3 cell donors.

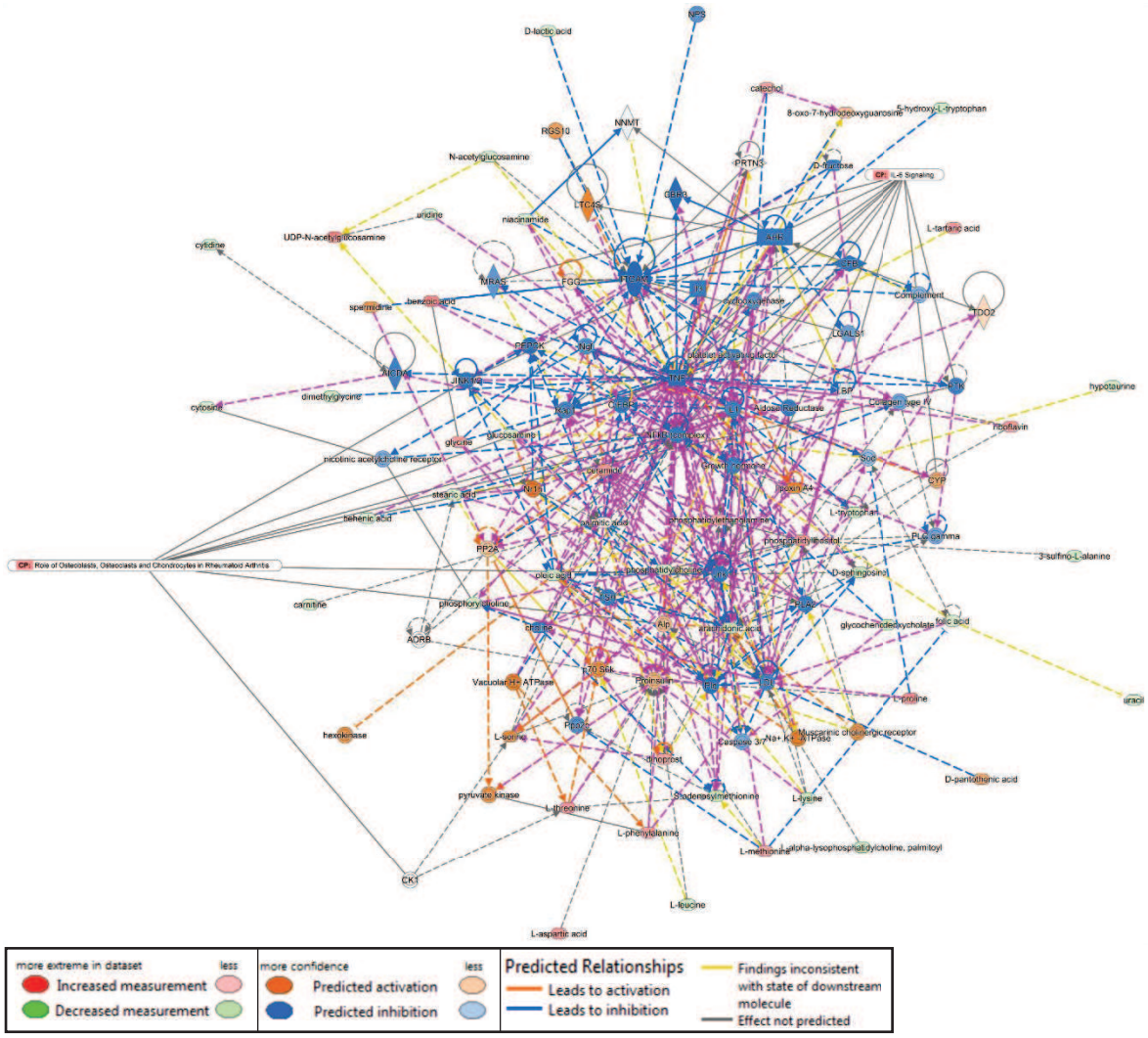

Figure 6:4 Metabolomics network and selected pathways for 2D day 21 co-culture.
IPA network analysis illustrating the top scoring networks identified. There were similar predicted trends identified at this time point to both day 14 co-culture and the CD14+ culture. This included inhibition of IL-1, NF-κB, LDL, C/EBP, TNF and JNK. Other potentially significant factors that were inhibited included Rap1 and ITGAM, both of which are important for osteoclast differentiation and function. The potentially significant complexes are indicated by the canonical pathway arrows for IL-6 and role of osteoblast and osteoclast in rheumatoid arthritis. Blue = inhibition, orange = upregulation. CP = canonical pathway. N=3 cell donors.

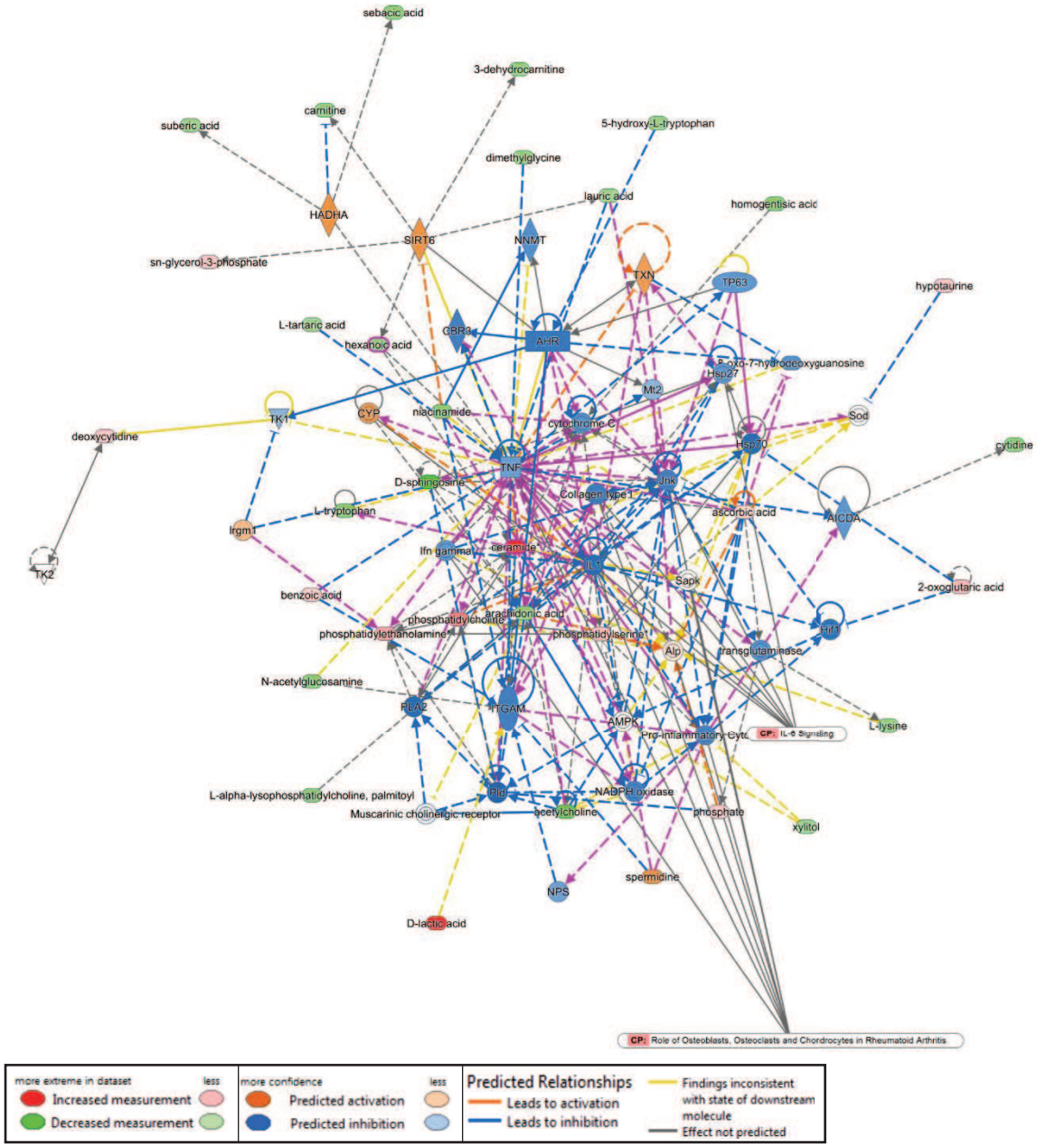

Figure 6:5 Metabolomics network and selected pathways for 3D day 14 co-culture.
IPA network analysis illustrating the top scoring networks identified. A number of inflammatory and osteoclast-stimulatory metabolomes were predicted to be inhibited. This included TNF, JNK, IL-1, HIF1, AhR and IFN-ϒ. The osteogenic marker ALP was increased. These complexes are highlighted in the overlaid pathways for IL-6 and role of osteoblast and osteoclasts in rheumatoid arthritis. In these pathways, all complexes were predicted to be inhibited, except ALP. The overall trends identified were comparable with the prior metabolomics experimental conditions. Blue = inhibition, orange = upregulation. CP = canonical pathway. N=3 cell donors.

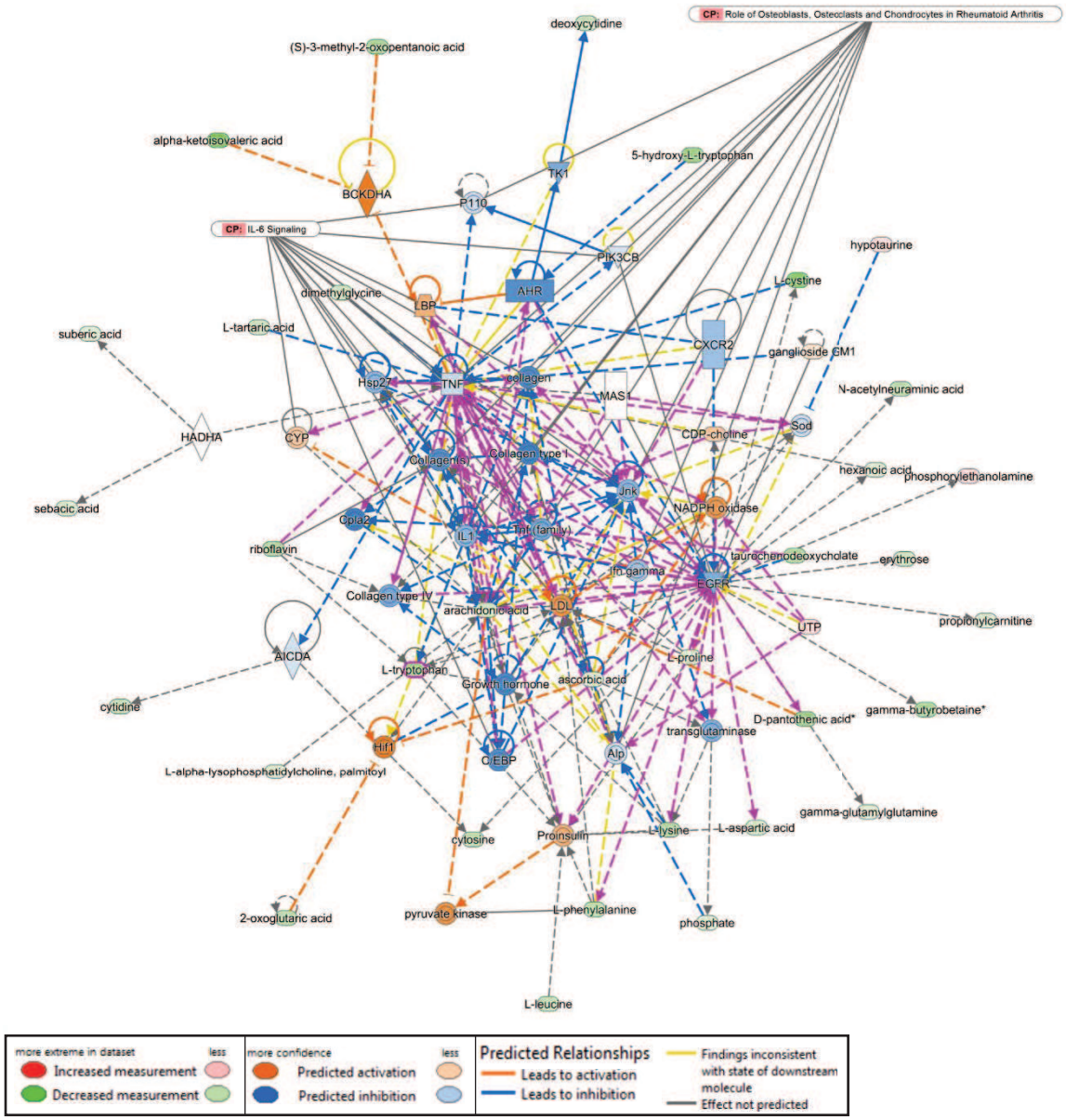

Figure 6:6 Metabolomics network and selected pathways for 3D day 21 co-culture.
IPA network analysis illustrating the top scoring networks identified. Similar to the prior experimental conditions, there was a predicted reduction in multiple inflammatory and osteoclast-stimulatory complexes, including TNF, IL-1, JNK, C-EBP, EGFR and CXCR2. Conversely, there was an increase in HIF1, LDL and NADPH oxidase which has not previously been noted in any other conditions. This therefore produces a more conflicting picture. These complexes are indicated by the canonical pathway arrows for IL-6 and role of osteoblast and osteoclasts in rheumatoid arthritis. Blue = inhibition, orange = upregulation. CP = canonical pathway. N=3 cell donors.